Title

Using Surface Networks to Infer CO2 and PM2.5 Emissions from On-road Vehicles

Author

Fitzmaurice, Helen Lorraine

Publication Date

2022

Peer reviewed|Thesis/dissertation

Using Surface Networks to Infer CO_2 and $PM_{2.5}$ Emissions from On-road Vehicles

By

Helen L. Fitzmaurice

A dissertation submitted in partial satisfaction of the

requirements for the degree of

Doctor of Philosophy

in

Earth and Planetary Science

in the

Graduate Division

of the

University of California Berkeley

Committee in charge:

Professor Ronald C. Cohen, Chair

Professor Inez Fung

Professor Fotini Katopodes Chow

Summer 2022

Using Surface Networks to Infer CO_2 and $PM_{2.5}$ Emissions from On-road Vehicles

by

Helen L. Fitzmaurice

Abstract

Using Surface Networks to Infer CO_2 and $PM_{2.5}$ Emissions from On-road Vehicles

by

Helen L. Fitzmaurice

Doctor of Philosophy in Earth and Planetary Science

University of California Berkeley

Professor Ronald C. Cohen, Chair

Cities and regional governments throughout the world are increasingly making commitments to reducing both total greenhouse gas (GHG) emissions and air quality (AQ) inequities within their boundaries. To plan emission reduction strategies, governments need information regarding the sector and subsector breakdown, spatial origin, and temporal variability in emissions, as well as strategies for tracking emissions changes over the policy-relevant time scales of 1-3yrs. While a wide variety of emission calculator tools are available, commonly used inventories disagree with one another by up to 100% and in different ways in different locations. The result is substantial uncertainty in how well we can describe the total quantity and the sectoral, spatial, and temporal distribution of emissions. One approach to reducing the uncertainty is to create inventories that account for spatially resolved processes with explicit sectoral details (e.g., fleet composition, congestion) using directly measured activity data and comparing these emission inventories with emissions inferred from atmospheric measurements.

In this dissertation, we use atmospheric observations to describe vehicle emissions of CO_2 and aerosol. Vehicles are the largest sector contributing to CO_2 emissions in US cities, and a substantial contributor to health inequities caused by exposure to co-emitted pollutants such as aerosol and aerosol precursors. We develop a novel method for using transportation data (vehicle flows, truck fraction) and near-road observations of aerosol and CO to derive Heavy Duty Vehicle (HDV) aerosol emission factors. We demonstrate that HDV primary aerosol emission factors derived using this method are in line with observations by other studies in the San Francisco (SF) Bay Area and elsewhere, that they decreased a by a factor of ~7 in the past decade, and that they are still 2-3 times higher than would be expected if all HDV were in compliance with California HDV regulations.

Second, we use the BErkeley Air quality and CO_2 Network ($BEACO_2N$), of low-cost sensors, paired with the Stochastic Time-Inverted Lagrangian Transport (STILT) model and a Bayesian inversion framework to estimate the variation of traffic emissions with speed on a stretch of road in the SF Bay Area. We show that the $BEACO_2N$-STILT-derived fuel efficiency estimates are within 3% of those predicted by the state of California's EMissions FACtor (EMFAC) model and that our network-inversion system should be able to detect changes in fuel efficiency of the fleet in 3 years or less.

Finally, we quantify the impacts of error in background concentration and meteorology, measurement density, and measurement duration on the ability of the BEACO$_2$N-STILT system to accurately constrain monthly and annual CO_2 emissions from the transportation sector in the SF Bay Area. We find large seasonal biases in posterior emissions and show that these biases may be significantly reduced by correcting for seasonal biases in background concentration and wind speed. We explore a method for determining thresholds for the number of nodes necessary for convergence of emissions estimates. In assessing the ability of the current BEACO$_2$N-STILT inversion framework to measure highway emissions, we find that this threshold is almost never met when less than 10 BEACO$_2$N nodes are operational, but almost always met when greater than 30 nodes are operational.

This dissertation illustrates two methods for using networks of sensors, paired with activity data to make sector and subsector-specific inferences about emissions in urban areas. These methods have the potential to observe both emissions at high resolution and changes in emissions over policy relevant time-scales, giving feedback to governments designing and implementing emissions reduction plans.

To Ben

Acknowledgements

The work done for this dissertation was supported by the NSF GRFP, the H2H8 Foundation, the Koret Foundation, and a Microsoft Research Internship.

Thanks to Ron. You have taught me to ask better questions and tell better stories. I am inspired by and grateful for all the things you balance and all the initiatives, projects, and most importantly, people that you manage to support. Thank you for your patience (perhaps more than you were hoping to supply) as I plotted my weird path through all this.

Thanks Inez and Tina, for reading this dissertation and offering your comments. You are both great teachers and I appreciate the time that you have spent with me in the classroom, through my quals, and in this dissertation.

Thanks to everyone who has worked on the BEACO$_2$N project over the years. You are the giants. None of this work would have been possible without you. Thanks to Alexis Shusterman for being my introduction to all this. Thanks to Alex Turner for teaching me so much and for being such an entertaining officemate. Thanks to Jinsol Kim, for always being someone I could bounce ideas off, and for being a such a creative wizard. Special thanks to Catherine Newman for keeping it all running through the years and for being a solid human being.

Thanks to the Cohen group, especially Jinsol, Kevin, and Hannah: I miss having lunch with the three of you. Garima, I appreciated all of our 2-hour conversations about the world beyond (in spite of) science. Josh, thank you for always being a teacher but a friend first. I appreciate that *someone* enjoyed my W(o)RF and (Lt. Commander) Data Assimilation jokes. Qindan, I'm so grateful for you, especially for being my partner in crime during our first year, when I was pretty sure that I didn't belong. Bryan, thanks for all the runs.

Thanks to the Education folks, especially Michelle Hoda Wilkerson for taking me under her wing, Jake Barton for being a thought partner, and David Hammer for being a sounding board through the past decade. Thanks to all the lovely writing group folks who made me feel less alone through this writing process.

Thanks to my extended EJC/OTACA fam: Sarah P. and Joe, you are both superheroes. Kate, you are a poet in all your (many) words. Deirdre, you always fight for what you believe in and never back down. Janan, your positive energy keeps us afloat. As much time as our work took away from this dissertation, all of you propelled me through it.

Thanks to Alicia, Alyssa, Nora, and Judy for listening to my complaints, trusting me with your own, for rendering the tragic comedic, judging me when called for, and generally just being there. Thanks to my pandemic trivia crew for keeping me sane in an insane time.

Thanks to my family and extended family. Thanks to Dad for truly making me believe that I could do anything I set my mind to and for showing me the importance of organizing, motivating, and doing work *for*, other people. (I think I can.) Thanks to Mom, for showing me how to power through, to move things forward, and *actually* get 'em done. You are a human

tractor: both the mother bird and the snort in the “Are you my mother?” book, wrapped into one. Thanks to Lorraine for all of your love: for listening to me, kvetching, and understanding. Thanks for the jelly sandwiches, the coffee, and for calling me (maybe). You are by far, my favorite sister. Thanks to Julie and David, for always making me feel like part of the family.

Thanks, most of all, to Ben. Words are not enough. Twelve years ago, when I was writing my undergrad thesis, I fell madly in love with you. In your vows, you promised to “take care of the little things,” so that I could “take care of the big things.” You have done that and more. You have taken care of me through the past five (really the past 12) years through all the grief and all the joy. You lift me up. You give me confidence. Thank you for teaching me how to code (even though I stuck with Matlab), for always being willing to help me think things through, and for reminding me to stop working every once in a while. I love you.

Table of Contents

List of Figures

List of Tables

Chapter 1 Introduction

1.1 – Mitigating climate change and poor air quality: The need to understand CO_2 and $PM_{2.5}$ emissions at the urban scale

Across the globe, climate change and poor air quality are among the most pressing challenges to human health and economic security. Already, an estimated 17 million people per year are displaced by climate-related disasters, and hundreds of millions are expected to be displaced by climate in the coming decades (UN, 2019). Climate change is already impacting food systems and is projected to reduce global crop yields by ~30% by 2080 (UN, 2019). Each year, air quality is estimated to be the cause of more than 4.2 million premature deaths worldwide (WHO) and nearly 100,000-200,000 premature deaths in the United States alone (Tessum et al., 2019). The human impacts of both phenomena are expected to increase in magnitude and severity over the coming decades, and the shifts in our climate are expected to endure for millennia (Soloman, 2007).

The causes and consequences of climate change and exposure to poor air quality, are tightly linked to combustion-related urban emissions. Combustion is the burning of oil, coal, natural gas, wood, or other materials, through which hydrocarbons combine with oxygen to produce CO_2, water, and heat. CO_2 is the primary emission from combustion and the most important greenhouse gas (GHG) contributing to climate change (the water from combustion condenses and is rapidly removed to the oceans). As a consequence of combustion of fuels, the amount of CO_2 in the atmosphere has increased from 280 parts per million (ppm) to 420 ppm since the start of the Industrial Revolution. Because CO_2 is a strong absorber of infrared (IR) radiation, reducing the amount of thermal radiation that escapes to space in regions of the spectrum where it absorbs IR energy, maintaining an energy balance causes the earth's surface to warm so that it emits increased amounts of IR radiation in regions of the spectrum where CO_2 does not absorb. This increase in surface warming propagates to ocean heat content, changes the equator to pole temperature gradient and consequently the intensity of storms that move energy from equator to pole. These impacts on earth's physical and chemical systems in turn impact the biosphere, stressing species adapted to historical climate conditions, launching a cascade of stress and increase in extinction events through the biosphere. Such changes in climate have happened before; however, the current pace of change is more rapid than those observed at the start or end of glacial periods and is unlike anything humans have tried to adapt to previously.

A variety of other products (including particulate matter) are also created, typically as a consequence of incomplete combustion. Fine particulate matter (PM) is the main driver of air-quality-related health impacts. $PM_{2.5}$ is a term used to describe particles smaller than 2.5 microns, composed of liquid and solids, and suspended in the atmosphere. $PM_{2.5}$ can be emitted directly into the atmosphere (primary $PM_{2.5}$) or formed as a secondary product via chemical reactions. Because of its small size (~ 1/30 the width of a human hair) , $PM_{2.5}$ can be absorbed directly through the surface of the lungs and lead to a number of serious heart (Rajagopalan et al., 2021) and respiratory conditions, as well as premature death (Di et al., 2017).

Both exposure to poor air quality (caused by $PM_{2.5}$ emissions) and climate change (caused largely by CO_2 emissions) exacerbate and magnify structural inequalities in health outcomes and economic stability within the United States and worldwide. For example, Tessum et. al (2021) showed that in the United States, race explains a larger percentage of the variance in $PM_{2.5}$ exposure than socioeconomic status, and that for most emission source types, people of color are more highly impacted than whites. Globally, air quality exposure is higher in cities than rural areas (Liu et al., 2021). Likewise, climate change is expected to push on the order of 100 million people worldwide into extreme poverty as climate change has a deleterious impact on human shelter, results in a loss of income for people in rural areas, and drives up food costs (Hallegatte, et al., 2016).

A focus on emissions reductions in urban areas is essential to mitigating both the health-related consequences of air pollution and the extent of global climate change. Using climate models, it is estimated that to keep anthropogenically-caused increases of global average temperature to less than 1.5 °C above pre-industrial levels, emissions of GHGs must be reduced by ~45% of 2010 levels by 2030 and to zero by 2050 (Rogelj et al., 2018). The 1.5 °C threshold is critical, because of the large differences in climate outcomes related to extreme heat, extreme precipitation and drought, and food security between scenarios in which the global mean temperature stabilizes at a 1.5 °C increase vs. a 2 °C increase (Hoegh-Guldberg et al., 2018). Worldwide, roughly 70% of CO_2 is attributable to urban areas, meaning that a swift reduction of CO_2 within and caused by cities is essential to achieving the less than 1.5 °C goal. Likewise, in the US, air quality is on average substantially worse in urban areas compared to rural areas (CDC, 2017), and in China the incidence of mortality attributable to $PM_{2.5}$ is ~5 times greater in urban as compared to rural areas (Liu et al., 2021). Because the share of people living in urban areas is expected to increase from ~50% to ~70% by 2050 (IPCC, 2014), without targeted emission reduction strategies, the share of CO_2 emitted and air pollution related deaths occurring in cities is likely to increase in the next three decades.

Although sweeping national and international policies are needed to bring CO_2 emissions to zero and decrease $PM_{2.5}$ concentrations to a level deemed safe by the World Health Organization, a substantial fraction of emissions can be reduced through local actions. Responding to the need for emissions reduction outlined above, local (city, regional) governments have increased efforts to reduce city-wide emissions of CO_2 and exposure to $PM_{2.5}$ at the neighborhood scale. For example, 88 major cities across the globe, totaling ~700 million in population, have committed to halving their CO_2 emissions by 2030 as part of the C40 program. This list of cities includes the three most populous cities in the United States: New York, Los Angeles, and Chicago, as well as San Francisco, one of the cities studied in this dissertation. At the regional scale, in California, 64% (Boswell et al., 2019) of residents reside within a city with a climate action plan that targets local reductions of CO_2 emissions. Because a fraction of $PM_{2.5}$ is co-emitted as product of combustion (through secondary processes enhanced by combustion products), concerted efforts in CO_2 emissions can lead to reductions of $PM_{2.5}$. Beyond $PM_{2.5}$ emissions reduction as a co-benefit of CO_2 emissions reduction, there are examples of local efforts to reduce PM2.5 exposure. For example, the California Air Resource Board's AB617 program (A.B. 617) enables local air districts to work with community stakeholders to collaborate to form emission reduction plans for health-impacting emissions, such as $PM_{2.5}$.

To create and continuously adapt and update emission reduction strategies, governments need information regarding the sector and subsector breakdown, spatial origin, and temporal variability in emissions. For example, to understand how to combat inequities in air quality exposure in an area near a port, neighborhood scale maps of emissions, and an understanding of the relative emission contributions by local emissions of cars, trucks, trains, watercraft, and other port activities and a comparison to regional contributions (e.g. Hamilton et al., 2021) are needed. Furthermore, to monitor the progress of these strategies, governments require the ability to track changes of emissions over the policy-relevant time scales of 1-3 years, so that course-corrections can be implemented on 5-10 year time scales. Consequently, there is a pressing need to understand urban emissions of both CO_2 and $PM_{2.5}$ emissions at the neighborhood scale and changes in these emissions over short periods of time.

1.2 – Using a high-density surface network to quantify urban emissions

The atmospheric science community has worked to develop tools to assess emissions progress at the sectoral level or to assess spatial and temporal changes in emissions. Briefly, these approaches can be characterized as either activity-based emissions models or those that use atmospheric measurements of concentration to infer emissions. Activity-based emissions models use quantifiable economic (e.g., utility or fuel sales) data, typically aggregated at the regional (for example, county) scale to estimate emissions by sector. These emissions models can then be given a spatial and temporal profile by applying high resolution activity (traffic counts), demographic (population density), or environmental (temperature) data that might indicate the location and timing of emissions. Several high-resolution (500m – 1km) (Oda et al., 2010; Gurney et al., 2012; McDonald et al., 2014; Gately et al., 2017a) or extremely high-resolution (10s of meters) (Gurney et al., 2019) emission inventories have been created for specific urban areas. In addition to emissions inventories created by researchers, a wide variety of emission calculator tools are available for use by municipalities and regional governments. However, activity-based inventories calculated by government agencies, and those created by researchers, can disagree with one another by up to 100% (Gately, 2017; Gurney, 2021). The result is substantial uncertainty in the total quantity and sectoral, spatial, and temporal distribution of emissions.

Atmospheric observations, obtained through a variety of platforms, have been used to estimate GHG emissions in urban areas across the US and globally, and have the potential to reconcile differences between activity-based emissions inventories. These platforms can roughly be divided into long-term networks, total column measurements, and mobile campaigns. A summary of measurement systems used to infer emissions estimates from atmospheric concentrations can be found in Table 1.

In practice, there are often tradeoffs between spatial and temporal resolution, spatial and temporal coverage, and biases created via representativeness error or errors in the meteorological model used to link atmospheric concentrations to emissions sources. For example, long-term measurements may monitor concentrations at elevation (~40-150 m above ground level) (Lavaux et al., 2016; Lavaux et al., 2020) or closer to the surface (Turner et al., 2016; Turner et al., 2020; Kim et al., 2021; Fitzmaurice et al., *2022a*; Fitzmaurice et al., *2022b*). Because of atmospheric mixing, emissions estimates inferred from measurements at elevation are sensitive to larger

areas, and therefore less likely to be biased by hyper-local sources, such as exhaust from individual buildings. However, because of the relatively larger areas to which each sensor is sensitive, and because of the sensitivity and corresponding instrument cost required for instruments to measure concentrations at height, tower networks are unable to achieve the spatial resolution of near-surface networks.

Similarly, total column measurements including satellite (e.g., Kort et al., 2012) and ground-based measurements (e.g., Sargent et al., 2018) measure the total integrated column of a particular species from ground to top of atmosphere, eliminating the need to model vertical atmospheric transport (a large source of error), but are unable to resolve emissions at high spatial resolution within an urban area. Mobile campaigns such as aircraft measurements, ground-based mobile monitoring (Mallia et al., 2020), tower networks and near-road plume capture (Kirchstetter et al., 1999; Bishop et al., 2015; Haugen et al., 2017; Haugen et al., 2018; Preble et al., 2018) capture snapshots of concentrations at extremely high resolution, but over short durations, making it difficult to track trends over time.

In Figure 1.1, we show the relative spatial and temporal resolution and coverage of each of the measurement systems described above. Only dense, low-cost measurement systems achieve neighborhood-scale (~1 km^2) resolution with city-wide (10^4 km^2) coverage at the time resolution (~1hr) required to track time of day changes over policy-relevant (1-3 yr) time periods.

1.3 - Using surface networks to study urban vehicle emissions

Vehicle emissions compose an important fraction of CO_2 emissions (29% in the United States, 14% globally) (IPCC, 2014) and have substantial public health consequences. In the United States, vehicles emit the largest sectoral fraction of CO_2 and a significant fraction of the $PM_{2.5}$ in urban areas (BAAQMD, 2011), and are estimated to cause 29% of deaths associated with poor air quality (Takrar, 2020).

Local and regional governments can influence emissions from vehicles via policies targeting subsector processes such as vehicle kilometers traveled (vkm) reduction, fleet make-up in terms of vehicle model, make, and fuel usage, and congestion, which can drastically alter vehicle emission rates of both CO_2 and $PM_{2.5}$. Across the globe, local and regional governments have enacted policies using these three levers to target emissions by vehicles. For example, in 2019 the city of London implemented an ultra-low emissions zone in which diesel and older gasoline vehicles are charged a flat rate per day to drive in the zone (Ma et al., 2021).

In this dissertation, we focus on quantifying emissions from surface-level networks, using data from both reference grade instruments with individual instrument calibrations traceable to standard materials and low-cost sensors calibrated as an ensemble network. Although questions remain about the sensitivity of low-cost sensor networks to interference from hyper-local signals and the challenges associated with modeling transport at sites so close to the surface, when deployed at high density and maintained over years and decades, they have the potential to shed light on long- (Lauvaux, 2020; Kim, 2022) and short-term (Turner, 2020) trends and spatial variability of emissions. Furthermore, both the high spatial resolution (Apte, 2017; Caubel, 2018; Fitzmaurice et al., *2022)* and colocation of sensors measuring several species (Fitzmaurice, *Chapter 2*) lend these networks to quantifying emissions by sector.

More specifically, we use network data to quantify emissions of $PM_{2.5}$ (Chapter 2) and CO_2 (Chapter 3) by on-road vehicles. We used data from both the Bay Area Air Quality Management District (BAAQMD) air pollution network, and the BErkeley Air quality and CO2 Network ($BEACO_2N$). The BAAQMD network consists of ~21 sites measuring criteria pollutants across the San Francisco Bay Area's nine counties, covering an area of 18,040 sq km. $BEACO_2N$ is a low-cost sensor network of ~65 nodes, spaced at ~2 km intervals located in San Francisco and the east and northeast parts of the Bay Area covering an area of ~500 sq km. Both networks have the temporal resolution and coverage to track changes over 1-3 years and the $BEACO_2N$ network has the spatial resolution to track changes at the neighborhood (~1-2 km) scale (see Figure 1.1). Locations of BAAQMD and $BEACO_2N$ sites, as well as the interior of a $BEACO_2N$ node are shown in Figure 1.2.

In the chapters described below, we make use of data from these to networks to quantify sub-sector processes by vehicles. In Chapter 2, we describe a novel method for using near-road regulatory sensors to infer emissions factors (grams $PM_{2.5}$ emitted per kilograms fuel) for heavy-duty vehicles (HDV). We track changes in these factors over a decade in the Bay Area. In Chapter 3, we use emissions derived from $BEACO_2N$ to track changes in fuel efficiency as a function of congestion and HDV fraction. In Chapter 4, we use ~2 years of traffic emissions estimated using $BEACO_2N$ data to understand the impact of node density and meteorological model error on emissions estimates.

1.4 – Chapter 2: Long-term trends in Aerosol Emissions from Heavy Duty Vehicles

In chapter 2, we outline a method for using regulatory surface networks in combination with measurements of vehicle number and type to estimate emissions factors (g $PM_{2.5}$ / kg fuel burned) from HDV. HDV contribute a small, but meaningful fraction of primary aerosol emissions in urban areas, for example ~7% in the county of San Francisco (BAAQMD, 2014). Previous studies have shown spatial heterogeneity in emissions as a consequence of variations in compliance with HDV emission control regulations (Preble et al., 2018). Consequently, location-specific emissions factors are necessary to describe primary particulate matter emissions by HDV. Using near-road observations from the BAAQMD network over the 2009-2020 period in combination with traffic measurements of vehicle number and type, we determine primary $PM_{2.5}$ emission factors from HDV on highways in the San Francisco Bay Area. We demonstrate that HDV primary aerosol emission factors derived using this method are in line with observations by other studies in the SF Bay Area and elsewhere, that they vary spatially, that they decreased by a factor of ~7 in the past decade, and that they are still 2-3 times higher than would be expected if all HDV were in compliance with California HDV regulations.

1.5 – Chapter 3: Using a Network of Low-Cost Sensors to Observe Fuel Efficiency in Vehicles

Turning from a focus on $PM_{2.5}$ emissions by HDV, in Chapter 3 we continue developing methodology for evaluating sub-sector vehicle emissions by using a high-density sensor network of low-cost CO_2 sensors to quantify changes in fuel efficiency from vehicles. Transportation represents the largest sector of anthropogenic CO_2 emissions in urban areas in the United States. Timely reductions in urban transportation emissions are critical to reaching climate goals set by

international treaties, national policies, and local governments. Transportation emissions also remain one of the largest contributors to both poor air quality (AQ) and to inequities in AQ exposure. As municipal and regional governments create policy targeted at reducing transportation emissions, the ability to evaluate the efficacy of such emission reduction strategies at the spatial and temporal scales of neighborhoods is increasingly important. However, the current state of the art in emissions monitoring does not provide the temporal, sectoral, or spatial resolution necessary to track changes in emissions and provide feedback on the efficacy of such policies at a neighborhood scale. The BErkeley Air Quality and CO_2 Network ($BEACO_2N$) has previously been shown to provide constraints on emissions from the vehicle sector in aggregate over a ~500 km^2 multi-city spatial domain. Here, we focus on a 5 km, high volume, stretch of highway in the SF Bay area. We show that inversion of the $BEACO_2N$ measurements can be used to understand two factors that affect fuel efficiency: vehicle speed and fleet composition. The CO2 emission rate of the average vehicle (g/vkm) are shown to vary by as much as 27% at different times of a typical weekday because of changes in vehicle speed and fleet composition. The BEACO2N-derived emissions estimates are consistent to within ~3% of estimates derived from publicly available measures of vehicle type, number, and speed, providing direct observational support for the accuracy of the Emissions FACtor model (EMFAC) of vehicle fuel efficiency.

1.6 – Chapter 4: Evaluating the Impact of Background Concentration Error, Transport Error, and Node Count on $BEACO_2N$-STILT Emissions Estimates

Finally, in Chapter 4 we further assess the $BEACO_2N$-STILT tool (developed by Turner et al., 2020) used to determine fuel efficiencies in Chapter 3. High-density, urban sensor networks, paired with Bayesian inverse models have been used to quantify sector-specific, temporally-specific, and spatially-specific CO_2 emissions and have, in some cases (e.g. Kim et al., 2022), been shown to have the precision necessary to evaluate whether annual emissions reductions are occurring as expected based on policy. A better understanding of the accuracy and precision of such emissions estimates, as well as the impact of real-world network conditions (background estimation error, meteorology, sensor down time) on these estimates is needed to support more general use of the tool. In this Chapter, we quantify the impacts of background error, meteorology, measurement density, and measurement duration on the ability of the $BEACO_2N$-STILT observation/inversion system as implemented by Turner et al 2020 to accurately constrain CO_2 emissions from the transportation sector in the SF Bay area. We find that there are seasonal biases in the inversion system. These biases are attributed to biases in CO_2 background (~80%) and biases in the modeled wind speed (~10-15%). We use $BEACO_2N$-STILT footprints to explore the node density necessary for convergence of highway emissions estimates in this inversion system. Finally, we make recommendations eliminating seasonal biases and for future evaluation of the system.

1.7 – Ch 5: Conclusions and Future Work

In this section, we summarize the findings in Chapter 2, Chapter 3, and Chapter 4 and make recommendations for future work. The novel contributions of this dissertation area as follows. In Chapter 2, we describe a novel method for using near-road regulatory sensors, paired with publicly available traffic data to track long term trends and spatial heterogeneity in HDV

emission factors. In Chapter 3, we use the BEACO$_2$N network to observe the dependence of CO_2 emission rates on vehicle speed and fleet composition on a short segment of highway in the SF Bay Area. To our knowledge, this is the first time that a network-inversion system has been used to quantify the impact of sub-sector processes on CO_2 emissions at the neighborhood scale. Finally, in Chapter 4, we investigate the impacts of node density, meteorological error, and background concentration error on emissions estimates.

In the future, we suggest that the method described in Chapter 2 could be applied widely across the United States to track long-term changes in HDV emission factors for $PM_{2.5}$ and other species or applied to dense, low-cost networks with many near-road sensors to understand the spatial heterogeneity in HDV emission factors. The work described in Chapter 3 could be extended to other species emitted by vehicles (for example CO) or sectors (with appropriate activity data for those sectors). Finally, based on the work describe in Chapter 4, we make recommendations to improve the BEACO$_2$N-STILT inversion system and for further evaluations of the system.

Technique	*Brief Description*	*Technique has been used to estimate total emissions from an urban area*	*Technique has been used to estimate sector-specific emissions from an urban area*
roadside plume capture	Instruments sample multiple species from individual vehicle plumes to ascertain emissions factors (g X / kg fuel burned) - rather than total emissions.		✓
flight campaigns	Instruments sample concentrations along flights in and around urban areas. Flight tracks typically not repeated.	✓	✓
mobile measurements	Instruments sample concentration along vehicle (car or light rail) driving path. Measurements are repeated many times (>10) at the same location via repeated paths.	✓	
tower measurements	Instruments sample concentration from elevated locations (10s -100s of meters) across an urban area.	✓	✓
satellite measurements	Measure total column absorption of a chemical species, integrated from the surface to the top of the atmosphere	✓	
regulatory networks	(5-15 sensors per urban area)		✓
low-cost sensor networks	A dense network of 20 or more sensors set up throughout an urban area, typically instruments are located near-surface (<10 m).	✓	✓
surface remote sensing	Instruments located on the surface measure total column absorption a chemical species, integrated to the top of the atmosphere	✓	

Table 1.1. Summary of techniques used to infer emissions from concentration measurements.

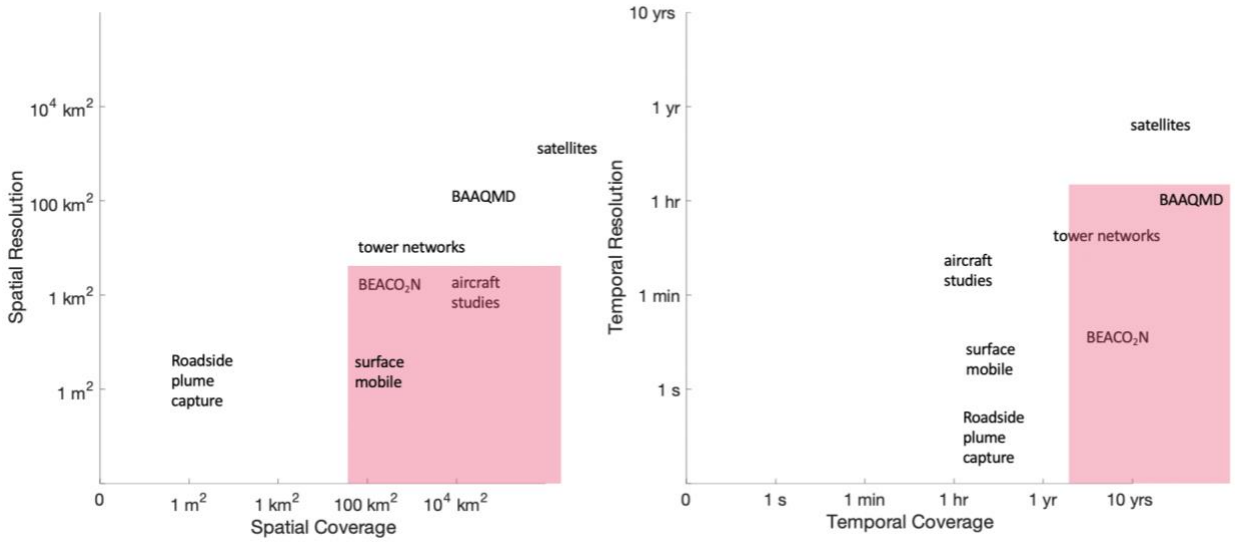

Figure 1.1. (left) Spatial resolution and coverage and (right) temporal resolution and coverage typically achieved by a variety of measurement systems. Pink boxes represent (left) the spatial resolution and coverage necessary to quantify neighborhood scale emissions for an urban area and (right) the temporal resolution and coverage required to understand daily patterns in emissions and track changes on policy relevant timescales.

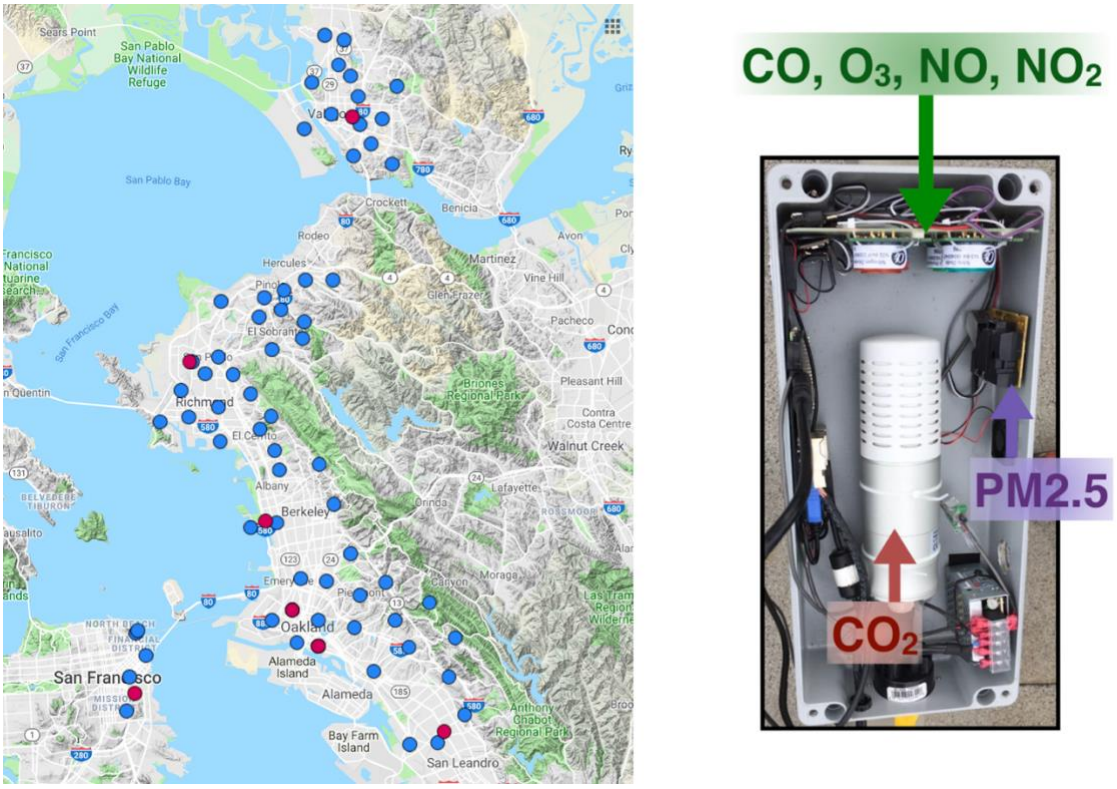

Figure 1.2. (right) Cut-away view of a BEACO2N node. (left) Measurement locations of the BEACO2N and BAAQMD networks in the SF Bay Area.

Chapter 2 A method for using stationary networks to observe long term trends of on-road emissions factors of primary aerosol from heavy duty vehicles

Adapted from Fitzmaurice, H.L. and Cohen, R.C., 2022. A method for using stationary networks to observe long term trends of on-road emissions factors of primary aerosol from heavy duty vehicles. *Atmospheric Chemistry and Physics Discussions*, pp.1-13.

Abstract Heavy-duty vehicles (HDV) contribute a significant, but decreasing, fraction of primary aerosol emissions in urban areas. Previous studies have shown spatial heterogeneity in compliance with regulation. Consequently, location-specific emissions factors are necessary to describe primary particulate matter (PM) emissions by HDV. Using near-road observations from the Bay Area Air Quality Management District (BAAQMD) network over the 2009-2020 period in combination with Caltrans measurements of vehicle number and type, we determine primary $PM_{2.5}$ emission factors from HDV on highways in the San Francisco Bay Area. We demonstrate that HDV primary aerosol emission factors derived using this method are in line with observations by other studies, that they decreased a by a factor of ~7 in the past decade, and that they are still 2-3 times higher than would be expected if all HDV were in compliance with California HDV regulations.

2.1. Introduction

Exposure to aerosols smaller than 2.5 microns in diameter ($PM_{2.5}$) at current ambient levels is estimated to cause 130,000 excess deaths per year in the United States (Tessum, 2019). Epidemiological studies have shown that health and mortality impacts from $PM_{2.5}$ persist at concentrations of $PM_{2.5}$ below current National Ambient Air Quality Standards and that small changes in $PM_{2.5}$ concentration may result in substantial health impacts (Di et al, 2017). Because of the health impacts resulting from small increases in $PM_{2.5}$, air quality academics, public health researchers, local regulatory agencies, and state governments have come to appreciate the importance of neighborhood scale differences in cumulative exposure to $PM_{2.5}$ (e.g. CARB, 2018). For example, regulatory agencies in California have begun to shift from a paradigm based primarily on compliance with annual and daily, regional scale air quality metrics to one also focused on mitigation of cumulative exposure, creating local remediation plans based on source apportionment. (BAAQMD, 2019). These source apportionment estimates are created from bottom-up emissions inventories using emissions factors and activity data. Consequently, accurate local emissions factors are vital to understanding and planning neighborhood-scale mitigation strategies.

On-road vehicles, specifically HDV, are a large contributor to aerosol in urban areas, both through direct emissions and through secondary formation in the atmosphere (e.g. Shah, 2018; BAAQMD, 2011). Total emissions can be thought of as the product of emissions factors (EFs) and the activity, where the EFs are expressed in units of grams of aerosol per unit activity (such as grams of aerosol per kg of fuel burned or per km travelled). EFs are estimated for on-road activity in a variety of ways including scaling based on measurements in a lab setting and/or on-road measurements (See references, Table 2.1). A summary of on-road studies for primary HDV and passenger vehicle PM EFs over the last 25 years is shown in Fig. 2.1 and Table 2.1. These

studies determined EFs of primary on-road aerosol by comparing ratios of aerosol enhancement (in grams) to CO_2 and/or CO enhancement (as a measure of fuel burned). Measurements included sampling directly in the exhaust of tunnels, and high frequency sensors near or above roads to sample and characterize individual vehicle plumes.

These prior observations show that typical heavy duty, diesel-powered vehicles dominated on-road emissions of primary aerosol in the 1990s and early 2000s. However, in recent years, emissions factors from typical heavy-duty vehicles have been dramatically reduced such that PM EFs of HDVs are now similar to those of light duty vehicles (LDV) and are less than 0.05 g aerosol/kg fuel burned. Control technologies such as diesel particulate filters and selective catalytic reduction are contributing to these reductions in EFs for HDVs.

While these improvements are seen in the "typical" HDV, previous studies indicate that compliance of HDV with emission technology requirements, and therefore HDV on-road emissions factors, vary by up to an order of magnitude from location to location (Preble, 2018 Bishop, 2015; Haugen, 2018; Haugen, 2019). For example, Bishop (2015) and Haugen (2018, 2019) found emissions factors measured at the Port of Los Angeles were as much as an order of magnitude lower than those measured along a highway in Cottonwood, California during the same season. While the gap between the two sites narrowed from 2013-2017, the mean emission factors measured in Cottonwood were still 3 times those measured at the Port of Los Angeles in 2017. Similarly, Preble (2018) found that while 100% of trucks at the Port of Oakland were registered by the state of California as being in compliance with HDV control technology regulations, compliance rates amongst HDV at the Caldecott tunnel (also in Oakland, CA) were below 90%.

These studies highlight that variability in emissions factors as a function of location may affect exposure. They point to the importance of characterizing spatial variation in HDV emissions if we are to understand aggregate emissions from the sector and its localized impacts. To assess the potential for existing data sources to supply the needed information, here we explore the use of regulatory sensor networks (near-highway, hourly $PM_{2.5}$ and CO (or CO_2) measurements), paired with coincident traffic data including LDV and HDV counts, to quantify spatial variation in HDV EFs. Such data is widely available. For example, in the US, there are more than 550 regulatory sites at which $PM_{2.5}$ and CO are collocated, some of which have measurements spanning more than a decade (https://www.epa.gov/outdoor-air-quality-data). Of these, 154 are located within 500 m of a highway. The large number of these sites and their longevity allow for examination of regional and temporal differences in EFs for HDV across the United States. In the future, the approach we outline should be even more widely applicable when dense low-cost sensor networks including aerosol and CO or CO_2 are available as a data source (e.g. Shusterman, 2016, Kim, 2018; Zimmerman, 2018). Because HDV emissions control regulations vary regionally in the US, this method has the potential to shed light on regional differences in HDV EF trends.

We begin by describing a general method for using such data to derive EFs of primary $PM_{2.5}$ from HDV (Section 2.2). We then (Section 2.3) test our method by using data from four near-highway sites operated by the Bay Area Air Quality Management District (BAAQMD) in the

San Francisco Bay Area (Figure 2.2a) over the period of 2009-2018. In section 4 we discuss the relationship of these findings to measures of exposure.

2.2. Data and Methods

2.2.1 Aerosol and CO Measurements

We use 1 hr averaged observations from 18 of the BAAQMD regulatory sites which measure $PM_{2.5}$ using Beta Attenuation Monitors and CO using the Thermo Scientific TE48i IR sensor. Some sites have been in operation since 2009, while others have been brought online as recently as 2018, or were operational for only a few years during this time period. Data was retrieved from https://aqs.epa.gov/aqsweb/documents/data_api.html. Site locations are summarized in Figure 2.2.

2.2.2. Meteorology

Boundary layer height and wind speed and direction are taken from the European Center for Meteorology and Weather Forecasting (ECMWF) ERA5 reanalysis, (https://cds.climate.copernicus.eu/cdsapp#!/dataset/reanalysis-era5-land?tab=form). Typical diel cycles for boundary layer height and total windspeed are shown in Fig. 2.10.

2.2.3. Traffic Data

Total vehicle flow and the percent of vehicles that are HDV are taken from the Caltrans' Performance Measurement System (PeMS) database (http://pems.dot.ca.gov), which records these parameters at over 1800 locations on highways in the Bay Area. We include all BAAQMD sites that are within 500 meters of one major highway and use traffic count data from the PeMS measurement site closest to each air quality site. In cases of missing PeMS data, data was filled in with the median value associated with that parameter for a particular site in a particular year, or if not possible, retrieved from the second or third nearest sites. More details about the PeMS data are presented in Fig. 2.5, Table 2.2, and Fig. 2.6.

2.2.4. Derivation of $EF_{PM(HDV)}$

Our derivation of HDV EFs assumes that the relationship between PM and CO, as observed near-road, can be scaled so that it represents PM per unit of fuel burned by HDVs (Equation 1):

$$EF_{PM(HDV)} = \gamma \frac{PM_{HDV}}{CO_{fleet}} \frac{gCO_{fleet}}{kg\ fuel_{,fleet}} \frac{kg\ fuel_{,fleet}}{kg\ fuel_{,HDV}}, \quad (1)$$

In this equation, γ=0.0008, and is the ideal gas law conversion factor, from ($\mu g/m^3 ppm^{-1}$-CO) to (gPM/gCO). Below, we describe the steps used to calculate each term in equation (1).

The first term $\frac{PM_{HDV}}{CO_{fleet}}$ in the equation is derived from observations as the slope of a linear fit of near-road $PM_{2.5}$ (assumed to be primarily emitted by HDV) and near-road CO (assumed to be emitted by both HDV and LDV). This term is derived by (1) isolating local enhancements of

$PM_{2.5}$ and CO, (2) isolating roadway enhancements by use of temporal filters and (3) fitting resulting roadway enhancements of $PM_{2.5}$ and CO to a line, as detailed below.

(1) To isolate local enhancements from total signal $PM_{2.5}$ and CO, we first leverage the entire BAAQMD network to derive an hourly regional signal for each species. The regional signal is defined as the 10^{th} percentile of the data across all 22 BAAQMD sites within a five-hour window of that hour (Figure 2.2b). This regional signal is assumed to be composed of background PM/CO transported to the region from elsewhere as well as region-wide sources of secondary aerosol/CO. We the find the enhancement by local primary emissions by subtracting the regional signal from total signal at each site.

(2) We isolate primary emissions from on-road sources by considering only the morning commute times and only during fall and winter. These are times coinciding with relatively high traffic emissions and too early in the day for significant accumulation of new secondary aerosol. We find the 6-8 am period represents the optimal overlap of low boundary layer height (Figure 2.10) and HDV emissions (Figure 2.6). To avoid observations of stagnant air, we only include observations with wind speed above 0.5 m/s. We also exclude known fire events. The result of these first two steps are enhancements, $\Delta PM_{2.5}$ and ΔCO above background.

(3) The slope of a linear fit of the median $\Delta PM_{2.5}$ in bins of ΔCO (see figure 2.3) is defined as the "enhancement ratio," α, in units of $\mu g/m^3 ppm^{-1}$-CO. Using the lengthy dataset, we are able to derive α for different percentages of HDV in the vehicle fleet on the road. There are some high $\Delta PM_{2.5}$ values uncorrelated with ΔCO as shown in Figure 2.3. In all cases, these points show little to no NO_x enhancement and thus are characteristic of a source that is not HDV. We make the assumption that LDV PM EFs are negligible and on-road primary emissions of aerosol are solely from HDV, implying that α is equivalent to the term $\frac{PM_{HDV}}{CO_{fleet}}$. This assumption is sound at the beginning of our period (2010s) of interest, because reported values of $EF_{PM(HDV)}$ were 2-3 orders of magnitude higher than $EF_{PM(LDV)}$ at that time (Fig 2.1). More recently, as $EF_{PM(HDV)}$ has decreased, this is less clear, especially without on-road estimates of $EF_{PM(LDV)}$. To understand the impact of LDV PM emissions on our findings, we establish an upper bound for $EF_{PM(LDV)}$ to be 0.002 g PM / kg fuel by insisting that all $EF_{PM(HDV)} > 0$ and find the impact of LDV PM on the long-term trends of $EF_{PM(HDV)}$ to be minimal (Figure 2.13).

The term $\frac{gCO_{fleet}}{kg\ fuel_{,fleet}}$ is the fleet EF for CO. We use truck percentage and CO emission factors from EMFAC2017 model and fuel efficiency estimates to calculate this term as follows:

$$EF_{CO,fleet} = \frac{EF_{CO(HDV)} t E_{HDV} + EF_{CO(LDV)} (1-t) E_{LDV}}{t E_{HDV} + (1-t) E_{LDV}}, \quad (2)$$

where t is the HDV fraction and E is fuel efficiency (miles / gallon). EF_{CO} for both LDV and HDV is defined for each time period using the EMFAC2017 model.

Finally, $\frac{kg\ fuel_{,fleet}}{kg\ fuel_{,HDV}}$ is the ratio of fuel burned by the total vehicle fleet to that burned by HDV alone. We find this ratio to be $\frac{t E_{HDV} + (1-t) E_{LDV}}{t E_{HDV}}$.

Because, at a given site, we expect $\frac{PM_{HDV}}{CO_{fleet}}$ (but not $EF_{PM(HDV)}$) to vary linearly with HDV fraction, we bin data by HDV fraction in increments of 0.02, use the process above to calculate $EF_{PM(HDV)}$ for each bin. We use the 95th percent confidence intervals to represent uncertainty in $EF_{PM(HDV)}$ for each bin, and finally, calculate $EF_{PM(HDV)}$ for each site during a particular time period using the average of the, weighted by uncertainty in $EF_{PM(HDV)}$ for each bin.

2.3. HDV Emissions Factors from Primary Aerosols in SF Bay Area: 2009-2018

The result of this procedure is HDV EFs at four near-highway BAAQMD sties (Redwood City, Berkeley Marina, San Rafael, Pleasanton) during the time periods: 2009-2011, 2012-2015, 2016-2018. (Figure 2.4.) HDV EFs decrease over the decade (Figure 2.1, Figure 2.4), amounting to a roughly seven fold reduction. Site to site differences in HDV EFs remain substantial. For example, during the 2018-2020 period, we see a range of more than a factor of 10 with a minimum of 0.02+/0.10 g PM / kg fuel to a maximum of 0.38+/0.07 g PM / kg fuel. Both the temporal decrease and the site to site differences are similar to prior reports derived using other approaches to data collection and interpretation (e.g. Haugen et al. 2017, 2018).

By 2020, California law required that all HDV models from the years 1995-2003 replace their engines with 2010 or newer models, and that all HDV model year 1994 or newer use diesel particulate filters (DPF) (California Code of Regulaitons). Assuming that the fleetwide average EF for models with 2010 or newer engines using DPF is 0.03 g PM / kg fuel as observed by Haugen (2018), we can use fuel usage by HDV model year in 2020 as well as emissions factors for vehicles older than 1994 estimated by the Emissions FACtor Model (EMFAC2017) to estimate a fleetwide average. Thus a fleetwide average should have an EF of 0.03-.06 g PM / kg fuel if the trucks were fully compliant in 2018-2020. We observe an average EF of 0.11 g PM / kg fuel, for 2018-2020, more than 2-3 times larger than expected for an HDV fleet compliant with current regulations. Possible explanations for this discrepancy include exemptions from truck regulations, under which certain classes of HDV travelling less than 15,000 miles per year are eligible for exemptions, meaning locally travelling HDV may have higher emissions factors than those travelling long distances (CARB, 2018), the fact that HDV registered in other states are not typically subject to CA regulations unless they enter specific areas, such as ports and failure of or tampering with installed equipment.

We also observe site to site variation in emission factors. For example, while emission factors at both Redwood City and Santa Rosa drop throughout the time period observed and each experiences a sharp drop between different two time periods, that sharp drop occurs earlier (2009-2011 to 2012-2014) at RWC than at SR (2012-2014 to 2015-2017), suggesting a difference in timing of compliance to control technologies at each place. Furthermore, in the 2018-2020 period, we see a wide range in emission factors, likely indicating a range in compliance.

We found reliable results using this procedure at 4 near-road locations that are well separated from other activity. However, at some at other locations apparent large emissions are observed, that we believe to be unphysical. For example, the EF_{HDV} calculated for Laney College in the

2015-2017 and 2018-2020 periods is significantly higher than EF_{HDV} observed at the four sites we deem reliably far from other sources. While it is possible that HDV on the highway near Laney College, are unusually high emitters, it is more likely that emissions from a nearby parking lot are responsible for the high inferred EFs. (See Fig. 2.12.) Slow moving LDV could be an important influence on local emissions, a factor that should be assessed more thoroughly.

2.4 Primary $PM_{2.5}$ exposure

To understand exposure from HDV $PM_{2.5}$, we calculate both a region-wide addition to aerosol burden by HDV emissions and an enhancement as a function of distance from a highway. Assuming steady-state, a box of 100 km in length, 160 m in height, and a wind-speed of 1.2 m/s (Figure 2.10), and using fuel sales data (Moua, 2020) to estimate total HDV fuel used, we estimate a maximum region-wide enhancement on the order of 0.2 $\mu g/m^3$ on a typical day in the 2018-2020 period, compared to an enhancement of 1.3 $\mu g/m^3$ during the 2009-2011 period (Figure S7). Decreases in emissions factors over the past decade are countered by the increase in diesel fuel usage (70%) (Moua, 2020) such that there has been only a small change in typical regional exposure to primary PM from HDV. (See Fig. 2.11 for diel cycle of modeled region-wide enhancement.) While an enhancement of 0.2 $\mu g/m^3$ is small in comparison to average ambient $PM_{2.5}$ (8.3-14.4 $\mu g/m^3$ for all BAAQMD sites in 2018), it is sizeable in comparison to average ambient BC (.4-1 $\mu g/m^3$ for all BAAQMD sites in 2018).

To gauge near roadway exposure, PM enhancement from HDV was calculated as a function of distance from a highway, modeled treating emissions from the highway as a gaussian plume flowing perpendicular to a line source. Assuming both highway and point of measurement at ground level, the simplified gaussian plume dispersion for a line source yields:

$$PM_{enh} = \frac{2\lambda}{\sqrt{2\pi}u\sigma_z} \quad (3)$$

where λ is an emissions rate per unit highway length, u is wind speed, and σ_z is a dispersion parameter. For a typical daytime HDV flow rate of 500 vehicles per hour (Figure 2.6) and windspeed of 1.2 m/s (Figure 2.10), we calculate PM enhancement as a function of perpendicular distance downwind of a highway. For unstable atmospheric conditions ($\sigma_z = \frac{0.102x}{\left(1+\frac{x}{927}\right)^{-1.92}}$), enhancements drop to values below 1 $\mu g/m^3$ in the first 200 m. For stable conditions ($\sigma_z = \frac{0.022x}{\left(1+\frac{x}{1170}\right)^{0.7}}$), such as those typical of early morning, enhancements of ~0.8 $\mu g/m^3$ are predicted up to a kilometer away.

2.5. Conclusions

We find that HDV EFs in the SF Bay Area have decreased by about a factor of seven over the last decade, consistent with trends reported in other analyses in this region and Los Angeles. We find spatial variation of HDV EFs remains large indicating a wide range in the application of retrofit technologies and possible that vehicles legally exempt from compliance with the current standards are a significant portion of those on the road at the sampling sites.

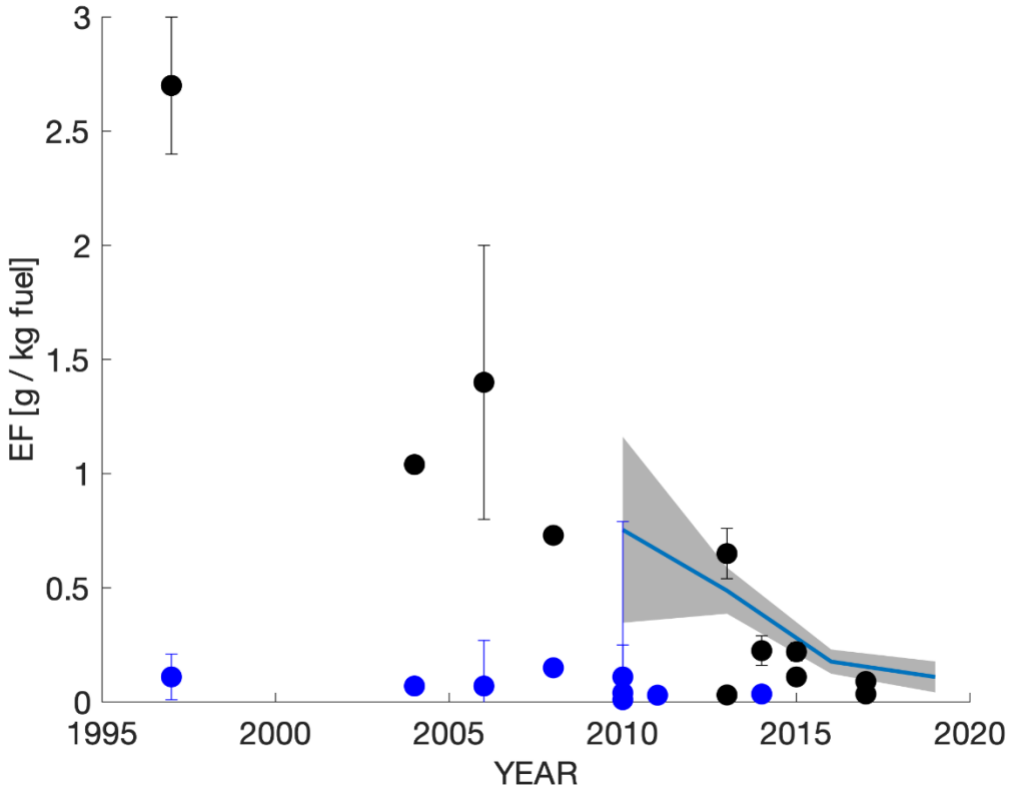

Figure 2.1: On-road measurements of emissions factors, from other studies. HDV (black) emissions factors converge on LDV (blue) emissions factors. Some studies do not give error bars. Grey patches and blue trendline indicate findings from this study for the two highway sites (RWC and SR) available during all three time periods. Patches span the mean and standard deviations of emissions factors from these two sites during each time period.

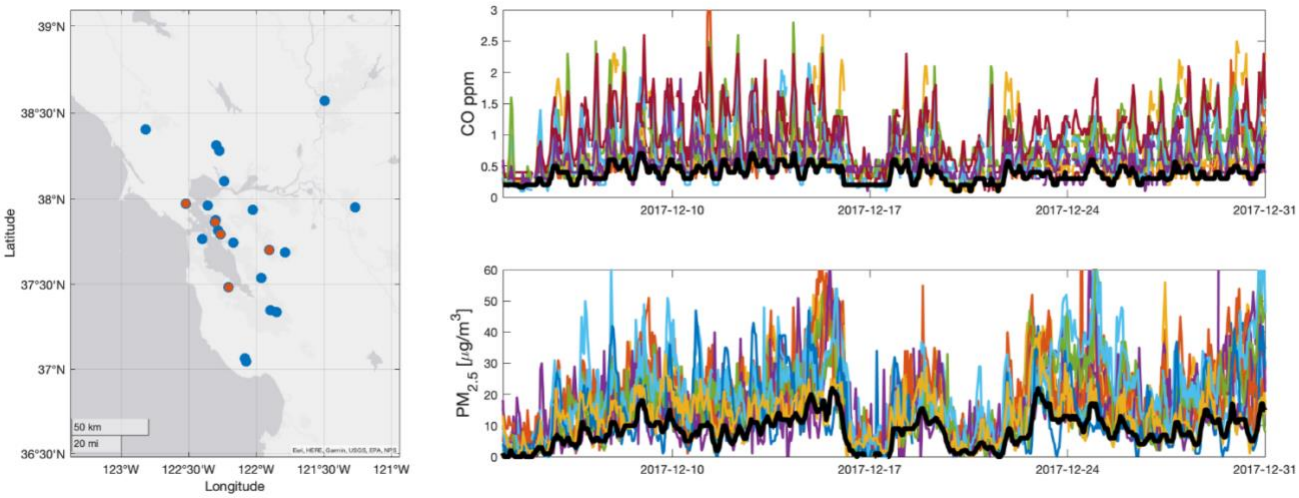

Figure 2.2. (Left): BAAQMD sites used in this study. Red dots show near-highway sites at which HDV emissions factors were determined. Blue sites were used only for determining regional signal. (Right): Aerosol and CO at each BAAQMD site (various colors). The regional background (black), is defined as the lowest 10th percentile of all signals within a rolling 4-hour window. Figure credit: Esri, HERE, Garmin, USGS, EPA, NPS.

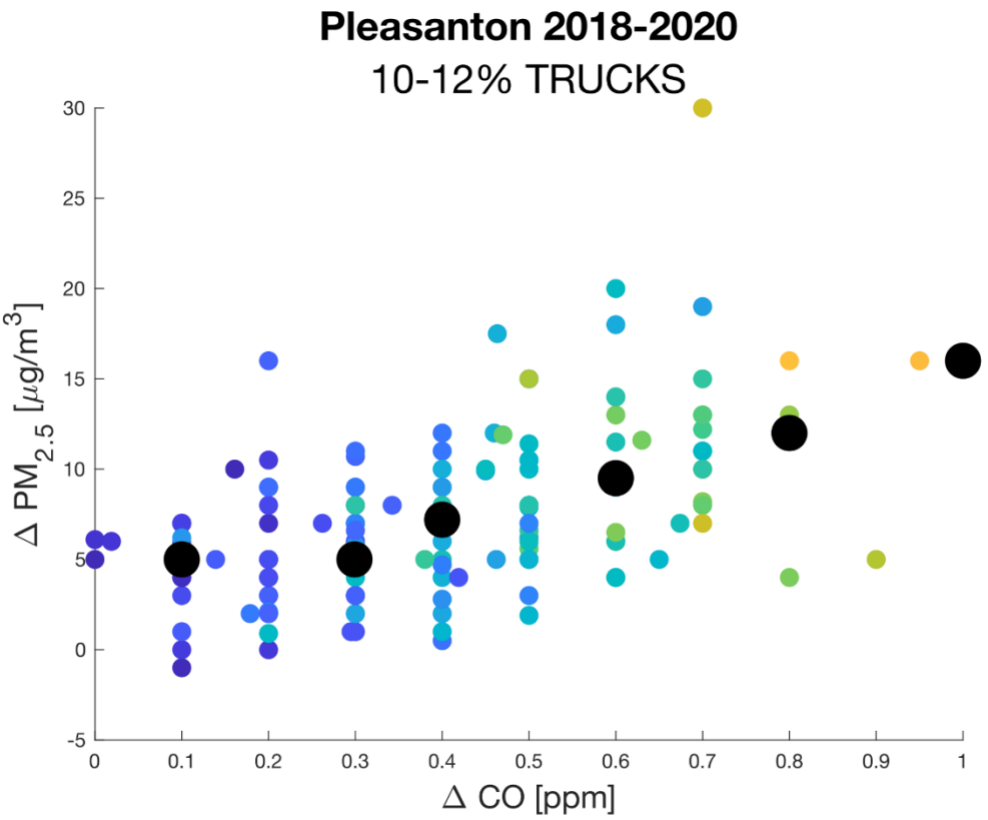

Figure 2.3. ΔPM vs. ΔCO at Pleasanton site during the 2018-2020 time period for which 10-12% of traffic flow is trucks. Data is colored by NO_x concentration. Black point represent the median ΔPM value falling within a 0.05 ppm bin of ΔCO. These points are fit linearly to find slope, α.

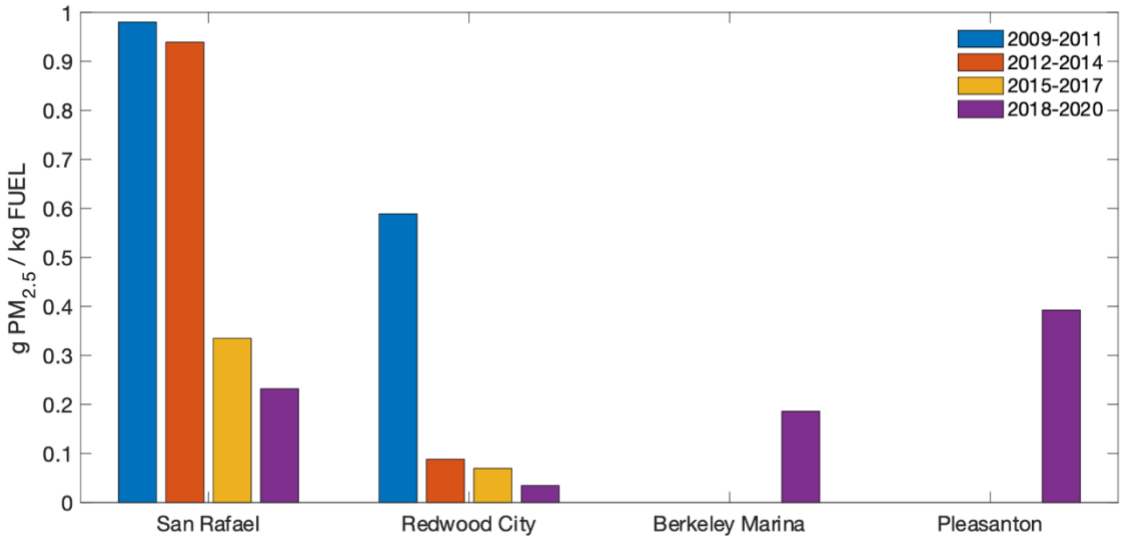

Figure 2.4. Top: Fleet emissions factors, derived from all sites, all years, binned by truck fraction. Bottom: HDV emissions factor at near highway sites during 2009-2011, 2012-2014, 2015-2017, and 2018-2020 time period.

Study	Year of Measurements	Vehicle Type	Measurement Location	EF_{CO} (g/kg fuel)	EF_{PM} (g/kg fuel)
Kirchstetter (1999)	1997	Light Duty	Caldecott Tunnel, Oakland CA		0.11 ± 0.1
Kirchstetter (1999)	1997	Heavy Duty	Caldecott Tunnel, Oakland CA		2.7 ± 0.3
Geller (2005)	2004	Light Duty	Caldecott Tunnel, Oakland CA		0.07 ± 0.02
Geller (2005)	2004	Heavy Duty	Caldecott Tunnel, Oakland CA		1.04 ± 0.02
Ban-Weiss (2008)	2006	Light Duty	Caldecott Tunnel, Oakland CA		0.07 ± 0.2
Ban-Weiss (2008)	2006	Heavy Duty	Caldecott Tunnel, Oakland CA		1.4 ± 0.6
Park (2011)*	2007	Light Duty	Los Angeles, CA (Wilmington)	47	0.15
	2007	Heavy Duty	Los Angeles, CA (Wilmington)	36	0.73
Dallman (2012)	2010	Heavy Duty	Caldecott Tunnel, Oakland CA	8.0 ± 1.2	
Dallman (2013)	2010	Light Duty	Caldecott Tunnel, Oakland CA	14.3 ± 0.7	0.038 ± 0.010
Bishop (2015)	2013	Heavy Duty	Cottonwood, CA		0.65 ± 0.11
Bishop (2015)	2013	Heavy Duty	Port of Los Angeles		0.031 ± 0.007
Park (2016)	2011	Light Duty	West Hollywood	15.2 ± 53.8	0.01 ± 0.01
	2011	Light Duty	Boyle Heights	36.8 ± 85.6	0.11 ± 0.68
	2011	Light Duty	Los Angeles, CA (Wilmington)	46.6 ± 117.9	0.04 ± 0.21
Haugen (2017)	2015	Heavy Duty	Port of Los Angeles	1.6 ± 0.4	0.11±0.01
	2015	Heavy Duty	Cottonwood, CA	3.0 ± 0.2	0.22 ± 0.04
Haugen (2018)	2017	Heavy Duty	Port of Los Angeles	1.7 ± 0.3	0.035 ± 0.01
	2017	Heavy Duty	Cottonwood, CA	2.8 ± 0.4	0.09 ± 0.005
Li (2018)	2014	Light Duty	Pittsburgh, PA		0.035±0.008
	2014	Heavy Duty	Pittsburgh, PA		0.225±0.065

Table 2.1. Summary of emission factors derived by previous studies.

* Note that in Park (2011), no error in emissions factors were reported.

2.6 Supporting Information for Chapter 2

Introduction

In 2.6.1 and 2.6.2, we provide additional details describing the traffic data used in this work. In 2.6.3, we define regional signal in more detail than in the main text and explore the sensitivity of derived emissions factors to the time window used to derive regional signal. In 2.6.4, we compare weekend and weekday truck flow, total flow, PM enhancement, and CO enhancement to demonstrate the sensitivity of PM and CO enhancement at each site to traffic signal. In 2.6.5, we detail the fitting process used to determine enhancement ratio and show fits for each site and time period. In 2.6.6, we show the mean diel cycles of boundary layer height and windspeed used to model enhancement of PM from HDV both near roadways and regionally. In 2.6.7, we show modeled PM from HDV. In 2.6.8, we show data from Laney College, near-highway site with signal interference from a nearby large parking lot and discuss the importance of using isolated sites for this analysis. In 2.6.9, we explore the possible impacts of LDV emissions on our calculations.

2.6.1. Transportation Data

The Caltrans Performance Measurement System consists of a network of in-road sensors (magnetic loop) that detect car and truck flow rate across the state of California. PeMS derives truck portion at a given site using vehicle length estimates (Kwon, 2003). Comparisons of this method with weigh-in-motion technology finds error in this method to be ~5%. (Kwon, 2003) Although network density varies across the state of California, coverage in the San Francisco Bay Area is quite dense, with over 1800 measurement sites along major highways (Figure S1). Total vehicle flow rate and truck percentage were retrieved from (http://pems.dot.ca.gov). For each near-highway BAAQMD site, traffic data was taken from the two closest (primary) PeMS sites (one in either direction). In cases when PeMS data from the closest sites were not available, data was (if possible) filled in with median values for hour of week for the given site and year (excluding 2020), or retrieved from pairs of second closest (secondary) or third closest (tertiary) sites on the same highway. PeMS site codes in Table S1. Example flow rates are shown below in Figure S2.1.

Figure 2.5. Map of Caltrans PeMS loop detector sites in the SF Bay Area from http://pems.dot.ca.gov. Copyright © 2022 State of California.

BAAQMD Site	PeMS – DIR 1 (primary)	PeMS – DIR 2 (primary)	PeMS – DIR 1 (secondary)	PeMS – DIR 2 (secondary)	PeMS – DIR 1 (tertiary)	PeMS – DIR 2 (tertiary)
Laney College (LC)	408138	400835	400609	400980	401710	400682
San Rafael (SR)	403317	403316	403314	403315	402412	402139

Redwood City (RWC)	404572	405673	401875	401874	401873	405679
Berkeley (BM)	400176	400728	400009	400432		
Pleasanton (PL)	402016	401006	400892	402018	402444	407964

Table 2.2. PeMS stations used in this study to capture truck flow near BAAQMD sites.

2.6.2. Example of weekly truck flow and truck percent at sites of interest.

Hourly flow rates and truck percent are found by combining data from paired traffic sensors in each direction of flow. Peak weekday flow rates vary substantially from site to site from ~300 to ~1000 trucks / hr.

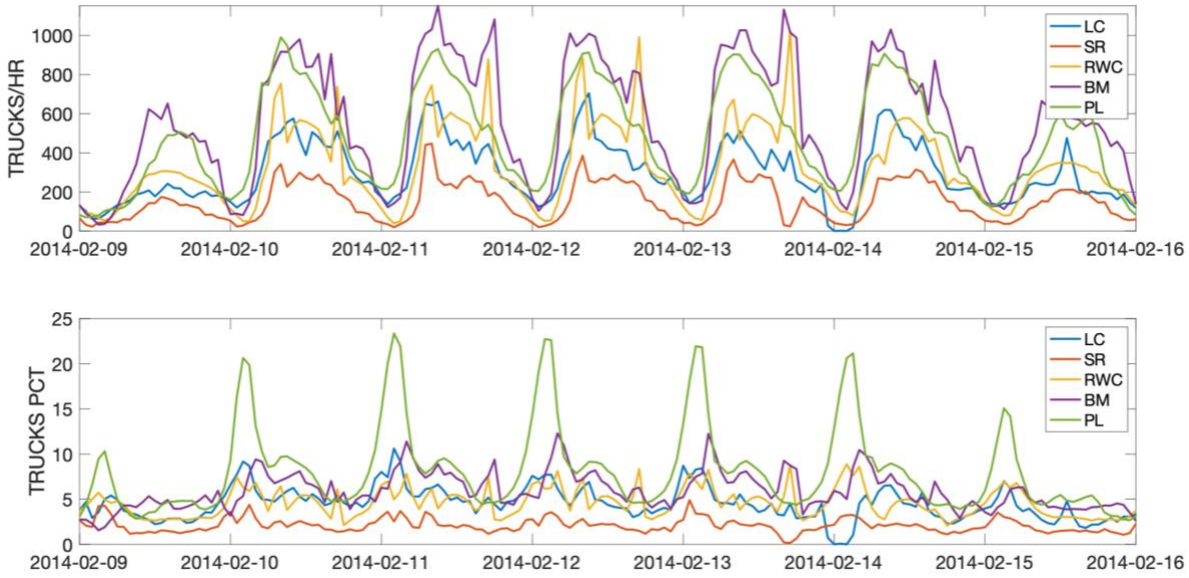

Figure 2.6. Hourly truck flow and truck % for PeMS sites located closes to the near-highway BAAQMD sites below.

2.6.3. Sensitivity of Results to Regional Signal method

We define regional signal of $PM_{2.5}$ as including $PM_{2.5}$ transported to the Bay Area from elsewhere, $PM_{2.5}$ emitted from area point, and line sources far enough away from a site to have mixed through the area, and $PM_{2.5}$ formed in the atmosphere through secondary chemical processes. We make the assumption that by taking the 10^{th} percentile of the signal from all sites, that we are able to approximate this regional signal, as in Shusterman (2018). By subtracting the regional signal from total signal at a given site, we are able to isolate enhancements that result from localized emissions. We furthermore make the assumption that within the nearfield of a highway during morning rush hour, that both $PM_{2.5}$ and CO enhancements are dominated by highway emissions. $PM_{2.5}$ emissions not from the highway should not correlate well with enhancements in CO and are eliminated from our analysis by taking the median value of $PM_{2.5}$ enhancement for each CO bin.

We choose to take a the 10^{th} percentile of a five hour window, based on the size of the region we are trying represent, but we recognize that depending on meteorology, different time windows may be more appropriate. In figure S3, we explore the sensitivity of emissions factors to the time window used to derive regional signal. While we observe some dependence of HDV emissions factors on time window, we note that with the exception of San Rafael in 2009-2011, (1) temporal trends for a given site are unchanged, and (2) the spatial pattern of differences in emissions factors for a given time period are unchanged.

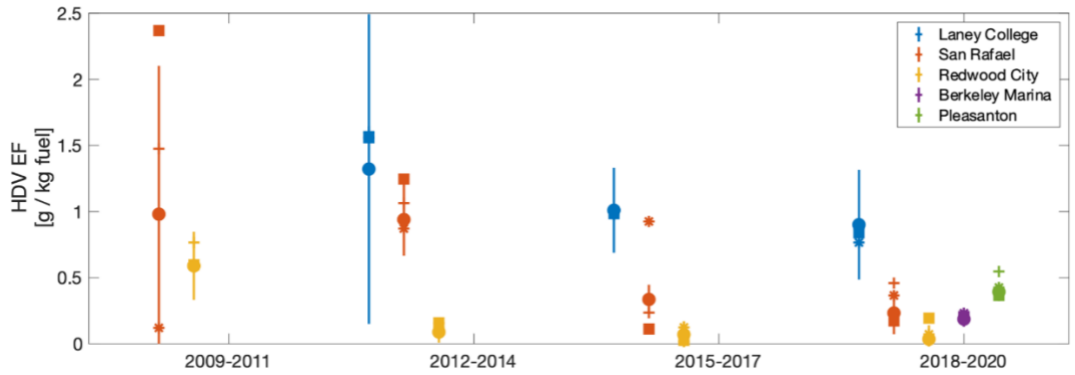

Figure 2.7. HDV emissions factors derived at each site during each time period, as in Figure 4 of the main text. Colors denote BAAQMD site: yellow denotes San Rafael, purple denotes Redwood City, blue denotes Laney College, and red denotes Berkeley. Each symbol represents a different time window used to derive regional signal: plus denotes one hour, square denotes three hours, circle denotes five hours, and the asterisk denotes seven hours. Error bars denote error calculated for 5 hour window.

2.6.4. Dependence of PM and CO enhancement on roadway emissions.

To illustrate the dependence of PM enhancement of HDV traffic and CO enhancement on total traffic, we show differences in truck flow, vehicle flow, PM enhancement, and CO enhancement at 8AM in Redwood City across all time periods in Figure S4. Although there is a large spread in enhancement of both PM and CO, weekend and weekday populations are distinct.

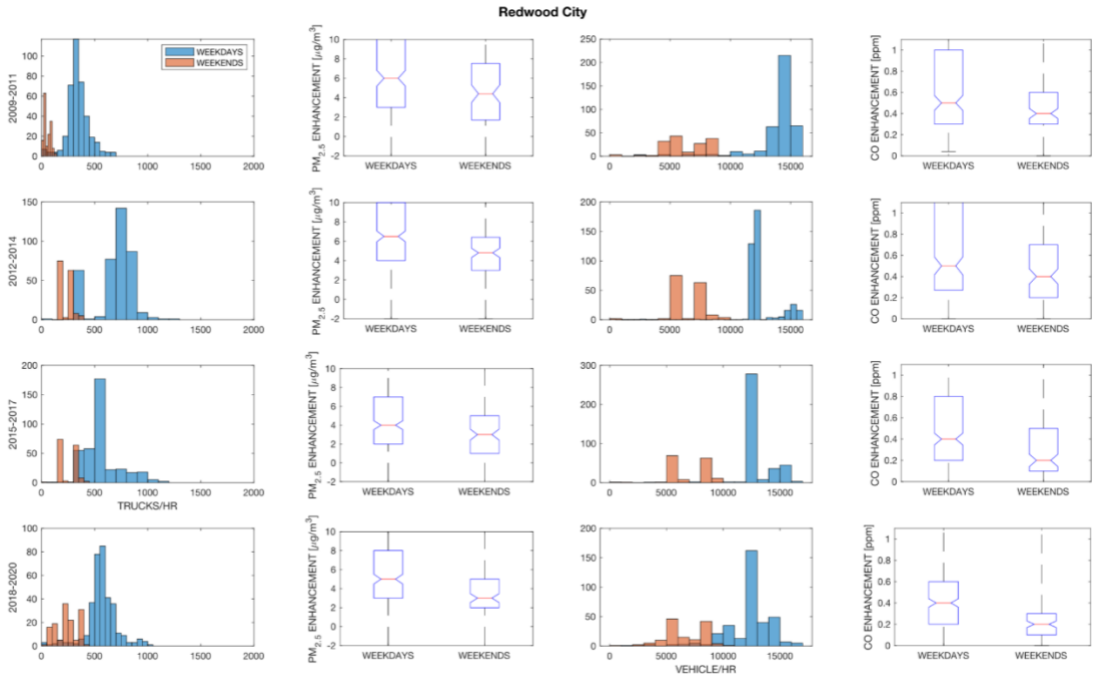

Figure 2.8. Truck and total flow rates, as well as $PM_{2.5}$ and CO enhancements on weekdays and weekends at 8 AM at RWC site during all time periods considered in this study.

2.6.5. Determining Emissions Factors

As described in the main body of the text, we use enhancement in local CO over background as a tracer for $PM_{2.5}$ emitted by HDV on the highway. Although most of the CO comes from LDV, when averaging over the course of an hour, $PM_{2.5}$ emissions from HDV and CO emissions from LDV and HDV can be thought of as originating from the same location and can be thought to have the same, meteorologically dependent dilution from the roadway. Using our knowledge of truck percentage and total flow rate from PeMS and assuming a fleet-wide emissions factor for CO from HDV and LDV, we use enhancement ratios of $PM_{2.5}$ to CO to find HDV emissions factors for $PM_{2.5}$, as described in the main text. Here we detail the process used to find these enhancement ratios.

(1) In figure S5, we show median $PM_{2.5}$ enhancement for every CO enhancement for each time period and truck percentage bin. (We insist on 5 data points to find a median.) These median $PM_{2.5}$ enhancements are fit to a line to find the enhancement ratio.

(2) We use the 95th percent confidence interval values from the fit and to define uncertainty in the slopes.

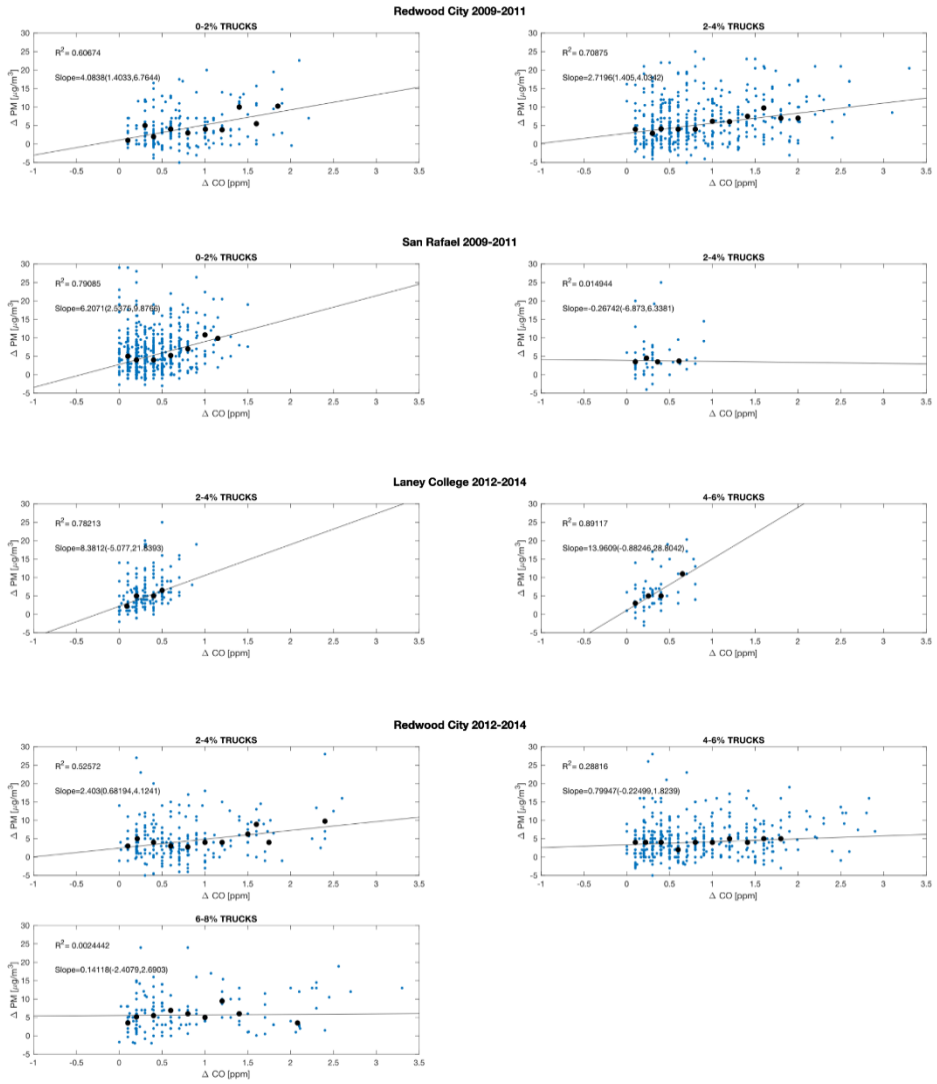

San Rafael 2012-2014

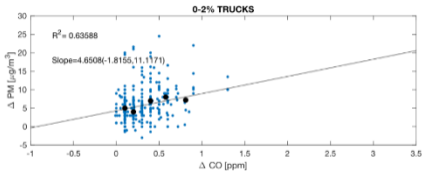

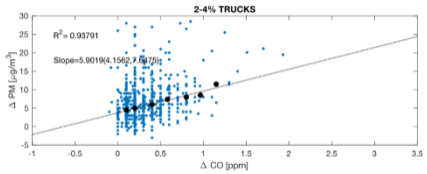

Laney College 2015-2017

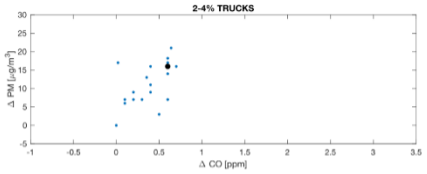

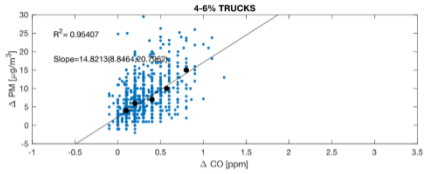

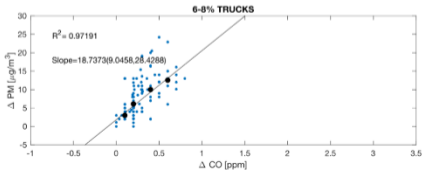

Redwood City 2015-2017

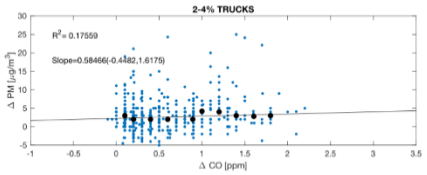

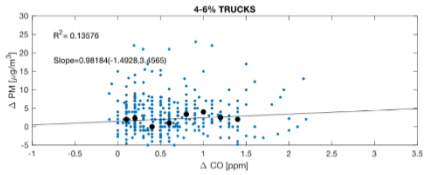

San Rafael 2015-2017

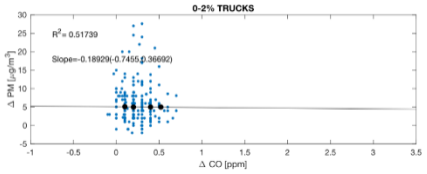

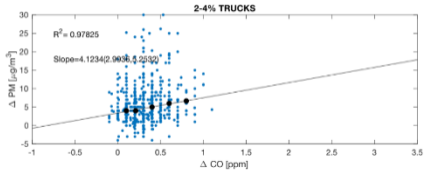

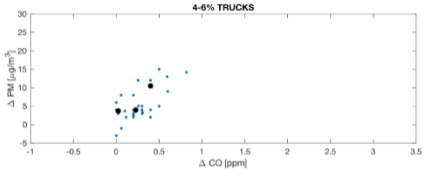

Berkeley Marina 2018-2020

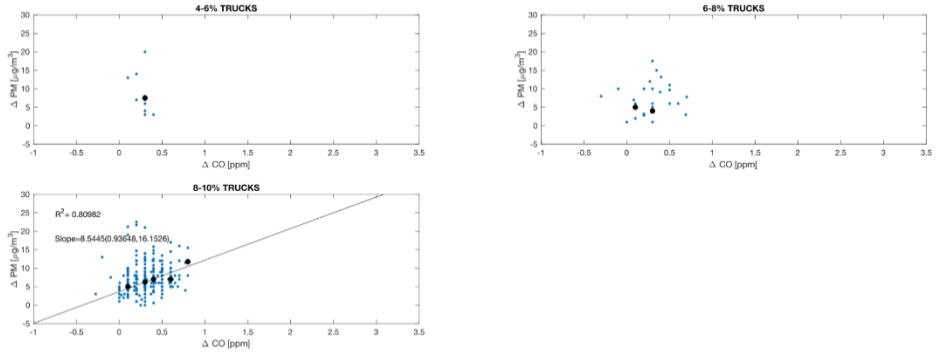

Laney College 2018-2020

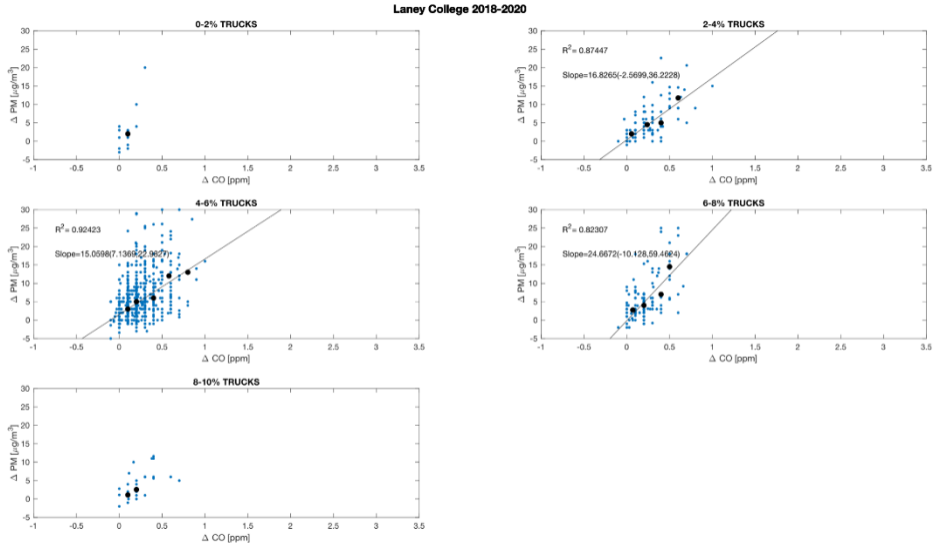

Pleasanton 2018-2020

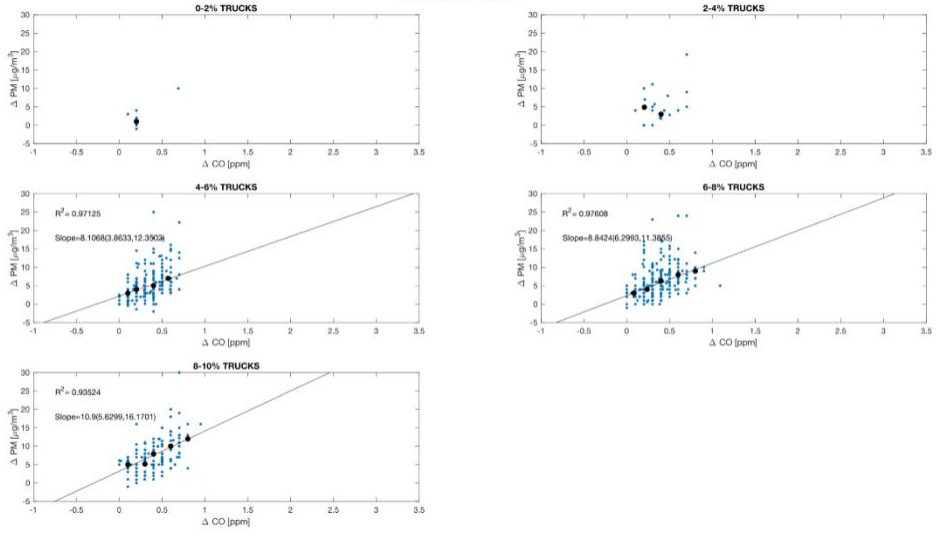

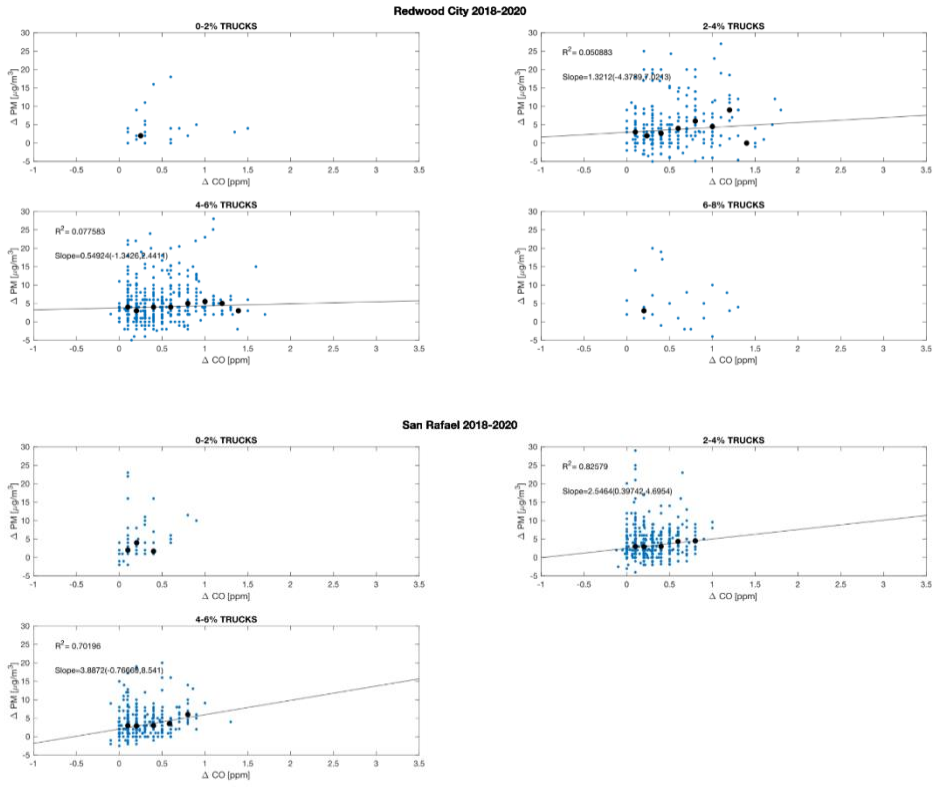

Figure 2.9. Binned PM enhancements and fits to CO enhancement.

2.6.6. Meteorology Used in Modeled PM Enhancement

In the main text, we make estimates of near roadway enhancement, using the continuity equation and gaussian plume dispersion. Here, we show diel cycles of the meteorology used in these calculations. Meteorological variables were taken from ECMWF ERA5.

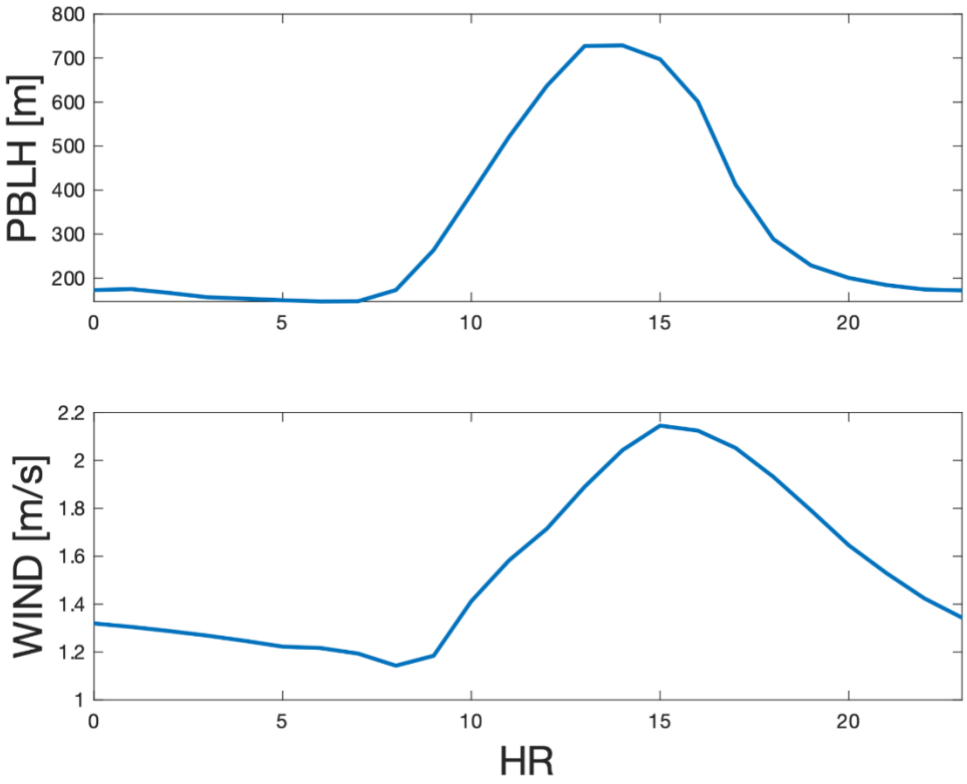

Figure 2.10. Mean diel cycle for total boundary layer height (top) and wind speed (bottom) in Bay Area during winter and spring. Data averaged across 2009-2018.

2.6.7. PM enhancement from HDV

As described in the text, we model PM enhancement from HDV across the region and as a function of distance from the highway.

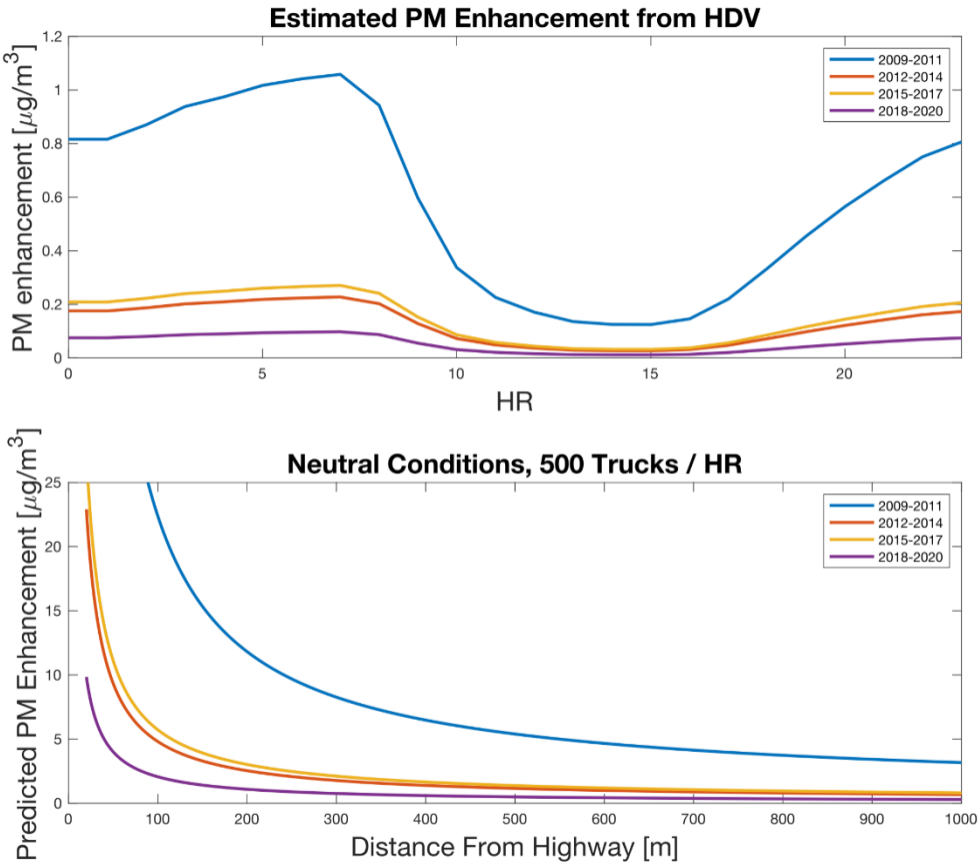

Figure 2.11. Modeled PM enhancement across Bay Area (top) and as a function of distance from a highway (bottom) during neutral conditions.

2.6.8. Laney College Site

Laney College is a near-highway BAAQMD site located in a large parking lot. We calculate much larger $EF_{PM(HDV)}$ than for other sites (FigS8, left). We believe that this is due, at least in part, to emissions from the parking lot. Here, we use EMFAC2017 emissions factors for PM and CO for both LDV and HDV, as well as typical 7 am LDV and HDV flow at that site to predict a PM:CO ratio due to highway traffic alone as well as the ratio that is expected from highway traffic plus 650 cars per hour driving into the parking lot at 5mph (FigS8, right). EMFAC2017 predicts $EF_{PM(LDV)}$ to be much higher at very low speeds, resulting in a substantially enhanced PM:CO ratio, that do not match, but are closer to the values measured at this site. This case highlights the need to screen near-highway sites for interfering emissions and the need to assess the role of slow moving LDV for their contribution to primary PM emissions.

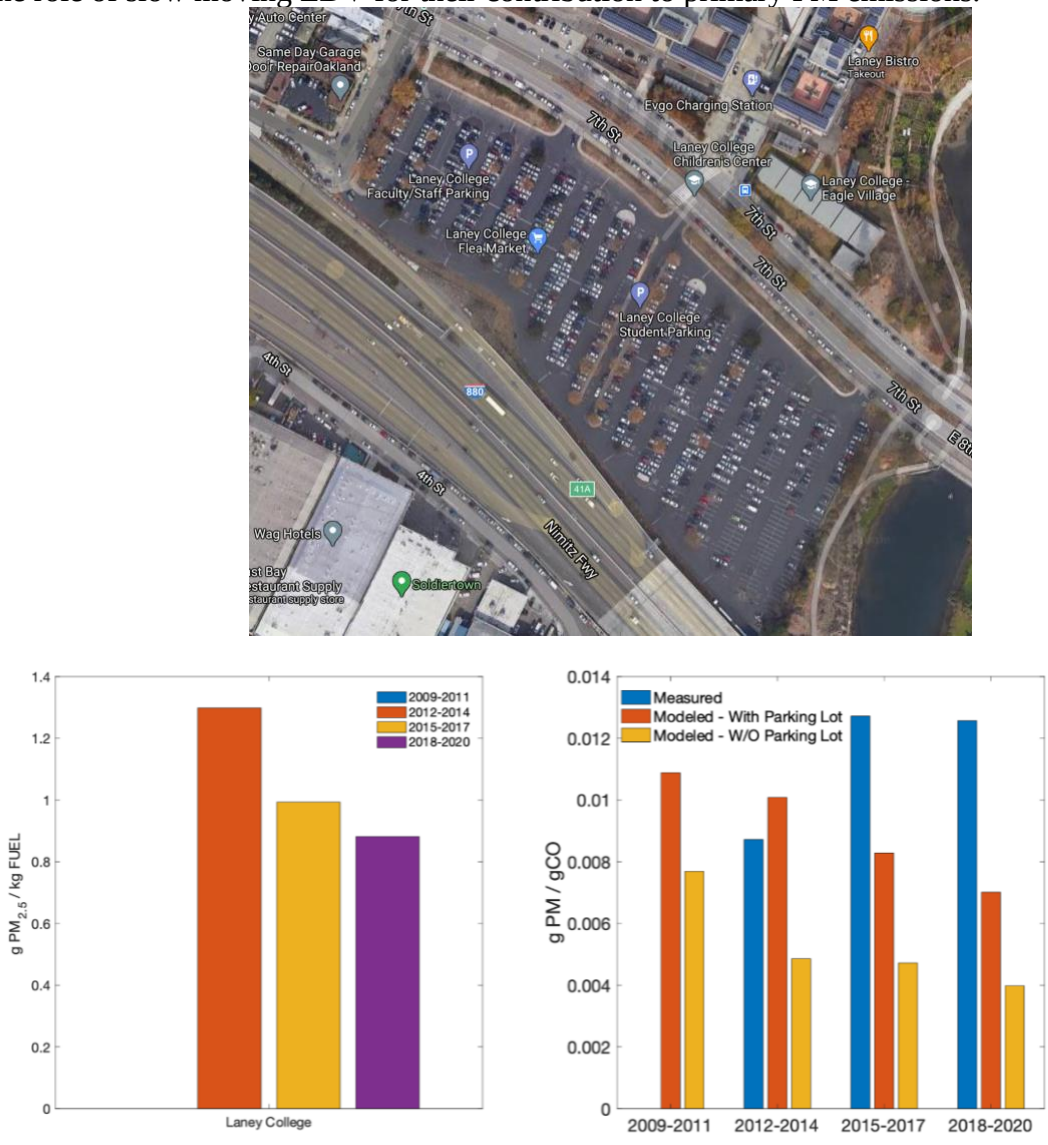

Figure 2.12. (top) Aerial photo of parking lot in which Laney College AQ sensors located. Image retrieved from google maps (© Google Maps 2021). (bottom left) $EF_{PM(HDV)}$ calculated by applying the procedure described in the text at Laney College. (bottom right) PM:CO ratios at

Laney College site that are measured, modeled to include highway emissions only, or modeled to include both highway and parking lot emissions.

2.6.9. Understanding the impact of LDV on emission factor estimates

In the procedure described in the main text, we assume that $EF_{PM(LDV)}$=0 and that all measured PM enhancements are due to HDV. This is a reasonable assumption in the early part of the period considered in our analysis when EF for HDV were measured to be 2-3 orders of magnitude larger than EF for LDV, but it is important to understand the impact of emissions from LDV during later time periods as emissions from HDV have dropped dramatically. We try to characterize $EF_{PM(LDV)}$ in two different ways.

1. We try to find $EF_{PM(LDV)}$, using the intercept of PM:CO ratios for all sites and truck bins during the 2018-2020 time period (Figure S9, right). We find this intercept to be within error of zero: -0.00087 (-0.005,0.004) g PM / g CO.
2. We use the idea that $EF_{PM(HDV)} \geq 0$ to constrain the possible impacts that PM from LDV might have on our results. If we do not assume that $EF_{PM(LDV)}$=0, our equation for calculating $EF_{PM(HDV)}$ becomes

   $$EF_{PM(HDV)} = \gamma \frac{t \cdot EF_{CO,fleet} \frac{fuel\ fleet}{fuel\ HDV} - EF_{PM(LDV)}(1-t)}{t}$$. (Equation S1)

   Applying Equation S1, and requiring $EF_{PM(HDV)} \geq 0$, we find that for highway driving, $EF_{PM(LDV)}$ should be less than 0.002 g PM / kg fuel in the 2018-2020 time period. Using the value of 0.002 for $EF_{PM(LDV)}$, Equation S1 in our analysis does little to change our final results (Figure S9, right).

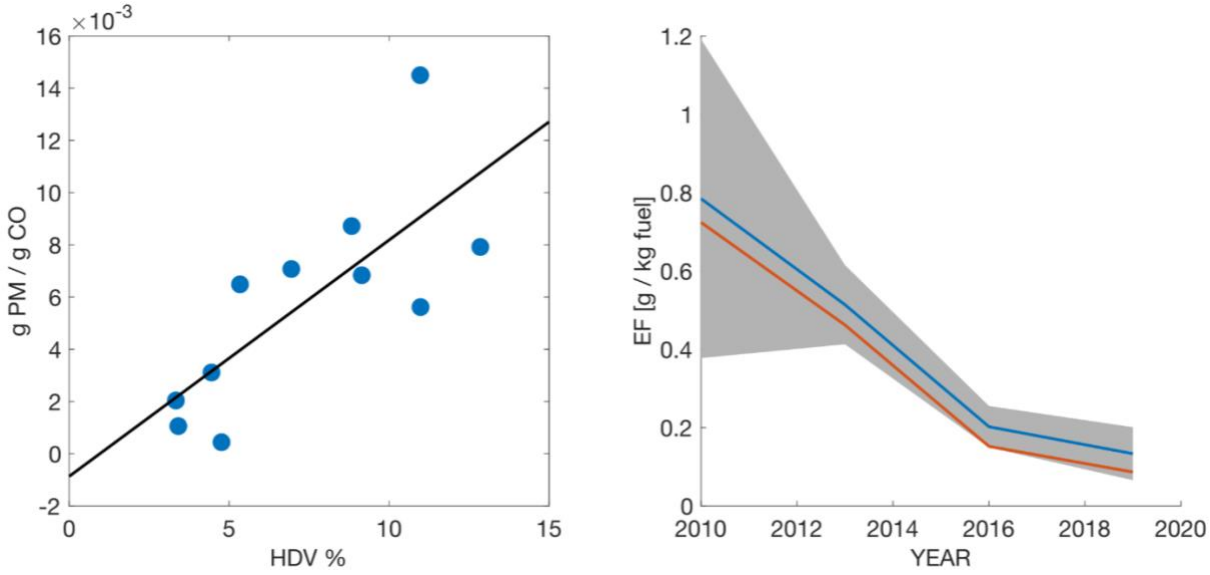

Figure 2.13. (Left) PM:CO ratio calculated from slope from for all HDV % bins and for BM, PL, RWC, SR during the 2018-2020 period. (Right) Trend in $EF_{PM(HDV)}$ for RWC and SR (as shown in Figure 1). The blue line indicates values calculated setting $EF_{PM(LDV)}$=0, while the orange line indicates values calculated using $EF_{PM(LDV)}$= 0.002 g PM / kg fuel.

Chapter 3 Assessing vehicle fuel efficiency using a dense network of CO_2 observations

Adapted from Fitzmaurice, H.L., Turner, A.J., Kim, J., Chan, K., Delaria, E.R., Newman, C., Wooldridge, P. and Cohen, R.C., 2022. Assessing vehicle fuel efficiency using a dense network of CO_2 observations. *Atmospheric Chemistry and Physics*, *22*(6), pp.3891-3900.

Abstract. Transportation represents the largest sector of anthropogenic CO_2 emissions in urban areas in the United States. Timely reductions in urban transportation emissions are critical to reaching climate goals set by international treaties, national policies, and local governments. Transportation emissions also remain one of the largest contributors to both poor air quality (AQ) and to inequities in AQ exposure. As municipal and regional governments create policy targeted at reducing transportation emissions, the ability to evaluate the efficacy of such emission reduction strategies at the spatial and temporal scales of neighborhoods is increasingly important. However, the current state of the art in emissions monitoring does not provide the temporal, sectoral, or spatial resolution necessary to track changes in emissions and provide feedback on the efficacy of such policies at a neighborhood scale. The BErkeley Air Quality and CO_2 Network ($BEACO_2N$) has previously been shown to provide constraints on emissions from the vehicle sector in aggregate over a ~500 km^2 multi-city spatial domain. Here, we focus on a 5 km, high volume, stretch of highway in the SF Bay area. We show that inversion of the $BEACO_2N$ measurements can be used to understand two factors that affect fuel efficiency: vehicle speed and fleet composition. The CO_2 emission rate of the average vehicle (g/vkm) are shown to vary by as much as 27% at different times of a typical weekday because of changes in these two factors. The $BEACO_2N$-derived emissions estimates are consistent to within ~3% of estimates derived from publicly available measures of vehicle type, number, and speed, providing direct observational support for the accuracy of the Emissions FACtor model (EMFAC) of vehicle fuel efficiency.

3.1. Introduction

Urban emissions currently account for ~75 % of all anthropogenic CO_2 emissions (IPCC, 2014). By 2050, roughly two-thirds of the earth's projected population of 9.3 billion is expected to reside within urban areas (IPCC, 2014), meaning that effective greenhouse gas emissions reductions strategies must focus on urban emissions reductions.

The transportation sector is responsible for ~23% of global greenhouse gas emissions worldwide (IPCC, 2014) and represents the greatest sectoral percentage (~25-66%) of emissions from within the boundaries of urban areas in the United States (Daw, 2020; Gurney et al., 2021). Although fuel efficiency of new internal combustion engine vehicles has increased by ~30% over the last 20 years and electric vehicles (EV) are becoming more prevalent (e.g. https://arb.ca.gov/emfac/emissions-inventory), emissions reductions resulting from fuel efficiency gains in newer vehicles are negated by an increasing percentage of heavy-duty vehicles (HDV) (Moua, 2020), speed-related reductions in fuel efficiency resulting from increases in congestion, and an increase of total vehicle kilometers traveled (vkm). Over the past 20 years, even in locations with aggressive climate change policy, these factors have resulted in CO_2 emissions from vehicles that have increased or stayed nearly constant. For example, California Air Resources Board estimates that in the state of California, per capita vehicle emissions in 2015 were only 2% lower than in 2000 and per capita vehicle kilometers traveled

(vkm) increased ~2.5% over that time period (California Air Resources Board, 2018). In addition to GHG emissions, the transportation sector is responsible for a significant share of $PM_{2.5}$ and NO_x emissions, exacerbating $PM_{2.5}$ and ozone exposure in low-income communities and communities of color already experiencing disproportionate health burdens associated with poor air quality (Tessum et al., 2021).

Municipal and regional governments have increasingly shown interest in tracking and reducing CO_2 emissions from all sectors, including transportation. For example, Boswell et al. (2019) found that 64% of Californians live in a city with a climate action plan. For urban and regional governments to plan, monitor, and responsively adjust emissions reduction policies, an up-to-date understanding of the spatial and temporal variations in total emissions and in emissions by sector and subsector processes is key.

For transportation, reductions in vkm, congestion mitigation, and rules affecting fleet composition (e.g., limiting road access to HDV, incentivizing use of electric vehicles, or buy-backs of older vehicles) are three levers that can be employed to reduce CO_2 and AQ emissions from vehicles, thereby affecting the climate footprint, air quality (AQ), and environmental justice (EJ) in a region. However, the current state of the art in emissions monitoring and modelling do not provide the temporal, sectoral, or spatial resolution necessary to track changes in urban emissions and provide feedback on the efficacy of each lever separately. Furthermore, current estimates of the magnitude and sectoral apportionment, of urban CO_2 emissions can vary widely. For example, Gurney et al. (2021) show how a consistent approach to total emissions from cities across the U.S. differs from locally constructed inventories in magnitude and sector by sector.

Spatial and temporal process-level maps of emissions are needed to improve the scientific basis for emission control strategies. The current state of the art involves finding aggregate emissions over large regions (counties, states) using economic data and downscaling those totals using proxies such as road length, building type or population density. These models meet the need for high spatial resolution (~500 m) and capture emissions from many detailed subsectors (Gately et al., 2015; Gurney et al., 2012; McDonald et al., 2014). Because fuel sales are well-characterized, these models are also likely to produce accurate region-wide CO_2 emissions totals from the transportation sector.

Yet even the most detailed of these inventories do not presently describe the temporal variability in processes that affect emissions, such as the direct response of home heating or air conditioning to ambient temperature or, with one exception (Gately et al., 2017b), the variations in emissions per km when comparing free-flowing to stop-and-go traffic. These models often disagree with one another spatially (Gately et al., 2017a), have been subject to only limited testing against observations of the atmosphere, and are not designed to be consistent with separately constructed AQ inventories that have been subject to much more extensive testing against observations.

Mobile monitoring campaigns and high-density measurement networks highlight the importance of characterizing and identifying the processes contributing to sharp neighborhood-scale AQ and GHG hotspots and point to the importance of traffic emissions on neighborhood scales. For example, Apte et al. (2017), showed that concentrations of NO_x and Black Carbon (BC) can vary by as much as a factor of ~8 on the scale of 10s to 100s of meters. Caubel et al. (2019), showed

BC concentrations to be ~2.5 times higher on trucking routes than on neighboring streets. Such gradients are not represented in inventories based on downscaled economic data.

Observations of CO_2 and other greenhouse gases can play an important role in improving and maintaining the accuracy of emission models—especially during a time of rapid proposed changes. CO_2 measurements paired with Bayesian inverse models have been shown to provide a quantitative assessment of emissions (Lauvaux et al., 2016; Lauvaux et al., 2020; Turner, et al., 2020a). To date, most attempts at quantifying urban CO_2 emissions have focused on extracting a temporally averaged (often a full year) total of the anthropogenic CO_2 across the full extent of city. A few studies have attempted to disaggregate emissions by sector or fuel type, or describe large shifts in aggregate emissions (Newman et al., 2016; Nathan et al., 2018; Lauvaux et al., 2020; Turner, et al., 2020a), but none characterize subsector processes of vehicle emissions.

High spatial density observations offer promise as a means to explore process-level emissions details. The BErkeley Air Quality and CO_2 Network ($BEACO_2N$) is an observing network deployed in the San Francisco Bay Area and other cities with measurement spacing of ~2km (Fig. 1, left). In a prior analysis, Turner et al. (2020a) showed that $BEACO_2N$ measurements can detect variation in CO_2 emissions with time of day and day of week in addition to the dramatic changes in CO_2 emissions due to the COVID-related decrease in driving.

Here, we analyze hourly, spatially-allocated CO_2 emissions derived from the inversion of $BEACO_2N$ observations (Turner et al., 2020a) to explore how well they constrain the CO_2 emissions from a 5km stretch of highway. This stretch chosen because of its location upwind of consistently active $BEACO_2N$ sites and for completeness of traffic data, and because emission rates are highly affected by speed (vehicles use more fuel per km at very low and high speeds) and fleet-composition (HDV emit more CO_2 per km than light duty vehicles (LDV)). The variation of the ratio of total fleet CO_2 emission per vehicle km traveled (g CO_2 / vkm) is used to explore variations in on-road fuel efficiency and the factors responsible for that variation. We show that average fuel efficiency of the vehicle fleet on the road varies by as much as 27% over the course of a typical weekday.

3.2 Methods and Data

3.2.1 The Berkeley Air quality and CO_2 Network

We use hourly CO_2 observations from the Berkeley Air quality and CO_2 Network ($BEACO_2N$) (Shusterman et al., 2016; Kim et al., 2018; Delaria et al., 2021). The $BEACO_2N$ network includes more than 70 locations in the SF Bay Area, spaced at ~2 km, and measures CO_2 with a network instrument error of 1.6 ppm or less (Delaria et al., 2021). All available data from January-June 2018-2020 are included in this analysis. During this time, more than 50 distinct locations had nodes that were active for a month or more (including 19 sites within 10 km of our highway stretch of interest). The number of nodes active at any given time ranged from 7-41, with a mean of 17. Figure 1 shows sites in operation at some point during analysis period and Fig. S1 shows a timeseries of the number of nodes available throughout the study period.

3.2.2 The BEACO$_2$N - STILT Inversion System

To infer CO_2 emissions from within the BEACO$_2$N footprint, we use the Stochastic-Time Inverted Lagrangian Transport (STILT) model, coupled with a Bayesian inversion as described in detail in Turner et al. (2020a). Briefly, we use meteorology from NOAA's HRRR product at 3 km resolution to calculate footprints from each hour at each site, weighted by a priori CO_2 emissions. The overall region of influence, the network footprint, as defined by a contour representing 40% of the CO_2 influence is shown in Fig. S2 (left). We construct a spatially gridded prior emissions inventory using point sources provided by the Bay Area Air Quality Management District (2011), home heating emissions as reported by BAAQMD (2011) and distributed spatially according to population density, on-road emissions from the High-resolution Fuel Inventory for Vehicle Emissions (McDonald et al., 2014) varying by hour of week and scaled by year using fuel sales data, and a biogenic inventory derived using Solar Induced Fluorescence (SIF) Satellite data (Turner et al., 2020b).

To ensure a focus on highway emissions, we subtract prior estimates associated with non-highway sources from posterior BEACO$_2$N-STILT fluxes. Non-highway sources are small (~12%) in comparison with highway emissions for the pixels corresponding with the highway stretch analyzed in this study (Fig. 2, left). We assume the error in prior estimates of these sources to be an even smaller fraction of the total. For reference, a diel cycle of sector-specific, weekday prior emissions for the pixels analyzed in this study is shown in Fig. S3.

We estimate the BEACO$_2$N-STILT inversion to be precise to at least 30% for a line source. This estimate is based on the results of Turner et al. (2016) who used Observation System Simulation Experiments to demonstrate that with 7 days of observations at 30 sites a 45 tC/hr line source could be constrained to 15 t C/hr. However, this paper also demonstrated that error in the posterior decreased as results were averaged over a longer period of time. Here we are using 18 months, rather than 7 days of observations, we expect and observe better precision than 30%.

3.2.3. PeMS-EMFAC – derived CO_2 Emissions Estimates

Total hourly vehicle flow, truck (HDV) percent, and speed, were retrieved from http://pems.dot.ca.gov for January – June 2018-2020. There are ~1800 traffic counting stations hosted by the Caltrans Performance Measurement System (PeMS) in the Bay Area, including more than 400 sites (Fig. S2) within the 2020 footprint of the BEACO$_2$N, as described in Turner et al. (2020a). These stations count vehicle flow using magnetic loops imbedded in roadways and estimate HDV fraction using calculated vehicle speed and assumptions about vehicle length (Kwon et al., 2003). For hours during which fewer than 50% of measurements were reported, we fill in total speed and light duty vehicle (LDV) flow gaps by using linear fits to nearest neighbor sites and gaps in HDV flow using hour-of-day- and weekend/weekday-specific median ratios between neighboring sites. We find that using this imputation method, mean absolute errors in speed are 5-10 km h^{-1}, in LDV flow are 500 vehicles h^{-1}, and in HDV flow are 50 vehicles / hour. (See Fig. S4.)

We calculate both LDV and HDV vkm for each highway segment during each hour, using downloaded flow data at each sensor location and segment lengths obtained from the PeMS

database. For highway segments within the BEACO$_2$N footprint, vkm are summed to obtain regional highway HDV and LDV vkm for every hour. Figure S2 (left) shows the extent of the PeMS network in comparison to the BEACO$_2$N-STILT footprint, as well as total HDV vkm and LDV vkm.

Vehicle fuel efficiency is dependent on both fleet composition and vehicle speed. We calculate an emissions rate at each location by combining speed and the HDV percentage with fuel efficiency estimates provided by the California Air Resources Board's Emissions FACtor Model (EMFAC2017). The EMFAC2017 model provides yearly fuel efficiency estimates for the Bay Area for 41 vehicle classes as a function of speed. We group these 41 vehicle types into the categories LDV or HDV. (Table S5) PeMS's vehicle-type classification system is length based, assuming that LDV have a median length of 3.7 m and HDV a median length of 18.3 m (Kwon et al., 2003). As a result, we group most light duty trucks into the LDV category. To find speed-dependent emissions rate values for the LDV and HDV groups, we find a vkm-weighted mean of emissions rates across all vehicle-classes within a group at a given speed

$$er_{speed,group} = \frac{\sum_{i=1}^{n} vkm_{i,speed} er_{i,speed}}{\sum_{i=1}^{n} vkm_{i},speed}, \quad (3.1)$$

where *we* is a vehicle class. From this, we generate LDV and HDV emissions rates at 8.02 km h^{-1} (5 mph) intervals. (See Fig. S6.) EMFAC does not provide data for several LDV vehicle classes at and above 96.8 km h^{-1} (60 mph). To fill in this gap, we estimate emissions rates for the LDV group by using emissions rate to speed slopes (g CO_2 vkm^{-1} km h^{-1}) for high speeds (88-145 km h^{-1}), using data from Davis et al. (2021).

We calculate emissions rates (g CO_2 / vkm) for each (< 1km) road segment between PeMS sensors at a moment in time

$$er(t, seg) = \frac{vkm_{LDV}(t,seg) er_{LDV}(t,seg) + vkm_{tHDV}(t,seg) er_{tHDV}(t,seg)}{vkm_{LDV}(t,seg) + vkm_{HDV}(t,seg)}, \quad (3.2)$$

where emissions rates for cars and trucks are found via spline fit between reported speed for that segment and time with our curves for the emissions rates of each vehicle group. A fit is used rather than an individual bins, because of the sharp gradients that exist at low speeds for LDV. From the emissions rate for each (~1km) segment, we calculate an emissions rate for a stretch of highway including several segments to find total emissions rate (*er*) along a "stretch" over a period of time:

$$er(t, stretch) = \frac{\sum_{all\ segments} \left(vkm_{LDV}(t,s) er_{LDV}(t,s) + vkm_{HDV}(t,seg) er_{HDV}(t,s) \right)}{\sum_{all\ segments} \left(vkm_{LDV}(t,s) + vkm_{HDV}(t,s) \right)}. \quad (3.3)$$

Total CO_2 emissions rates for the highway stretch analyzed in this work are shown in Fig. 2 (right, bottom).

3.3. Results

To gain insight into the relative impacts of congestion and fleet composition, we calculate fleet-wide vehicle emission rates (gCO_2/vkm) using two different methods. For both methods, the Caltrans Performance Measurement System (PeMS) provides vehicle counts, speed and categorizes HDV vs. LDV (http://pems.dot.ca.gov). Using this data and estimates of fuel per km from the EMissions FACtor 2017 (EMFAC) Model, we calculate the CO_2 emissions per km for the average vehicle with hourly time resolution as described above. Second, we use the PeMS data in combination with g CO_2 per unit area derived from the BEACO_2N-STILT inversion system. We focus on the ~5 km stretch of Interstate-80 just north of the San Francisco-Oakland Bay Bridge (Fig. 2). Interstate 80 is an East-West Highway whose orientation in this stretch is mainly North-South, with eastbound lanes traveling north and westbound lanes traveling south. The road has 5 lanes in each direction and is often subject to high congestion (vehicles traveling slower than the posted speed).

PeMS-EMFAC-derived emissions rates give us insight into (1) the expected variation in emissions rates across a typical day (Fig. 2) and (2) the relative impacts of congestion vs. HDV percentage as factors leading to this variation (Fig. S7). For example, while the west-bound segment experiences speeds significantly below free-flow during both morning and evening rush hours, the east-bound segment experiences significant congestion only during the evening. Because of a steep gradient in LDV emission rates between 20 and 50 km h^{-1} (Fig. S6), the west-bound congestion in this segment occurs at speeds that are more fuel efficient than free-flow. The overall variance in emissions rates over the whole stretch is significantly smaller than in either of the directions shown individually.

From PeMS-EMFAC-derived emissions factors, we predict a median diel cycle with emissions per km travelled ranging from ~247 to ~314 g CO_2 / vkm. For reference, if all vehicles were driving at the speed limit of 104.6 km h^{-1} (65 mph) and the fleet mix was 6% HDV and 94% LDV, we calculate an emission rate of 265 g CO_2 / vkm. The range of predicted emissions are narrower on the weekend (238 to 276 g CO_2 / vkm), both because fewer HDV use the road and because there is a smaller range in speed.

Figure S7 shows the hourly variation in the relative contributions of LDV speed, HDV percentage, and HDV speed to the deviation in g CO_2 / vkm from the reference value of 265 g CO_2 / vkm. The solid line is the mean and the shaded envelope represents the day-to-day variance. In the morning and mid-day, HDV percentage and LDV speed have opposite impacts on g CO_2 / vkm, leading to small variations in g CO_2 / vkm over the day, despite substantial variations in the separate effects of speed and HDV %. During evening rush hour, low vehicle speeds result in higher emission rates, leading to large positive deviations. High day-to-day variance in vehicle speed contributes to high day-to-day variance in emission rates. At times near midnight, large, positive deviations are observed, mostly as a consequence of high HDV percentage, but also because traffic flows at rates higher than 104.6 kph, leading to higher emission rates. Night-to-night variance in HDV percentage is low, thus variance in nighttime predicted g CO_2 / vkm is small. HDV speed has little impact on g CO_2 / vkm.

We use CO_2 measurements from 50 BEACO_2N sites across the Bay Area, combined with the BEACO_2N-STILT inversion system to assess highway emissions from our stretch of interest. In

Fig. 1, we show the location of BEACO$_2$N sites, the stretch of interest, and emissions estimates for this stretch. Note that the posterior emissions move substantially from prior emissions towards what is estimated from PeMS-EMFAC, particularly during evening rush hour, when the prior overestimates emissions by ~20%.

We compare BEACO$_2$N-derived and PeMS-EMFAC-derived emissions rates (CO$_2$ / vkm) and find remarkable agreement. The PeMS-EMFAC-derived emissions rates range from 225-300 g CO$_2$ / vkm and include effects of both fleet composition and variation in speed. For BEACO$_2$N, we use the total CO$_2$ emissions from the inversion at times corresponding to narrow bins of PeMS-EMFAC g CO$_2$ / vkm. Figure 3 (left) shows an example of data selected at times with with PeMS-EMFAC-derived fuel efficiency in the range 271.4-279 g CO$_2$ / vkm. There is a range of emissions at each vkm because of noise in the inversion, variation in speed and variation in fleet composition. The slope of a fit to the data in Fig. 3 (left) is an estimate of the emissions rate *(equation 4)*, where *CO$_2$ emissions* is defined as hourly emissions summed over BEACO$_2$N pixels corresponding to our highway stretch of interest (Fig. 2)

$$er(\ g\ CO_2/vkm) = \frac{CO_2\ emissons}{vkm}.\ \text{(Eq. 3.4)}$$

Using 18 months of data for weekdays between 4 am and 10 pm, we compare PeMS-EMFAC-derived and BEACO$_2$N-derived CO$_2$ / vkm (Fig. 3, right). These hours were chosen, because they represent the hours for which we expect traffic emissions to be substantially larger than emissions from other sources in our area of interest (See Fig. S3). Fitting to a line forced through the origin, emissions rates found via the BEACO$_2$N inversion are within 3% (0.97 +/- 0.01) of those predicted using PeMS-EMFAC traffic counts. A more complete description of this fitting and error calculation process can be found in Text S8 and a comparison to results from applying this method to the prior can be found in S9. Using the definition of limit of detection as three times our uncertainty, we calculate that we would be able to detect an 11% change in individual points (representing bins of fuel efficiency from a combination of HDV percent and speed) and a 3% change in the slope. Because 18 months of data was required to reach this level of certainty, if we assume the 2.3-3.8% per year decrease in emission rate found by Kim, et al. 2021, we should be able to detect a change in overall fuel efficiency with three full years of BEACO$_2$N-STILT output.

We also consider how emissions rates compare throughout the day (Fig. 4, top). During the evening, PeMS-EMFAC-derived and BEACO$_2$N-derived emission rates are in good agreement. The BEACO$_2$N g CO$_2$/vkm increases from 256 g CO$_2$ / vkm before rush hour (2 pm) to 324 g CO$_2$/ vkm during peak rush hour (5 pm). Likewise, the PeMS-EMFAC-derived CO$_2$/vkm increases from 256 CO$_2$ / vkm to 320 CO$_2$ / vkm over the same time period. The BEACO$_2$N prior has a slightly larger increase in emission rate over this period (256 g CO$_2$/vkm at 2PM to 361 g CO$_2$/vkm at 5PM). In contrast, during the morning rush hours, we see less agreement between PeMS-EMFAC-derived and BEACO$_2$N-derived emission rate estimates. The BEACO$_2$N inversion is similar to the PeMS-EMFAC estimate at 5 am local time (280 g CO$_2$ / vkm) and then the BEACO2N estimate increases over the morning rush hour to 330 g CO$_2$ / vkm at 8 am. This behavior is different than either the BEACO$_2$N prior (175 at 5 am and 275 at 8 am) or the PeMS-EMFAC calculation which decreases over this period (275 at 5 am and 250 at 8 am).

The discrepancy in the morning between emissions derived from PeMS-EMFAC and BEACO$_2$N can potentially be reconciled by congestion. There is a non-linear relationship between vehicle speed and the rate of emissions. As such, congestion involving non-constant speeds can result in higher emissions than would be estimated using the average vehicle speed. This can be seen from a simple example. Consider two cases: 1) a LDV travelling at a constant 50 km h^{-1} for one hour and 2) a LDV traveling at 100 km h^{-1} for 20 minutes and 25 km h^{-1} for 40 minutes. Both vehicles travel 50 km in one hour and therefore have the same average speed. However, the emissions rate is 461.5 g CO_2/vkm at 25 km h^{-1}, 195 g CO_2/vkm at 50 km h^{-1}, and 221 g CO_2/vkm at 100 km h^{-1}. Using these emission rates, the vehicle in the first case would emit 9.75 kg CO_2 whereas the vehicle with the variable speed in the second case would emit 15 kg CO_2.

Contrasting the speeds (Fig. 4 bottom, right) during these two periods, we see that while both show a bi-modal speed distribution, a greater fraction of morning speeds fall into the 40-100 kph range, whereas a greater fraction of evening speeds are < 40 km h^{-1} or > 100 km h^{-1}. We show in Fig. S10, emission rate estimates based on hourly averaged speeds between 0-40 km h^{-1} and 100-140 km h^{-1} (more common in evening rush hour) are likely an upper bound on possible emission rates corresponding to those hourly averaged speeds, whereas emission rate estimates based on hourly averaged speeds between 40-100 km h^{-1} (more common in morning rush hour) likely represent a lower bound of emissions. The predicted range in emission rate resulting from non-constant speeds, combined with a larger HDV % in the morning (Fig. 4 bottom, right), is large enough to explain the mismatch observed during morning rush hour.

3.4. Discussion

Strategic reduction of emissions from transportation is important to both reducing total GHG emissions and improving AQ. To make informed decisions that reduce GHGs and exposure to poor AQ, policy makers need to know (1) how much is being emitted, (2) location and timing of emissions, and (3) the relative impact of various sub-sector processes (vkm, fleet composition, congestion).

To effectively capture emissions from sub-sector processes, models are also reliant on emissions factor models, such as the EMFAC2017 emissions model used in this paper. While our BEACO$_2$N-STILT based estimates largely agree with the EMFAC2017 emissions model for CO_2, tracking on-road changes in emission factors will be especially important as the impacts of congestion and fleet composition evolve rapidly, making timely updates essential to creating spatially accurate inventories. For example, the EMFAC model predicts an 18% decrease in overall CO_2 emission rates by 2030, resulting from the improved fuel efficiency of combustion engine vehicles and a transition to hybrid and EV (~6.8% of LDV vkm and ~6% of HDV vkm are expected to be traveled by EV by 2030). While the increased share of hybrid and EV should work to decrease the impact of congestion, a projected increase in total congestion and congested-vkm share by HDV (Texas A&M Transportation Institute, 2019) is likely to work against that trend, making the overall result difficult to predict.

To our knowledge, this paper represents the first demonstration that a high-density atmospheric observing network can both diagnose and quantify relative contributions of sub-sector processes at the neighborhood scale. We demonstrate that the BEACO$_2$N network (~2 km spacing) of low-

cost CO_2 sensors, can be used to quantify emission rates at a specific location (~5 km stretch) and by time of day. We show that on the highway stretch, activity-based emissions estimates that account for speed and HDV % match the inference from atmospheric measurements to within 3%. Finally, we demonstrate that the BEACO$_2$N-STILT system detects daily changes in fuel efficiency that range from 200-300 g CO_2 / vkm and this system would be capable of detecting fleet-wide changes in fuel efficiency in ~3 years.

3.5 Outlook

In this work, we have demonstrated that the BEACO$_2$N-STILT system was able to infer emission rates from vehicles along a specific stretch of highway. To understand the extent to which this method can be applied to other contexts, future work should investigate the extent to which various elements of the BEACO$_2$N-STILT system, including measurement density, error in meteorology used to calculate STILT trajectories, and the quality of the prior, impact the ability of similar systems to estimate emissions.

For example, it is possible that the mismatch we observe during the morning rush hour may be due to a larger relative meteorological model error during the morning as compared to the afternoon and early evening in which the boundary layer is relatively well mixed. Because a highly mixed boundary layer is important for minimizing discrepancies between particle trajectories in the STILT model and real transport (Lin et al., 2003), inversions typically use only measurements taken during the afternoon, (Lauvaux et al., 2016; Nathan et al., 2019; Lauvaux et al., 2020) when the boundary layer is relatively well mixed. However, as discussed by Martin et al. (2019), the impacts of meteorological mismatch during the morning may be offset by stronger signal, and future work should explore the extent to which averaging results over long time periods or strategic filtering of meteorological mismatches can combat emissions error.

Beyond further exploration of the elements influencing the sensitivity and precision of the BEACO$_2$N-STILT system, because each BEACO$_2$N node measures CO, NO_x, and $PM_{2.5}$ in addition to CO_2 (Kim et al., 2018), the method presented in this paper has the potential to shed light subsector processes impacting emission factors of these co-emitted species. This is salient because plume-based emission factor measurements of co-emitted pollutants show various emissions factor models systematically underestimate emissions (Bishop, 2021), fail to capture spatial heterogeneity in these factors due to fleet composition (age and compliance with control technologies) for PM (Haugen et al., 2018; Park, et al., 2016) and Black Carbon (Preble et al., 2018), or fail to capture the impact of temperature on emissions factors.

Applying these methods across a broader spatial area and to other species ($PM_{2.5}$, NO_x, CO) should yield information of interest to both scientists and policy makers by:

1. Revealing spatial and temporal trends in emission rates and emission factors across an urban area and quantifying the contributions of congestion, fleet composition, or other factors to spatial variations.
2. Identifying and diagnosing the causes of traffic-related AQ hotspots that contribute to exposure inequities.
3. Tracking trends in the above over periods of years to decades.

Figures and Tables

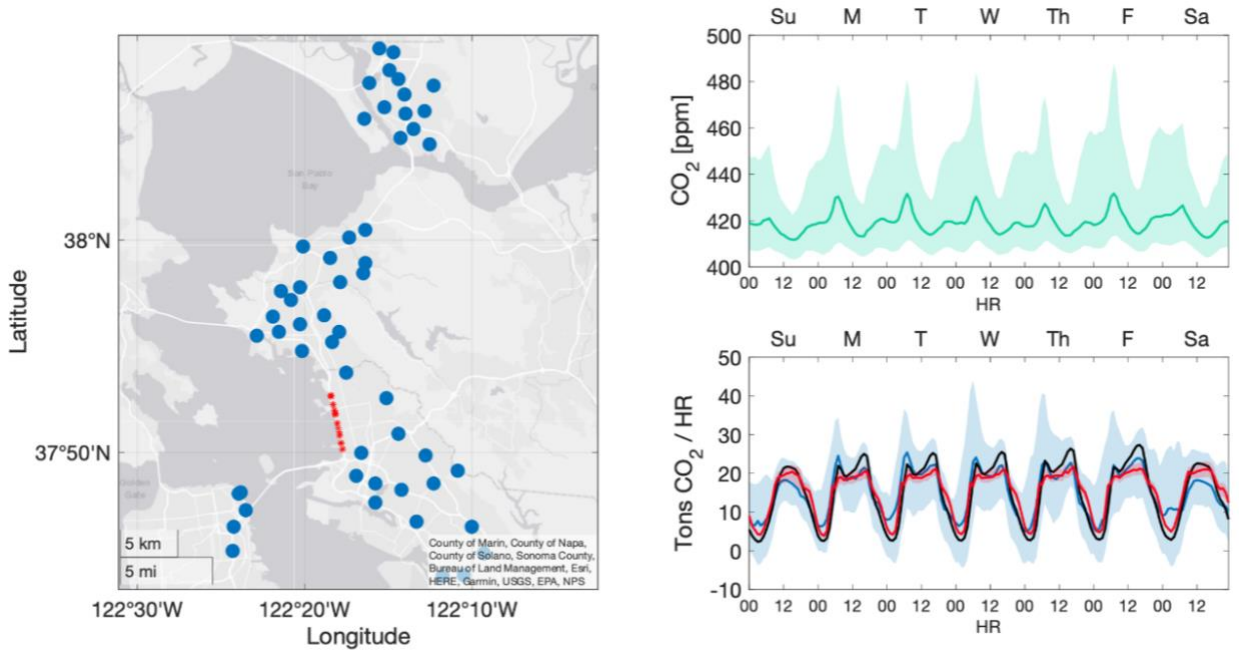

Figure 3.1. Left: Map of the BEACO$_2$N Network shows all sites (blue dots) for which there are more than 4 weeks of data during the period analyzed (Jan-June 2018-2020). Red stars indicate location of PeMS monitors used in this study. Right (top): CO_2 values shown for a 'typical week' during time period observed. Dark line represents the median value observed across all sites and times. Shaded envelope represents 1 sigma variance across the network and over the 2 year period. Right (bottom): CO_2 emissions on all highway pixels in the domain as derived from the inversion of BEACO$_2$N observations (blue), BEACO2N prior (black), and PeMS-EMFAC-based estimate (red). Shaded envelope shows variance in emissions during the 18-month analysis window.

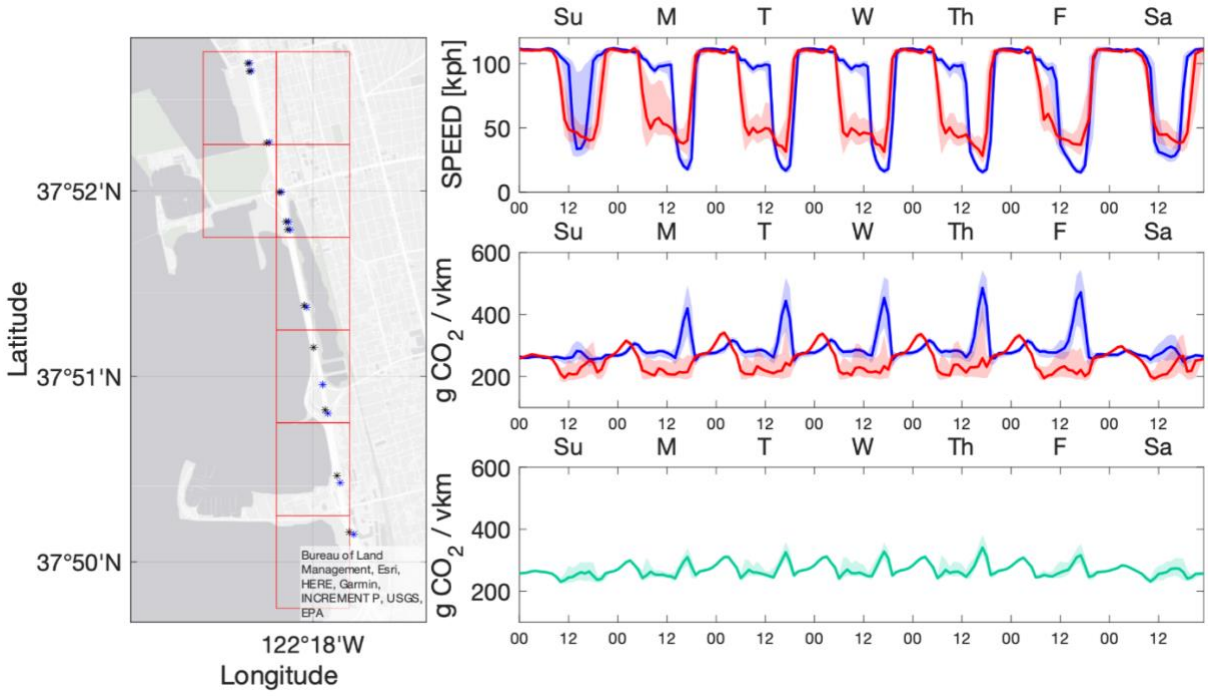

Figure 3.2. Left: ~5km stretch over which we analyze g CO_2/ *vkm*. Points show the location of PeMS stations. Squares show pixels associated with BEACO$_2$N STILT output which we use for comparison for 5km stretch. Right (top): Hourly average speed shown for two opposite (West in red, East in blue) PeMS measurement stations for a typical week. Right (middle): PeMS-EMFAC-derived emissions rates calculated for two opposite (West in red, East in blue) PeMS measurement stations for a typical week. Right (bottom): Aggregate PeMS-EMFAC-derived estimated emissions rates from the two directions of traffic for a typical week for this highway stretch.

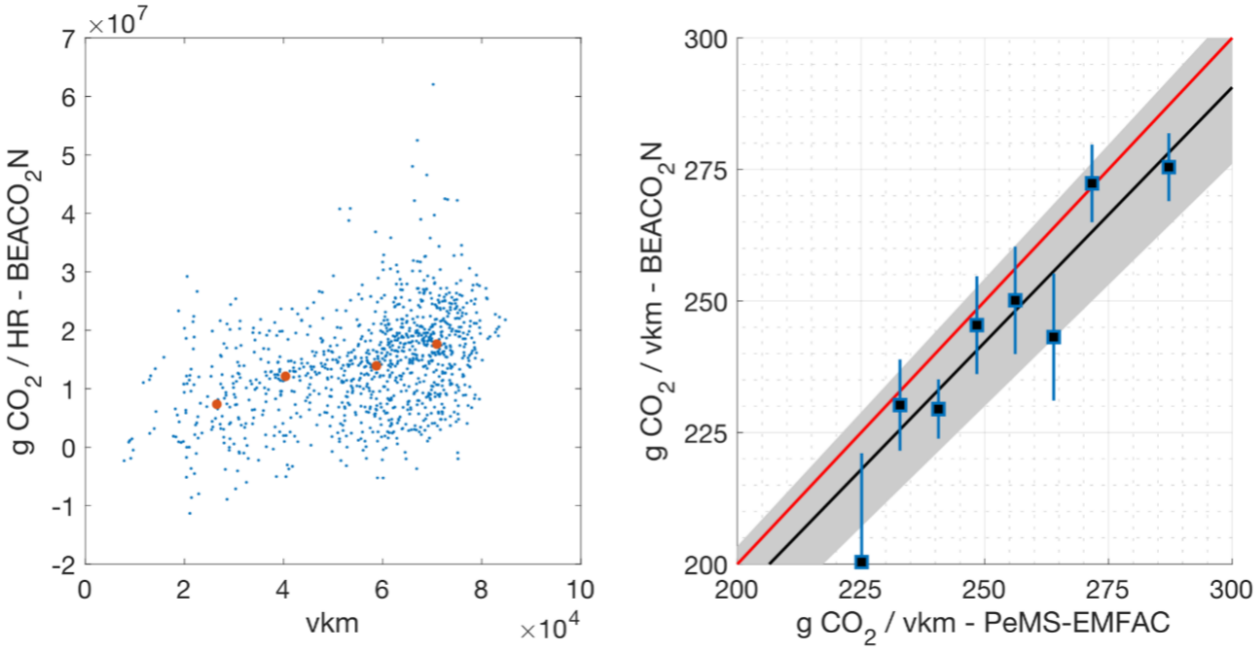

Figure 3.3. Left: $BEACO_2N$-derived emissions vs. vkm for times corresponding to modeled emission rates of 271.4-279 g CO_2/ vkm. Red points represent binned medians used in fitting. **Right:** $BEACO_2N$-derived vs. PeMS-EMFAC derived emissions rates with uncertainty estimate. Black line shows fit weighted by variance: y = 0.97(.01)x . Grey envelope is 5% deviation from fit. Red line represents 1:1 line.

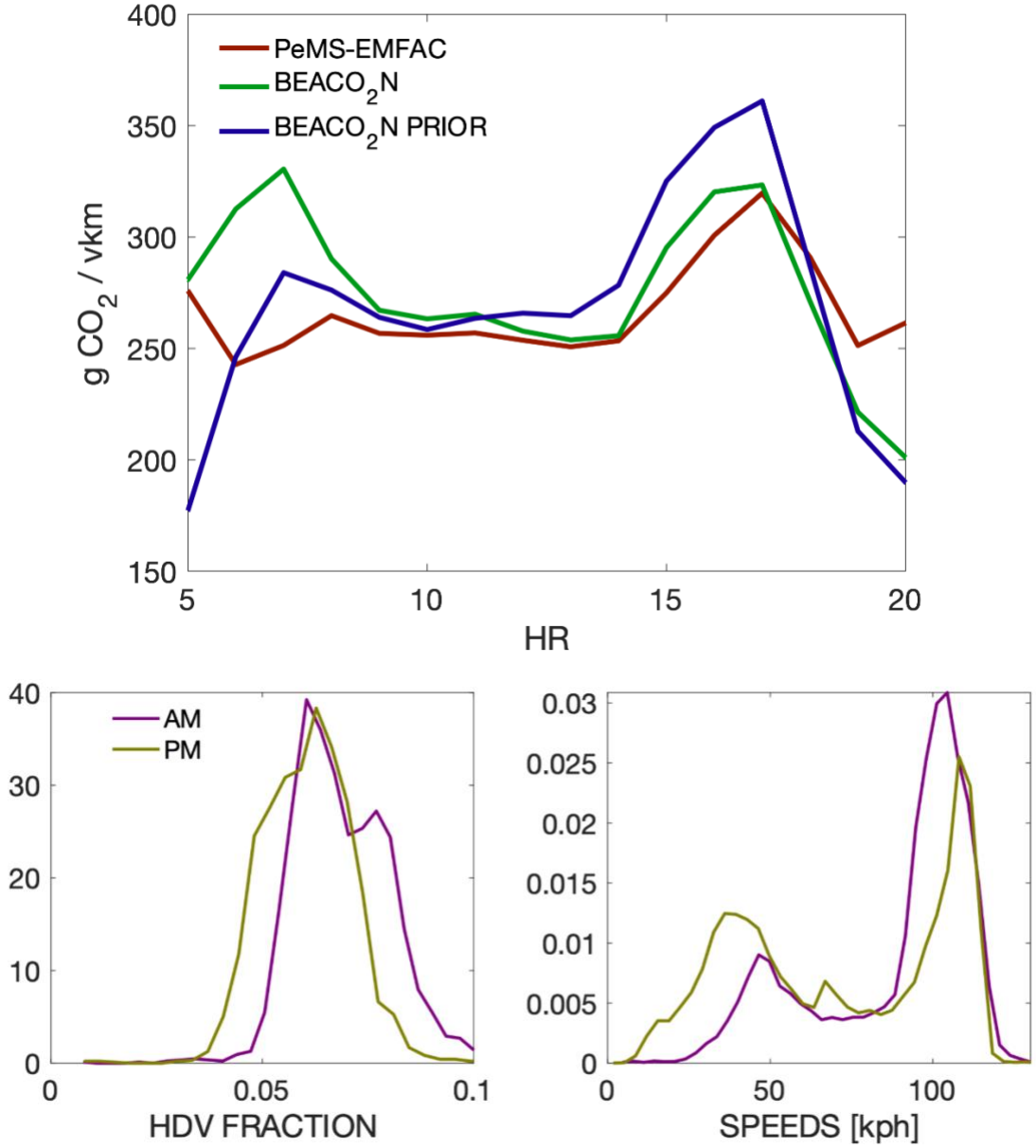

Figure 3.4. Top: Emissions rates by time of day on weekdays for PeMS-derived (red), BEACO2N-prior (blue), and BEACO$_2$N posterior (green). **Bottom:** Probability density functions of truck fraction (left) and speed (right) from weekday morning (5-9 am) and evening (4-8 pm) rush hour period on the segment of I-80 analyzed in the Results section. Y-axis represents the relative probability of HDV fraction (left) or averaged hourly speed (right). Speeds are from individual PeMS sensors, while truck fraction is aggregated over the whole stretch under consideration (both directions).

3.7. Supplemental Information to Chapter 3

Introduction

In 3.7.1, we describe the time series of the number of BEACO$_2$N nodes reporting CO$_2$ during the from January through June for the years 2018-2020. In 3.7.2, we show the locations in the PeMS measurement network in the region of the SF Bay Area shown on the map, as well as an estimate of LDV and HDV VMT for a typical week in this domain. In 3.7.3, we describe the hourly BEACO$_2$N-STILT prior for the typical weekday for CO$_2$ emissions in the 1km pixels that encompass the highway stretch that is the focus of our analysis. The figure also shows vkm traveled for each hour on this stretch of highway. In 3.7.4, error analysis for PeMS values for speed, LDV and HDV volume is described. In 3.7.5, we list EMFAC2017 vehicle classes and indicate whether we have classified them as LDV or HDV based on estimated vehicle length. In 3.7.6, we show both LDV and HDV emissions rates as a function of speed. We also compare a piece-wise linear to a spline fit of these two curves. In 3.7.7, we show the diel cycle for contribution to total emissions by congestion and vehicle type as estimated using PeMS-EMFAC. In 3.7.8, we describe the calculation of uncertainty in emissions rates derived using the BEACO$_2$N-STILT system. In 3.7.9, we derive emission rates from the BEACO$_2$N-STILT prior and discuss improvements of the posterior over the prior. In 3.7.10, we explore how non-constant speed may impact emissions rates for a given hourly average speed.

3.7.1. Site Availability

Throughout the period examined in this study, the number of BEACO$_2$N sensors reporting data varied from due to power or instrument failure.

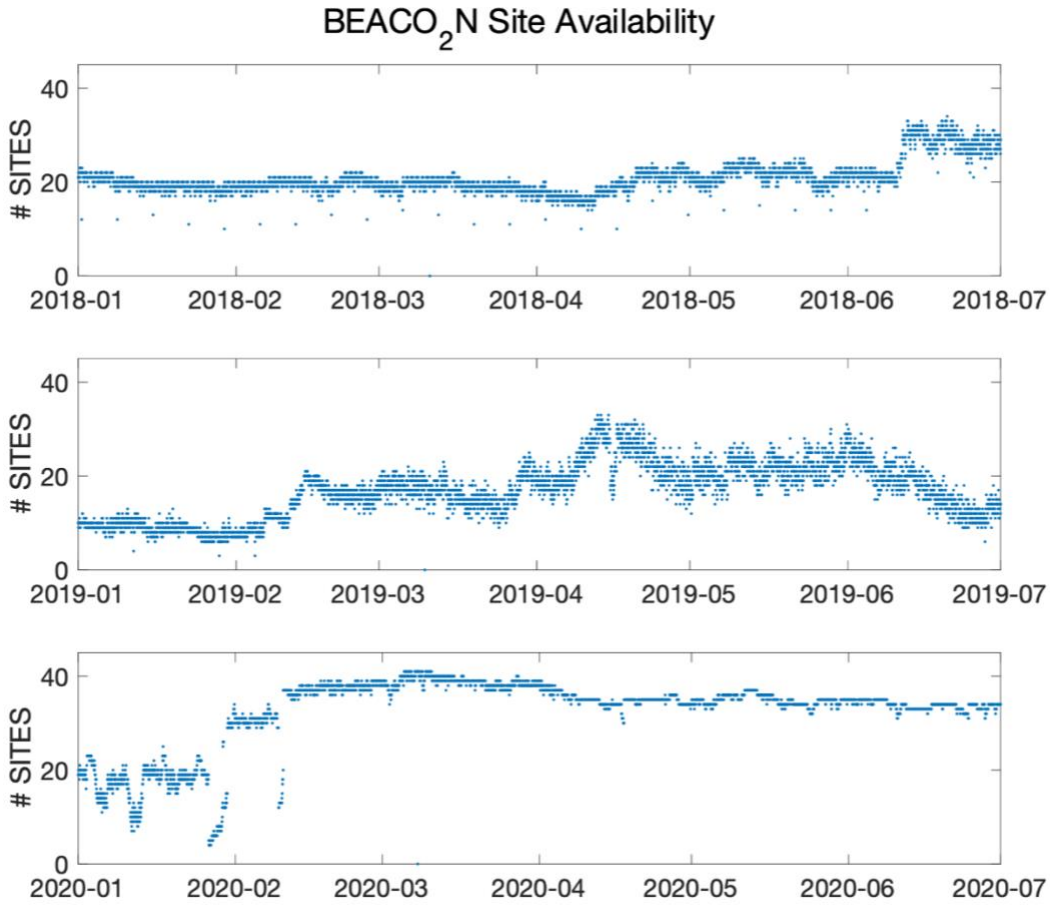

Figure 3.5. Number of BEACO$_2$N sites reporting CO_2 data used in BEACO$_2$N-STILT inversion for January-June in 2018 (top) 2019 (middle) and 2020 (bottom).

3.7.2 – PeMS Emissions Estimates

The Caltrans Performance Measurement System Network consists of thousands of magnetic loop monitors imbedded in highways across the state of California (http://pems.dot.ca.gov). Each station consists of loop sensors in each lane that report hourly values for total vehicle flow, HDV percentage, and average speed. Using station locations, vehicle flow, and HDV percentage, hourly vkm can be calculated as outlined in the main text.

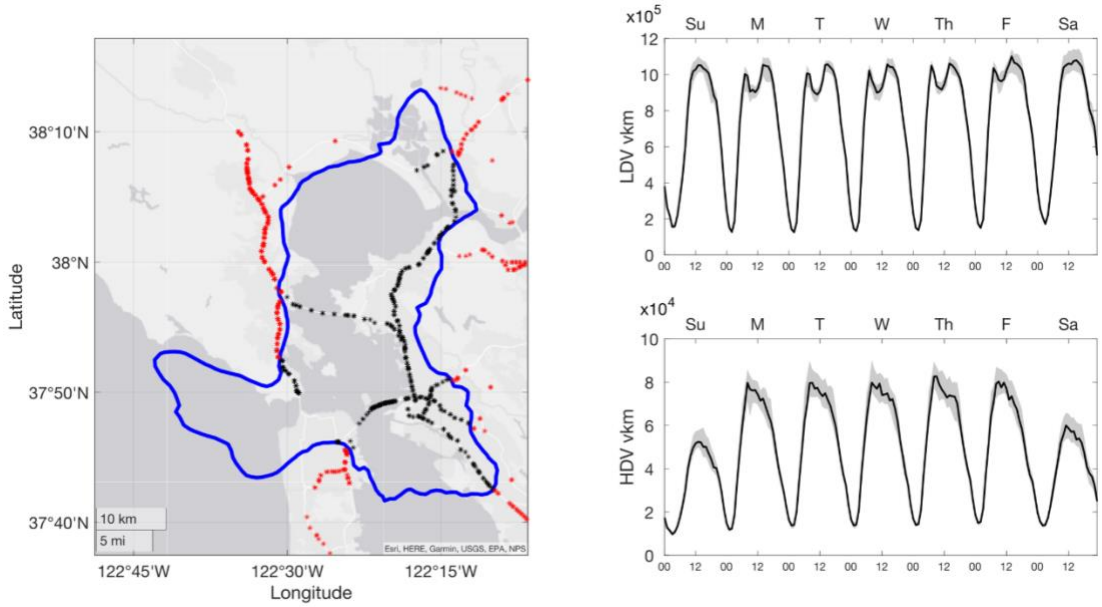

Figure 3.6. Left: Locations of Caltrans PeMS monitoring stations (black and red). The solid blue line marks the 40% contour of the $BEACO_2N$ cumulative influence function during January – June 2020. **Right:** LDV vkm, HDV vkm estimated based on PeMS data.

3.7.3. Daily Cycles of Traffic and Prior Emissions Estimates

We focus our analysis on the hours 4am – 10pm. During this period, emissions from traffic are much larger than all other sources in the pixels used in this analysis. From 11pm – 3am, total vkm and therefore emissions from traffic are low.

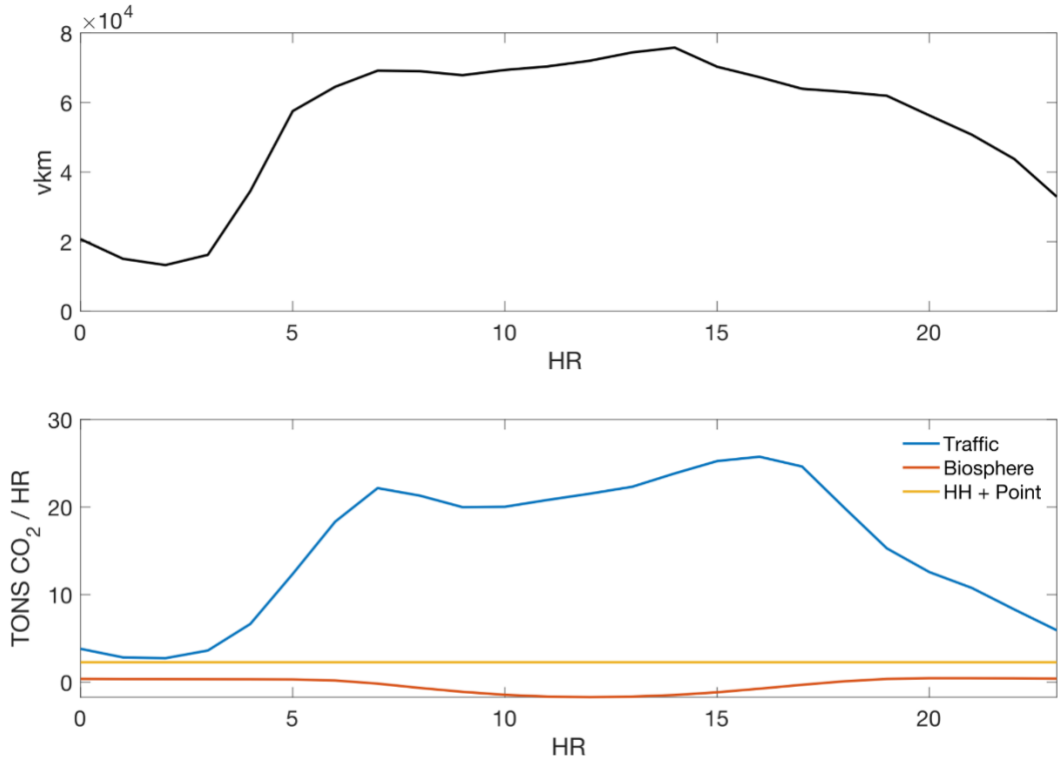

Figure 3.7. Top: Diel variation of total vkm (from PEMS observations) for the stretch of roadway indicated in Figure 2 for a typical weekday. **Bottom:** Prior estimates of emissions from biogenic sources (orange), vehicle emissions (blue), point sources and area sources (yellow).

3.7.4. Imputation of Traffic Data

We apply linear fits (for speed and LDV) and hourly ratios (for HDV) to nearest neighbors, second nearest neighbors, and third nearest neighbors to create modeled values for all times for which we have observations. Using these modeled values we estimate mean error and spread for all PeMS sites over the time period studied, finding that speed accurate to about 5km hr^{-1}, LDV/hr to ~300 vehicles and HDV to ~55 vehicles for the east and west directions of flow on I-80. Precision is much higher than these values as shown on the right.

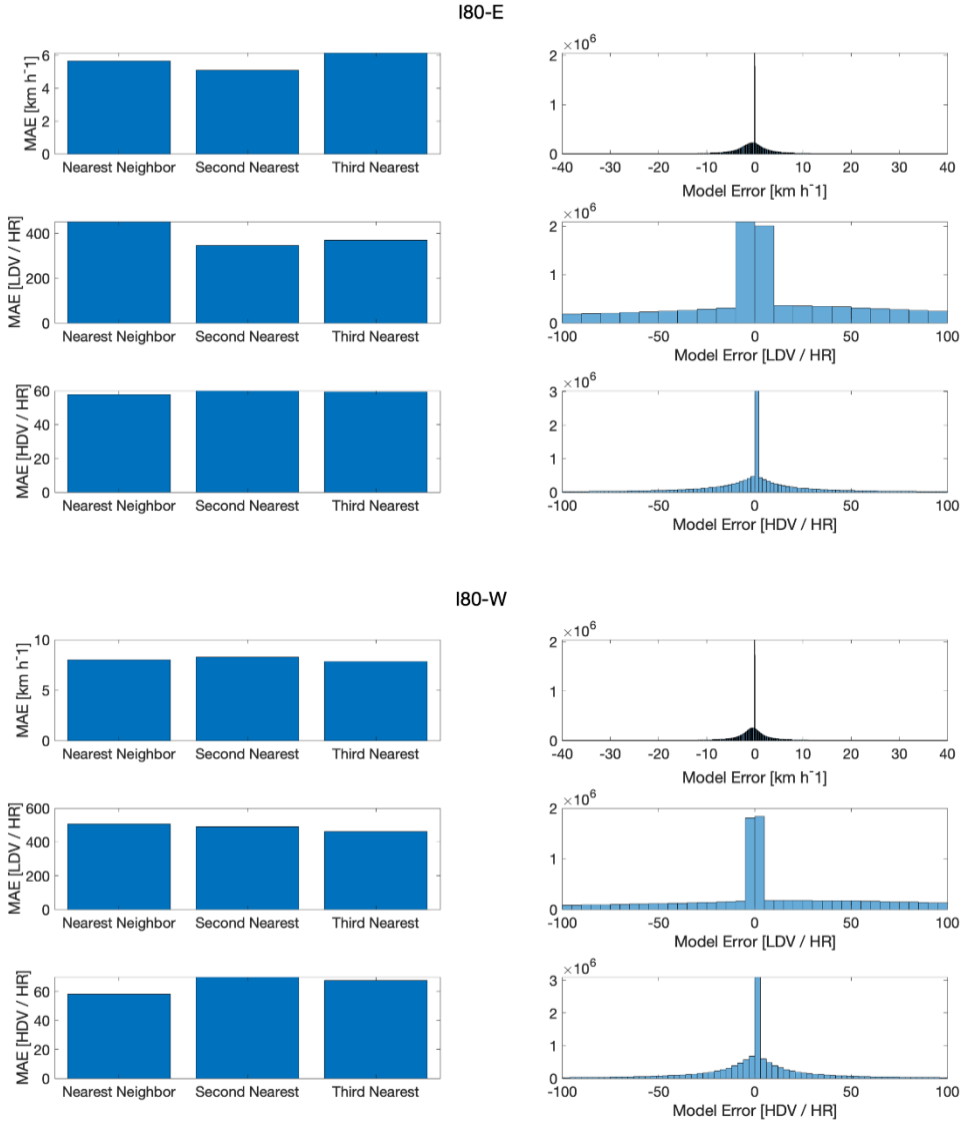

Figure 3.8. Mean average error (left) and distribution of error (right) for modeled speed (top), LDV flow (middle), and HDV flow (bottom).

3.7.5. EMFAC2017 Vehicle Classes

While EMFAC2017 provided speed-dependent emission rate estimates for 41 vehicle classes, PeMS characterizes vehicles in two categories based on length. In order to use EMFAC2017 emission rates in combination with PeMS traffic counts to estimate total emissions, we classify EMFAC2017 categories as LDV or HDV based on length.

EMFAC Vehicle Class	Grouping for this work
All Other Buses	0
LDA	1
LDT1	1
LDT2	1
LHD1	1
LHD2	1
MCY	1
MDV	1
MH	0
Motor Coach	0
OBUS	0
PTO	0
SBUS	0
T6 Ag	0
T6 CAIRP heavy	0
T6 CAIRP small	1
T6 OOS heavy	0
T6 OOS small	1
T6 Public	0
T6 instate construction heavy	0
T6 instate construction small	1
T6 instate heavy	0
T6 instate small	1
T6 utility	0
T6TS	0
T7 Ag	0
T7 CAIRP	0
T7 CAIRP construction	0
T7 NNOOS	0
T7 NOOS	0
T7 POAK	0

T7 Public	0
T7 SWCV	0
T7 Single	0
T7 other port	0
T7 single construction	0
T7 tractor	0
T7 tractor construction	0
T7 utility	0
T7IS	0
UBUS	0

Table 3.1. Breakdown of EMFAC vehicle classes we characterize as LDV or HDV based on length. “1” denotes LDV and “0” denotes HDV.

3.7.6. EMFAC2017 Emissions Rates

As described in the main text, emission rates for LDV and HDV on each road segment between individual PeMS monitoring stations are computed hourly as a function hourly average speed. Here we show emission rates as a function of speed.

We also compare piece-wise linear fits to the spline fits used in this study. With the exception of emissions rates for LDV at speeds lower than 20 km h^{-1}, there is little difference between these fits. High uncertainty in emission rates at low hourly average speeds because of travel at non-constant speeds is likely to outweigh any difference between these fits (see Fig S7).

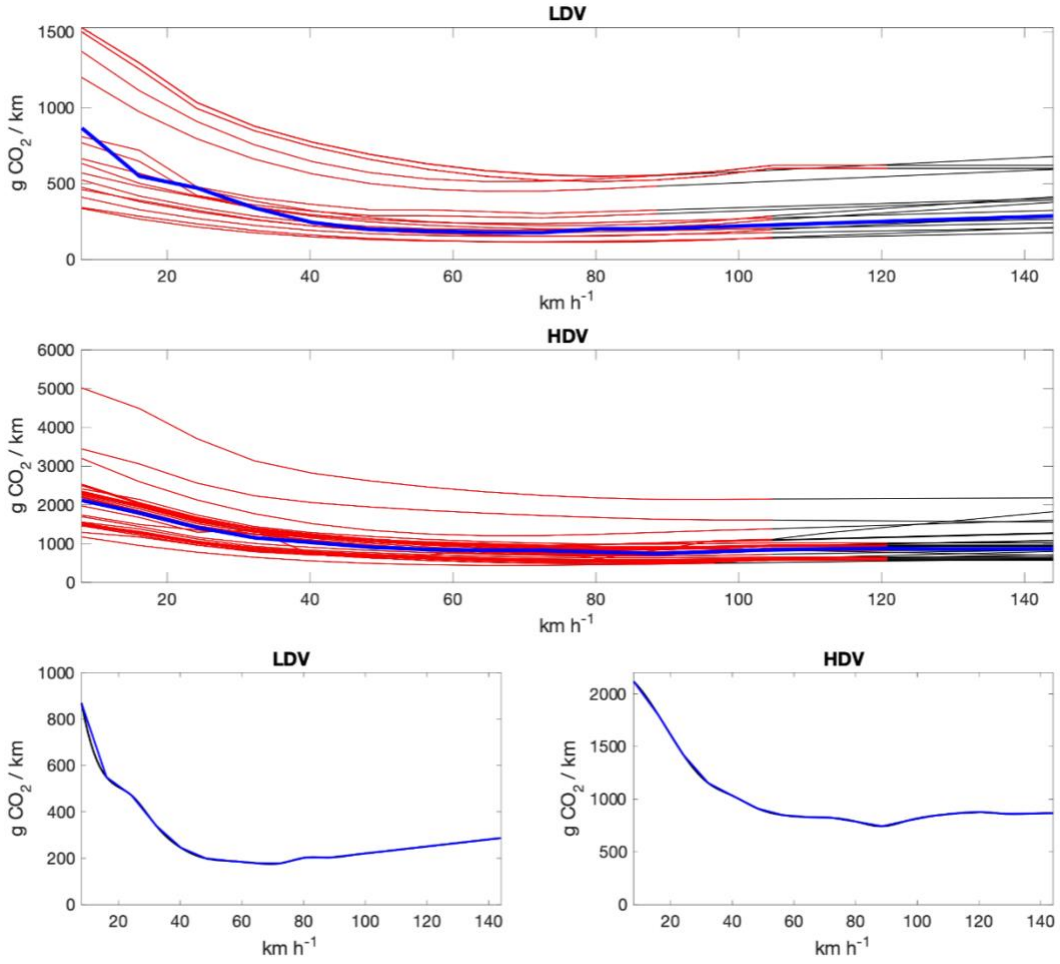

Figure 3.9. We show emission rates (g CO_2 / km) of different vehicle classes as a function of speed. **Top and middle:** Red lines indicate emission rates for individual vehicle classes as reported by EMFAC2017. Black lines indicate extrapolation using Oakridge National Lab data. Heavy blue lines indicate emission rates for LDV and HDV groups calculated by taking the vkm-weighted mean of emission rates for all vehicles within a group at a particular speed. **Bottom:** We compare piecewise-linear fits of this data to spline fits. Black lines indicate spline fit. Blue lines indicate piecewise-linear fits.

3.7.7. Contribution to Emissions by Speed and Fleet Composition

Figure S5 shows the hourly variation in the relative contributions of LDV speed, HDV percentage, and HDV speed to the deviation in CO2 / vkm from the reference value of 265 g CO2 / vkm. The solid line is the mean, and the shaded envelope represents the day-to-day variance. In the morning and mid-day, HDV percentage and LDV speed have opposite impacts on CO2 / vkm, leading to smaller variations in CO2 /vkm than the variations in the separate effects of speed and HDV %. During evening rush hour, low vehicle speeds result in higher emission rates, leading to large positive deviations. High day-to-day variance in vehicle speed contributes to high day-to-day variance in emission rates, shown as the envelope surrounding the solid line. At times near midnight, large, positive deviations are observed, mostly as a consequence of high HDV percentage, but also because traffic flows at rates higher than 104.6 kph, leading to higher emission rates. Night-to-night variance in HDV percentage is low, thus variance in nighttime predicted CO2 / vkm is small. HDV speed has little impact on CO2 / vkm.

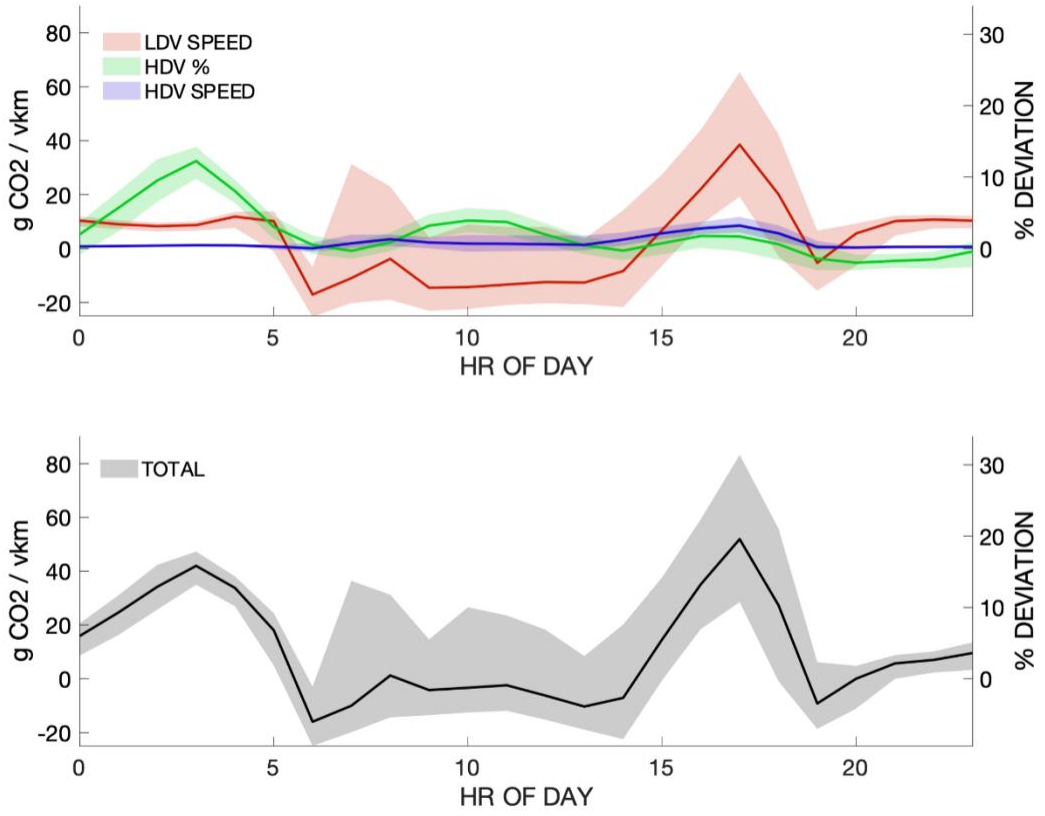

Figure 3.10. Top: PeMS-EMFAC-derived emissions rate deviations from baseline of 6% of all vehicles HDV, and vehicle speed constant at 105 kph resulting from car speed, truck percentage, and truck speed for the average day on the week shown in Figure 3.3. **Bottom:** Total deviation in emissions rate by hour of day. % Deviation (right axis) shows percent deviation for all curves from emissions rate of 6% HDV at 105 kph. For all plots, solid line represents median values and shaded area represents variance.

3.7.8. Determination of Uncertainty in Emissions Rate Estimates

For the set of BEACO2N emissions corresponding in time to the data in each 7.8 g CO_2 / vkm bin of PeMS-derived emissions rates, we find a BEACO2N-derived emissions rate estimate. To do this, we take all BEACO2N traffic emissions occurring simultaneously with the PeMS-derived emissions rates and further bin these points based on vkm, as shown in Figure 3. For each vkm bin, we then find the median emissions value and the variance of emissions values, $\sigma 2$. We assume the error in our estimate of the median emissions for each vkm bin to be $\delta ems = \frac{\sigma}{\sqrt{n}}$.

We then fit median emissions values to the line

$ems = \frac{gCO_2}{vkm} vkm,$

to find $\boldsymbol{\frac{gCO_2}{vkm}}$, using $\boldsymbol{\delta ems}$ as weights in the MATLAB fitlm function, and take the reported SE in slope to be the error in our calculated $\boldsymbol{\frac{gCO_2}{vkm}}$.

3.7.9. Posterior Emission Rates

The prior inventory was constructed to reflect vehicle type (LDV v. HDV) dependence on emissions, but not speed-dependence in emissions. In order to illustrate improvement of the posterior (Figure 3) over the prior, we repeat the analysis described in the main text to show emission rates calculated for the prior. Calculated emissions rates for the prior are nearly constant over a wide range (237.5 – 262.5 g CO_2 / vkm) of PeMS-EMFAC emission rates. Where they do vary, they are substantially different than those estimated in the posterior.

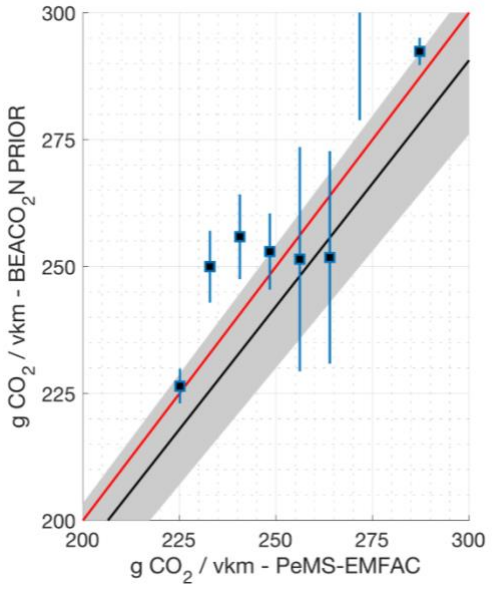

Figure 3.11. Emission rate estimates calculated for the $BEACO_2N$-STILT prior in the same manner in which they were calculated for the posterior vs. PeMS-EMFAC emissions estimates with uncertainty estimate. Black line shows fit of to posterior (Fig 3) weighted by variance: y = 0.97(.01)x . Grey envelope is 5% deviation from fit. Red line represents 1:1 line.

3.7.10. Impacts of Non-Constant Vehicle Speeds

While PeMS reports hourly averaged speeds for each sensing station, non-constant speeds due to congestion can result in range of possible emissions rates that can occur for a particular hourly averaged speed.

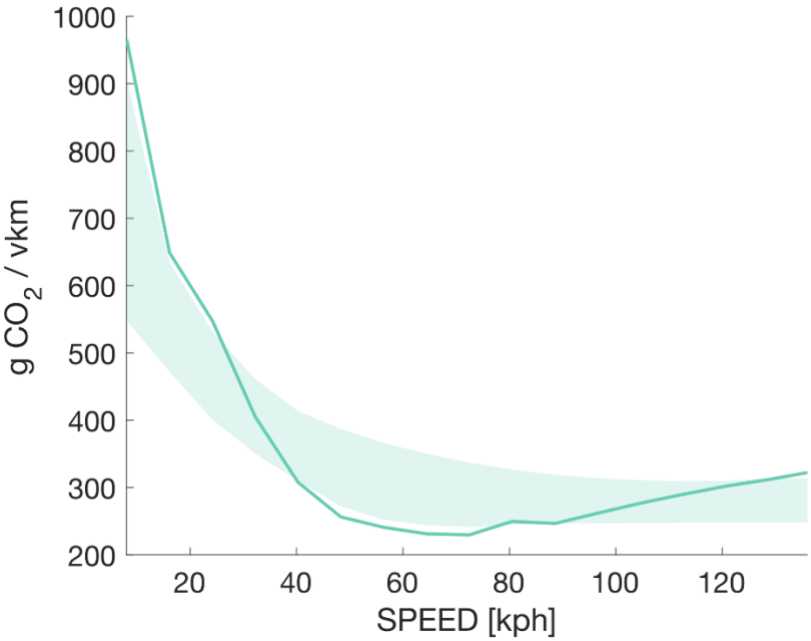

Figure 3.12. The dark line indicates the emissions rate corresponding to driving the speed indicated on the x axis at a constant velocity. The shaded region represents *er* distribution resulting from vehicle travel at non-constant speeds. For each speed, we calculate all possible emissions rates (g CO_2 / vkm) that could be generated assuming that the vehicle fleet (here, 8% HDV as is common during AM rush hour) drives at 2 different speeds between 8 kph and 130 kph for the times required to result in the average speed represented on the x axis. The spread for each speed represents the 16^{th}-84^{th} percentiles of possible emissions rates.

Chapter 4 – Evaluating the Impact of Background Concentration Error, Transport Error, and Node Count on BEACO$_2$N-STILT Emissions Estimates

4. 0 Abstract

High-density, urban sensor networks, paired with Bayesian inverse models have been used to quantify sector-specific, temporally-specific, and spatially-specific CO_2 emissions and have, in some cases (e.g., Kim et al., 2022), been shown to have the precision necessary to evaluate whether annual emissions reductions are occurring as expected based on policy. A better understanding of the accuracy and precision of such emissions estimates, as well as the impact of real-world network conditions (background concentration error, meteorology, sensor down time) on these estimates is needed to support more general use of the tool. In this chapter, we quantify the impacts of background error, meteorology, measurement density, and measurement duration on the ability of the BEACO$_2$N-STILT observation/inversion system as implemented by Turner et al. (2020) to accurately constrain CO_2 emissions from the transportation sector in the SF Bay area. We find large seasonal biases in the inversion system. These biases can be largely attributed to biases in CO_2 background (~80%) and biases in the modeled wind speed (~10-15%). We also use BEACO$_2$N-STILT footprints to explore the number of nodes and node density required for convergence of highway emissions estimates in this inversion system, estimating that one node per ~16.3 km^2 may be sufficient. Finally, we make recommendations for eliminating seasonal biases and for future evaluation of the system.

4.1. Introduction

Globally, cities are responsible for ~70% of GHG emissions. Because the urban share of the world population is expected to increase by 2.5-3 billion, making up ~67% of the world's population by 2050 (IPCC, 2014), global emissions reduction strategies must necessarily focus on reductions in urban emissions. Locally enacted policies are predicted to be able to drive a large (~30%) decrease in urban emissions and cities, and regional governments throughout the world are increasingly making commitments to reducing total greenhouse gas (GHG) emissions within their boundaries (e.g., Boswell, 2019). To plan GHG emission reduction strategies and then evaluate their effectiveness, governments need information regarding the sector and subsector breakdown, spatial origin, and temporal variability in emissions, as well as strategies for tracking emissions changes over the policy-relevant time scales of 1-3yrs. A large repertoire of activity-based, high-resolution emissions inventories have been created with fine resolution (~1km) at the urban scale (Gurney et al., 2012; Oda et al., 2011; McDonald et al., 2014; Gately et al., 2017a) However, there is a substantial lag in updates in the databases describing activities, and these emissions inventories often disagree with one another spatially (Gately et al., 2017b), in sectoral distribution, or in total estimates of emissions (Gurney et al., 2021). Because of these discrepancies and additional discrepancies with locally created inventories, it is desirable to use atmospheric observations of CO_2 to provide independent evaluation of emissions and emission trends.

Several recent studies have combined CO_2 measurements with atmospheric transport models and a Bayesian inverse system to estimate urban greenhouse gas emissions (Lauvaux et al., 2016; Turner et al., 2020, Hedelius, et al., 2018; Lian et al., 2022; Kort et al., 2012; Wu et al., 2016, Bréon et al., 2015; Staufer et al., 2016; Lauvaux, 2012). Applications to CO (Nathan et al.,

2018), and particulate matter (Nathan et al., 2021) have also been described. Using data from tower networks, Staufer et al., (2016) was able to reduce uncertainty in urban CO_2 measurements across the Paris metropolitan area by 9-50% and Lauvaux et al., 2020 was able to match city-wide CO_2 emissions to within 3% of a highly detailed emissions inventory. The latter was ~35% different from the inventory estimated by the local government. Using data from a surface network and tower network respectively, Turner et al. (2020) and Lian et al., (2022) were both able to observe a short term (~6 week) shifts in traffic emissions resulting from COVID-19 shelter-in-place orders. Furthermore, Fitzmaurice et al. (2022, Chapter 3) used a surface network to observe changes in highway fuel efficiency as a function of speed and fleet composition.

The above projects represent the promise of the network-inversion approach. However, the choices made by the different research groups in measurement density, sensor height, and instrument cost, imply wide variations in the labor and capital costs for expanding these initial studies to most cities on the planet. Furthermore, all network-inversion systems are subject to noise and bias because of representativeness error, background error, and error in modeled meteorology. Because different network-inversion setups may respond differently to these challenges, it useful to document system characteristics such as number of days required for emissions estimates to converge, the impact of meteorological and background concentration error on emissions estimates, and the node density required for convergent emissions estimates for each network-inversion system. For example, the approach used in this dissertation relies on a high spatial density (~2 km spacing), low capital cost, distributed network with an internal calibration approach that limits the need for reference grade standards and instruments. The design of the network followed from some hypotheses based on observations that urban emissions mix into the background on length scales of order ~1km, thus necessitating 2km spacing between nodes if every source is to be directly observed at a node in the network. However, because the inversion system allows for advection and diffusion to be represented, the reach of each node is extended, making it plausible that a lower network spacing is truly required.

Turner et al. (2016) explored the time required for emissions estimates to converge for a network similar to that described in this dissertation in a simulation showing that for network density, instrument precision and capital costs could be viewed as trade-offs. They estimated the precision of a networks of varying numbers of instruments and with varying, Gaussian distributions of model-measurement mismatch error. Estimates of the accuracy of inversions for a point, line and area source were described and the time for convergence to 1.3% was estimated. Turner et al., 2016 estimated that ~2 days would be enough time for convergence of emissions estimates for dense, near-surface measurements. This analysis was a model examination of the limits of performance but did not involve a suite of observations and a model of weather that might not perfectly match. The purpose of the paper was comparison of two approaches to an observing system. Analyses of convergence of real implementations of observation and modeling systems are expected to be different. Lauvaux et al., 2020 found for a tower network, 5 days were inadequate for emissions estimate convergence, 1 month to be substantially better, and 1 year to be as good as 3 years, in correcting bias in prior emissions. In this chapter we begin a similar exploration of the BEACO$_2$N-STILT inversion system.

In addition to noise, systematic errors in background concentrations contribute to biases in emissions estimates of network-inversion systems. There is no standard method for the determination of background concentrations, and inversion studies have used a variety of methods including a running lowest percentile, upwind measurements, or modeled concentration data. One study explicitly included the background as a parameter to be derived from the inverse (Henne et al., 2016). Several studies have documented large background concentration differences resulting from the use of different methods (Karion et al., 2021; Balashov et al., 2020). Henne et al., 2016 and Lauvaux et al., 2016 both tested the sensitivity of emissions to different strategies for finding background, finding up to 30% and 9% variation in emissions output respectively.

Transport errors are a large contributor to bias in any atmospheric inversion system. In the inversion process, transport models serve as a link between measurements (3-d concentrations at locations at points in time) and emissions (a 2D grid of emissions estimates for every moment in time); noise and bias in transport models lead to noise and bias in emissions estimates. For example, wind speeds biased high will result in lower concentrations than correct winds and thus emissions estimates with such biased winds will be higher to compensate. Previous work has documented transport errors in models over large regions (Lin 2005; Gerbig 2008; Martin et al., 2019) and across smaller, urban areas (Sarmiento et al., 2017; Lian et al., 2020). While observed variance and bias in the meteorological parameters are highly dependent on the specific location, transport model, and parameterizations used, higher relative error in windspeed and boundary layer height is typically seen during the nighttime and early morning hours. As a consequence, many inverse modeling studies attempt to avoid transport-induced bias by using data only from afternoon hours, during which the boundary layer is well-mixed and relative error in windspeed and boundary layer height are lower. Other approaches go further and use only data from mid-afternoon that meet certain wind-speed and direction criteria, resulting in the filtering of more than 90% of afternoon data points (Staufer et al., 2016).

In addition to documenting error in transport models, several studies have examined the relationship between transport error and error in emissions estimates, either through OSSEs (Deng et al., 2017) or the by studying the relationship between transport error and concentration error in forward models (Martin et al., 2019; Lian et al., 2020). For example, Deng et al. (2017) evaluates the impact of transport error on posterior emissions and finds reduced transport error substantially enhance the performance of the posterior at correcting bias in the prior. While both Lian et al. (2020) and Martin et al., (2019) attribute bias in modeled concentrations to bias in meteorological factors, they interpret the implications of this bias differently. Lian et al. (2020) suggests that higher nighttime bias in modeled concentration supports the practice of using only afternoon emissions, while Martin et al. (2019) report the existence of significant bias (both in modeled concentrations and meteorological variables) during the afternoon as well, suggesting that data used for estimating emissions via inversions should be filtered by meteorological error, rather than time of day.

Finally, because of the cost of instruments and the labor involved in maintaining urban networks, it is important to understand the impact of measurement density, which impacts the footprint of urban networks, on emissions estimates. Studies exploring this relationship using OSSEs suggest that a higher instrument density can substantially decrease uncertainty in emissions estimates

(Wu et al., 2016; Turner et al., 2016; Deng et al., 2017). However, because of costs, network plans must consider the trade-offs between sensor density and instrument precision. High-precision CO_2 (< .1 ppm) instruments are costly (~50K USD per instrument), making networks with dozens of sensors infeasible. Low-cost CO_2 instruments (~2K USD per instrument) can be deployed at higher density but are precise to ~1 ppm (e.g. Delaria et al. 2021).

Findings regarding the relative importance of instrument precision and sensor density seem to vary by network type (tower v. near surface). Turner et al. (2016) found that for near-surface, dense networks (25 sites at ~2km spacing) a model-measurement mismatch error corresponding to a Gaussian precision smaller than 1 ppm does not substantively reduce errors in emissions estimates. In contrast, Deng et al (2017) found that for a tower network, error in emissions estimates was greatly increased by a 1 ppm instrument precision. Turner et al. (2016) also found that optimal site density varied by emissions type. For an area source (~150 km^2) no significant information was gained by adding more than 10 measurement sites to the domain, estimation of a 32 km long line source was improved by adding up to 20 sites and estimation of a point source continued to improve as more than 35 sites were added. Because the labor costs associated with maintaining and calibrating sensor networks are substantial, finding the optimal site density for estimating emissions is critical for planning the scaling of such systems to multiple cities. Importantly, all three of the studies discussed were OSSEs. To our knowledge, there has been no real-world test of the relationship between node density and a system's ability to infer emissions.

In this chapter, we evaluate the inversion-network system characteristics discussed above: the impacts of errors in background concentration and meteorology on estimated emissions, the time required for emissions estimates to converge, and the number of nodes required to estimate highway emissions. Specifically, we use CO_2 measurements from the BErkeley CO_2 and Air quality Network ($BEACO_2N$), paired with the Stochastic Time Inverted Lagrangian Transport model (STILT) and a Bayesian inversion.

4.2 Data and Methods

4.2.1 The BErkeley Air quality and CO_2 Network

The BErkeley Air quality and CO_2 Network ($BEACO_2N$) (Shusterman et al., 2016) consists of ~65 sites, spaced at ~2km, across the San Francisco Bay. (See Fig. 1, left.) Each site measures CO_2, as well as CO, NO, NO_2, O_3, $PM_{2.5}$, temperature, and relative humidity (Kim et al., 2018).

In this study, we make use of $BEACO_2N$ CO_2 data from January 2018 to March 2020 (before the start of the COVID-19, related shelter in place in the SF Bay Area), during which time the number of $BEACO_2N$ nodes reporting data ranged from 1 to 41. The data used in this study was calibrated using the temperature-correction method described in Delaria et al. (2021) and precision of the CO_2 measured by individual nodes in the network is estimated to be 1.4 ppm.

4.2.2 $BEACO_2N$ – STILT Inversion System

Data from the $BEACO_2N$ network has been used to infer emissions changes as a result of the COVID-19 shelter in place (Turner et al., 2020), year over year changes in fuel efficiency of the

vehicle fleet (Kim et al., 2022*)*, and changes in fuel efficiency resulting from congestion and fleet composition (Fitzmaurice et al., 2022). In two of these studies (Turner et al., 2020; Fitzmaurice et al., 2022), emissions estimates were derived using the Stochastic Time Inverted Lagrangian Transport (STILT) model, paired with a Bayesian inversion. The STILT model follows particles transported backwards in time from $BEACO_2N$ measurements to generate a footprint ($\frac{ppm}{\mu mol\, m^{-2} s^{-1}}$), expressing the area to which $BEACO_2N$ measurements are sensitive. The inversion then uses an error-weighted comparison of prior emissions estimates (Turner et al., 2020a; Turner et al., 2016; McDonald et al., 2014), transformed into observation space using the STILT model, with $BEACO_2N$ measurements to calculate posterior emissions for the domain on the same grid as emissions estimates.

The inversion step of this process is carried out via the equation

$$\hat{x} = x_{prior} + (HB)^T (HBH^T + R)^{-1}\left(y_{obs} - Hx_{prior}\right), \text{ (Equation 4.1)}$$

in which x_{prior} (m x 1) is the prior emissions estimate, $\hat{x}$ (m x 1) is the posterior emissions estimate, y_{obs} (n x 1) are the $BEACO_2N$ observations of CO_2 enhancement over background values, R(n x n) is the model-data mismatch error covariance matrix, B (m x m) is the prior error covariance matrix, and H (n x m) is the measurement footprint. Note that m is 96 times the number of spatial elements in the prior domain, as the covariance matrices contain temporal as well as spatial elements and n is the number of observations made at a specific time point. More details surrounding the construction of these matrices can be found in Turner et al. (2020a).

CO_2 enhancement is found by subtracting background values from calibrated $BEACO_2N$ measurements. For each measurement (location, hour) the background value is estimated using either the NOAA Pacific curtain (for most trajectories) or AmeriFlux measurements in the Sacramento Delta, if the back-trajectories pass within 25 km of an AmeriFlux site.

In this work, we make use of *H,* the footprint of $BEACO_2N$ measurements as a spatial measure of sensitivity of the inversion system, and to explore the relationship between convergence and node density. While inversion footprints for a given measurement are dependent on meteorology, areas closer to measurements tend to have higher footprints (Fig. 4.1, right). We refer to the non-normalized sum of all individual measurement footprints at a given hour as the cumulative influence (CI). CI (m/96x1) is given in units of $\frac{ppm}{\mu mol\, m^{-2} s^{-1}}$, thus translating prior emissions into concentration. When comparing CI to emissions estimate convergence, we sum CI over the pixels for which we are tracking emissions.

Because we want to understand the impact of meteorology and node density on emissions estimate convergence, we choose to focus on a set of emissions unlikely to change abruptly or seasonally: highway traffic emissions. To examine these emissions, we evaluate weekday emissions from pixels associated with major highways. (See Fig 4.1, left.) We isolate traffic emissions in these pixels by subtracting emissions from the prior associated with other sectors, as described in Chapter 3.

4.2.2 Modeled Meteorology

The transport model used to generate Lagrangian back-trajectories for the BEACO$_2$N-STILT system is the High Resolution Rapid Refresh (HRRR) model, a reanalysis product created by NOAA (https://rapidrefresh.noaa.gov/hrrr/), simulating meteorology at a 3 km x 3 km scale across the United States.

4.2.3 Meteorological Measurements

We use wind speed and direction measurements recorded by a Vaisala WXT520 anemometer is in Richmond California to compare to the HRRR.

To understand biases in boundary layer height, we use data from soundings released at 0 UTC and 12 UTC daily at the Oakland airport. We calculate the bulk Richardson number (Zhang et al., 2014) as:

$$R_i = \frac{g}{\theta_v} \frac{(\theta_v - \theta_{v0})(z - z_0)}{(u - u_0)^2 + (v - v_0)^2}, \text{ (Equation 4.2)}$$

where g is gravitational acceleration, θ_v is virtual temperature, z is height above ground level, and u and v are the horizontal components of horizontal wind speed. We then find the boundary layer height to be the point at which $R_i = 0.25$.

4.3 Results

4.3.1. Relative Impact of Background Concentration and Windspeed Error on STILT Emissions Estimates

The STILT emissions from highway pixels are observed to have an unphysical seasonal variation that is too large to be attributed to uptake by the biosphere or seasonal changes in anthropogenic emissions. For example, inferred highway emissions are ~60% lower than the annual mean in mid-July 2018. In contrast, uptake by the biosphere is estimated to peak in late-April 2018 and result in a 19% deviation from average values in the pixels we examine.

To understand the source of the seasonal bias, we assess seasonal biases in background CO_2 concentrations, wind speed, and boundary layer height. To estimate error in background CO_2 estimates, we follow Kim et al., (*in prep*) and estimate the true background of the network for a given hour to be the running six-hour average of the 5th percentile of measured CO_2 concentrations. We then calculate error in enhancement for a given hour to be the difference between the mean background used in the STILT inversion (detailed in Turner et al., 2020a) and background calculated using the 5th percentile method. We also find the error in windspeed by comparing HRRR output to wind measurements at the RFS and error in boundary layer height to that estimated using OAK sounding data.

In Fig. 4.3, we show 30-day averages in fractional difference from mean emissions, wind error, enhancement error, and boundary layer height error. We see that background error and wind speed also exhibit seasonal bias, and that these biases are roughly synced in time with that of the bias in emissions estimates, with positive values peaking in winter and negative minima in

summer. In contrast, boundary layer height, while exhibiting positive bias, does not show a seasonal trend. This is reflected in much higher correlations in the timeseries of windspeed and background concentration error with fractional emissions difference (0.92 and 0.89 respectively) compared to boundary layer height (0.29).

To estimate the impact that seasonal bias in background concentration and windspeed have on emissions, we make use of a simplified version of the continuity equation, which assumes that we are estimating emissions from a uniform box at steady state with no substantial entrainment.

$$Q = \left(C - C_{bkg}\right)\frac{Uh}{W}, \text{ (Equation 4.3)}$$

where Q is emissions, C is CO_2 concentration, h is boundary layer height, U is windspeed and W is the width of the domain from which emissions arise. Kim (*in prep*) parameterized W using STILT posterior output, BEACO$_2$N concentrations, background values used, and HRRR meteorological parameters, and found

$$W = \alpha_1\sqrt{Uh} + \alpha_2, \text{ (Equation 4.4)}$$

where $\alpha_1 = 3436$ and $\alpha_2 = -1.58 \cdot 10^4$. Using Kim's (*in prep)* parameterization, we estimate fractional seasonal bias in emissions estimates due to background, wind, and boundary layer height error to be:

$$\frac{Q_0}{Q_c} = \frac{(C-C_{bkg,0})}{(C-C_{bkg,c})}\frac{\alpha_1\sqrt{U_c h_c}+\alpha_2}{\alpha_1\sqrt{U_0 h_0}+\alpha_2}\frac{U_0 h_0}{U_c h_c}, \text{ (Equation 4.5)}$$

in which variables with subscripts "0" are the values used as inputs to the BEACO$_2$N-STILT system as described in Sect. 4.2 and variables with subscripts "c" are "correct" values: measured values for windspeed and background values generated with the rolling 5th percentile method for background. We use Eq. 3.5 to evaluate the plausibility that windspeed and background error are the primary causes of the season bias we observe in emissions estimates. To isolate the impact of background error and windspeed separately, we compute the ratio described by Eq. 3.5 in three separate ways: assuming only background error with no windspeed error, assuming only windspeed error with no background error, and assuming both background and windspeed error. To avoid unphysical estimates, we omit times when enhancement (in either numerator or denominator) is less than 2 ppm, when W (Eq. 3.4) is estimated to have values less than zero, and when the uncertainty in modeled error is greater than 0.2×10^{-6} kg m^{-1} s^{-1}. Because we have only twice-daily measurements giving us boundary layer height and because percent error in boundary layer height is smaller than percent error in windspeed, we use modeled boundary layer height in these estimates.

We find fractional seasonal bias expected from background concentration error alone, background concentration error and windspeed error, and windspeed error alone and compare this expected bias to a normalized, 30-day running average of emissions. We see that the bias due to background error is expected to be substantially larger (maximum of 52%) than that due to seasonal bias in wind speed (up to 18%). In Tbl. 4.2, In winter, the expected fractional bias due to both background error and windspeed error is similar in magnitude to fractional bias

observed in posterior emissions (0.50 v. 0.45). In summer, the match between observed seasonal bias and bias expected because background and windspeed error is not as good (-.17 v. -.43). It is unclear whether this is due to other seasonal biases or because of substantial uncertainty in the bias ratio during summer, largely because of small (and negative) enhancements over background lead to large variations in the denominator of Eq. 4.5.

We hoped to use our knowledge of the error in these two factors to correct STILT emissions output, evaluating the correction by its ability to create a highway traffic signal with no seasonality. However, we found the correction factor (especially during the summer months) to be highly sensitive to our choice of data filtering thresholds and were therefore not able to create such a corrected set of emissions.

4.3.2 The Impacts of Short-Term Noise on Emissions Estimates

Despite the seasonal biases discussed in 4.3.1, it is still possible to address the question of how many days of observation are needed to overcome short-term noise in the BEACO$_2$N-STILT system. To answer this question, we compare contiguous sampled subsets of emissions output for a given area to the eventual mean emissions over that area. We find the fractional mean average error of these subsets as a function of number of days of emissions output included in the subset (sampling the maximum possible number of contiguous subsets available given number of days included and the availability of emissions data described in the above section). Regardless of area sampled, we find the mean average error follows a double exponential decay function (e.g., Fig. 4.2, left.), in which we see a sharp drop in error in the first few days, followed by a long decay in error. While the long decay represents seasonal bias, the short time constant, τ_1, and its corresponding coefficient, C_1, represent the impacts of short-term noise Fitting the curve produced using all traffic data in the whole footprint area averaged over an entire weekday, we find $\tau_1 = 3.8\ days$, $C_1 = 4.7\%$. Because performing the same analysis on background and meteorological error yields similar time constants, we assume that τ_1 is a product of day-to-day noise in background and meteorological error (Table 4.1).

We also perform this analysis on each of the pixels pictured in Fig. 1, left. In Fig. 4.2, we see that (at least within the footprint region) time constants and coefficients associated with individual pixels are uncorrelated with CI and similar to those estimated for all highway traffic across the footprint region (3-7 days and ~5-10%).

4.3.3 Emissions Estimate Convergence and Measurement Density

Because of the labor and costs associated with maintaining a dense network of low-cost sensors, it is desirable to quantify the number of nodes required for convergence of emissions estimates. In principle, it would be possible to repeat inversions with a subset (different numbers of) measurements at each (as in Turner et al., 2016). However, the realities of our data record (see Fig. 3.5) make this challenging. Instead, we use the relationship between CI (summed over traffic pixels) and emissions estimate convergence to establish a threshold CI value required for convergence of emissions and link this CI threshold to number of nodes.

We examine the relationship between fractional change from prior for each hour of the weekday, as we expect that area-wide, weekday highway emissions to be fairly constant for a given hour.

We show that for emissions across a large area, averaged emissions estimates converge at a threshold value of CI. We then relate CI of convergence to node density.

Figure 4.4 shows and example of the relationship between CI and emissions estimates, in which we show percent deviation of prior emissions to posterior emissions. At times associated with low CI, posterior emissions stay close to the prior, as expected from Eq. 4.1. Note that as H approaches zero, $\hat{x}$ approaches x_{prior}. In contrast, in areas where CI is high, $\hat{x}$ moves from the prior towards emissions rates implied by the translation of $BEACO_2N$ measurements into emissions space by H. However, the number of $BEACO_2N$ nodes reporting CO_2 data at any one time varies from 1-41. Because of substantial fluctuations in total number of sites reporting as well as *which* nodes were reporting (for example, before June 2018, no nodes were located in Vallejo, CA), both the total value and spatial distribution of CI area highly variable. Over the two-year period we explore, even pixels with high average CI may experience times of zero CI, during which emissions estimates move only a small distance from their posterior value.

To further understand the relationship between CI and emissions convergence for the footprint area, we plot percent change of posterior from prior vs. CI for each hour. (For example, Fig. 4.4, left.) Based on Eq. 4.1, we expect $\Delta ems_{posterior}$ to (roughly) follow the form

$$\Delta ems_{posterior} = \frac{bCI^2}{bCI^2+R}\left(ems_{obs} - ems_{prior}\right), \text{ (Eq 4.6)}$$

where ems_{obs} is the emissions implied by our observations. Because data points from Eq. 4.6 fit the form of a decaying exponential

$$\Delta ems = \Delta ems_0(e^{-\frac{CI}{CI_0}} - 1), \text{ (Eq 4.7)}$$

we can fit the binned median values of shift from prior as a function of CI using Eq. 4.7, interpreting Δems_0 as the shift from prior at convergence and CI_0 as roughly the CI necessary for convergence of emissions estimates. Averaging across CI_0 for fits with $R^2 > 0.5$, (nighttime fits are worse than daytime fits), we find the average threshold CI value to be 2.25 $\frac{ppm}{\mu mol\ m^{-2}s^{-1}}$.
To understand the relationship between this threshold CI and node density, we show CI for the footprint area vs. number of $BEACO_2N$ nodes reporting CO_2 data. We see that at times when the network has 10 or fewer nodes reporting data, the threshold CI (represented by the red line) is almost never met, while the threshold CI is nearly always met during times where 30 or more nodes report data, which translates roughly to a density of one node per ~16.3 km^2 across the $BEACO_2N$ footprint region.

4.4. Implications for the BEACO2N-STILT system

In this chapter, we investigate the (1) the impact of transport and background concentration error on $BEACO_2N$-STILT emissions estimates, (2) the time needed to resolve those estimates, and (3) the measurement density required to arrive at those estimates. Here we discuss the implications for the $BEACO_2N$-STILT system: how our findings impact our understandings of previous emissions estimates and how we can use these new understandings to improve emissions estimates going forward.

4.4.1. Implications for Understanding Previous Work

The seasonal bias in background concentrations and windspeed discussed in this chapter has undoubtably influenced previous work (Turner et al., 2020; Fitzmaurice et al., 2022) using $BEACO_2N$-STILT to constrain CO_2 emissions. It would be prudent to repeat the analysis for these works after seasonal bias in background CO_2 and windspeed have been addressed. However, we have several reasons to believe that the results of those works will be similar after seasonal bias is addressed. Turner et al., 2020 saw larger emissions decrease due to the COVID-19 shelter in place than would be expected from PeMS highway emissions (48% v. 41%). This may have been in part due to a decrease in fractional bias over the period examined (February 2020 to May 2020). However, the question is whether we expect $BEACO_2N$-STILT to be able to converge on emissions estimates in the time Turner considered (~6 weeks). By considering the sharp reduction in error associated with using a few days in emissions estimates, we find error reduction timescales similar to, but slightly longer than those predicted by Turner et al., 2016 (3.8 d v. 2 d). These values represent a $BEACO_2N$-STILT time to convergence in the best-case scenario in which seasonal biases in background concentrations, windspeed, and other factors impacting emissions estimates are eliminated, and that in the absence of seasonal bias, $BEACO_2N$-STILT should be able to converge on emissions estimate over 6 weeks, the time period examined in Turner et al, 2016.

Results from Fitzmaurice et al. (2022, Chapter 3) rely on median values across 18 months of data (January – June), binned by fuel efficiency modeled using traffic data. Although we see day-to-day fluctuations in fuel efficiency in the area examined, fuel efficiency is highly dependent on hour of day (Figs. 3.2, 3.4). Across the period used, median values for expected fractional bias from background concentration and windspeed are relatively even (less than 0.1 spread from 0 fractional bias) across the times of day sampled (4 am – 10 pm). Because the spread in fuel efficiencies observed is much higher (~50% over minimum values) than hour-to-hour differences in median bias, we expect that we are in fact observing changes in fuel efficiency, and that observed fuel efficiencies are within 10% of true fuel efficiencies.

4.4.2. Implications for Improving BEACO2N-STILT Emissions Estimates

We find that on seasonal timescales, $BEACO_2N$-STILT emissions estimates are subject to substantial biases influenced by errors in the background CO_2 concentration and the HRRR reanalysis product. Seasonal biases in emissions (up to 60% of mean emissions) are much larger than those associated with day-to-day noise (5-10% of mean). A significant portion of seasonal emissions bias can be explained by bias in background concentration and windspeed. We predict that correcting background error prior to inversion may eliminate up to 80% of the observed seasonal bias in emissions output, and future work should prioritize eliminating background error, either by using an alternate calculation process before inverting emissions estimates or by solving for background concentrations through the inversion (e.g., Henne et al., 2016; Nickless et al., 2018). Greater precision in concentrations will be required during the summer when enhancements are smaller relative to noise in background. In principle, seasonal bias in windspeed error may be reduced through careful choice of transport model or by assimilating meteorological variables at a higher resolution and over a smaller domain than used by HRRR. However, because we expect seasonal meteorological bias to produce emissions estimate bias on

the order of only ~10%, the relative gains would likely be smaller than those realized by correcting background concentration values.

Finally, we present a method for examining the relationship between node density and emissions estimate convergence, by identifying a threshold CI below which emissions estimates have not converged. This method, which circumvents problems posed by node down-time in repeating OSSEs (e.g., Wu et al., 2016; Turner et al., 2016) which vary the number of nodes used in inversions, has the potential for use in planning field maintenance or node siting around areas of interest. For example, our analysis implied that consistently reach this threshold CI for the whole footprint region when we have more than 30 nodes active. Several caveats must be applied to these results. Before being used for planning purposes, this analysis should be repeated after seasonal biases are corrected. Furthermore, we assessed only the CI threshold needed for convergence of highway traffic emissions. Smaller emissions may require different CI thresholds and future work should investigate the relationships between CI thresholds and emissions magnitude and area of interest. Despite these caveats, we see this analysis as a useful planning tool. The threshold we find corresponds to ~ 1 node / 16 km^2, meaning that roughly half of all BEACO2N nodes are sufficient for detecting changes in highway emissions. This density metric could also be applied to historical BEACO$_2$N data (which dating back to ~2012) to evaluate the utility of applying the STILT-HRRR system and Bayesian filter to these time periods. Beyond network and inversion planning, this analysis also presents a potential filtering criteria for posterior emissions. Time points for which CI is below the convergence threshold represent time points at which BEACO$_2$N measurements are not sufficiently sensitive to areas of interest and could be filtered.

Future work could also evaluate whether CI convergence thresholds are similar across geographical locations. Networks using the same instruments as BEACO$_2$N have been established in Los Angeles, Glasgow, and Leicester, and will soon be deployed in Providence. While place to place differences in meteorology may result in different node densities required for convergence of emissions estimates, CI is a more direct indicator of the sensitivity of the measurement network to local emissions. If CI thresholds are similar across geographic locations, CI convergence thresholds, paired with Lagrangian back-trajectory models, could be used in planning networks in new cities.

	WINDSPEED ERROR τ_1 **(DAYS)**	***WIND DIRECTION ERROR*** τ_1**(DAYS)**	***PBLH ERROR*** τ_1 **(DAYS)**
06:00 LT	**4.4**	**3.7**	
12:00 LT	**3.0**	**5.3**	
18:00 LT	**4.7**	**4.5**	
00:00 LT	**2.6**	**4.0**	
00:00 UTC			**6.4**
12:00 UTC			**3.0**

Table 4.1. Shorter time constants for meteorological error fit to double exponential function.

Fractional Bias	*Summer (JJA)*	*Winter (DJF)*
Expected from Windspeed Error	*-0.0896 (0.0521)*	*0.0687 (0.2349)*
Expected from Background Concentration Error	*-0.0825 (1.6511)*	*0.4029 (0.1970)*
Expected from Windspeed Error and Background Concentration Error	*-0.1651 (1.5060)*	*0.4995 (0.5024)*
Observed in Posterior (compared to mean in Posterior)	*-0.4282*	*0.4501*

Table 4.2. We show expected bias from windspeed error, background concentration, windspeed and background concentration error, as well as observed bias in the posterior both in summer (JJA) and winter (DJF). Numbers in parentheses represent variance in correction factors.

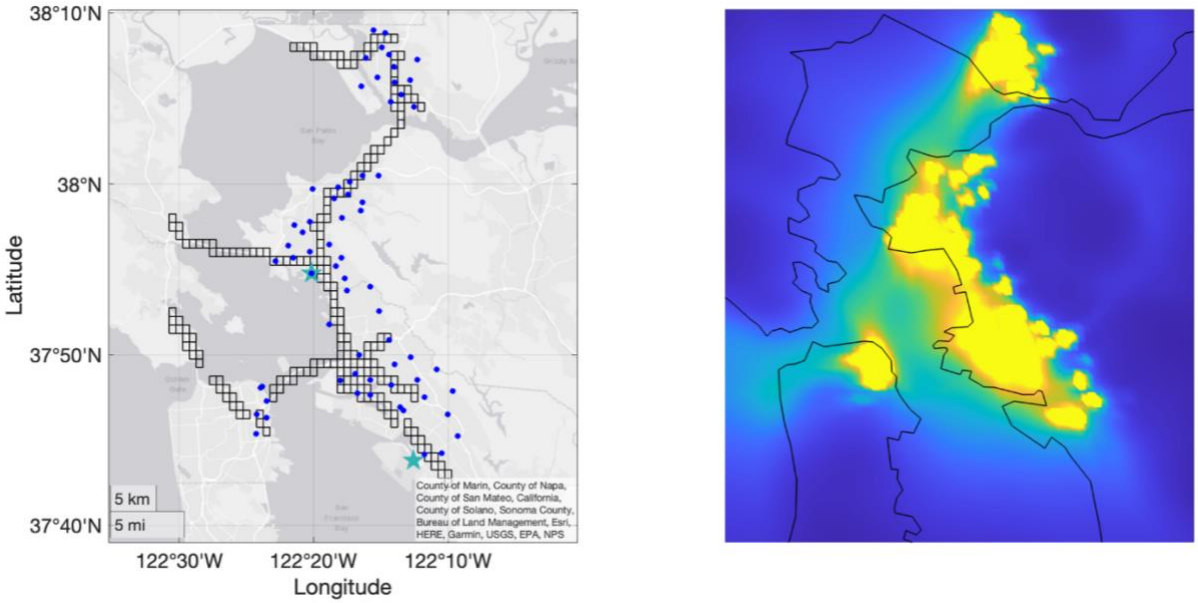

Figure 4.1. (Left) Map of pixels used (black boxes), BEACO$_2$N sites (blue dots), and meteorological measurements. (Right) CI averaged in time for each pixel across domain.

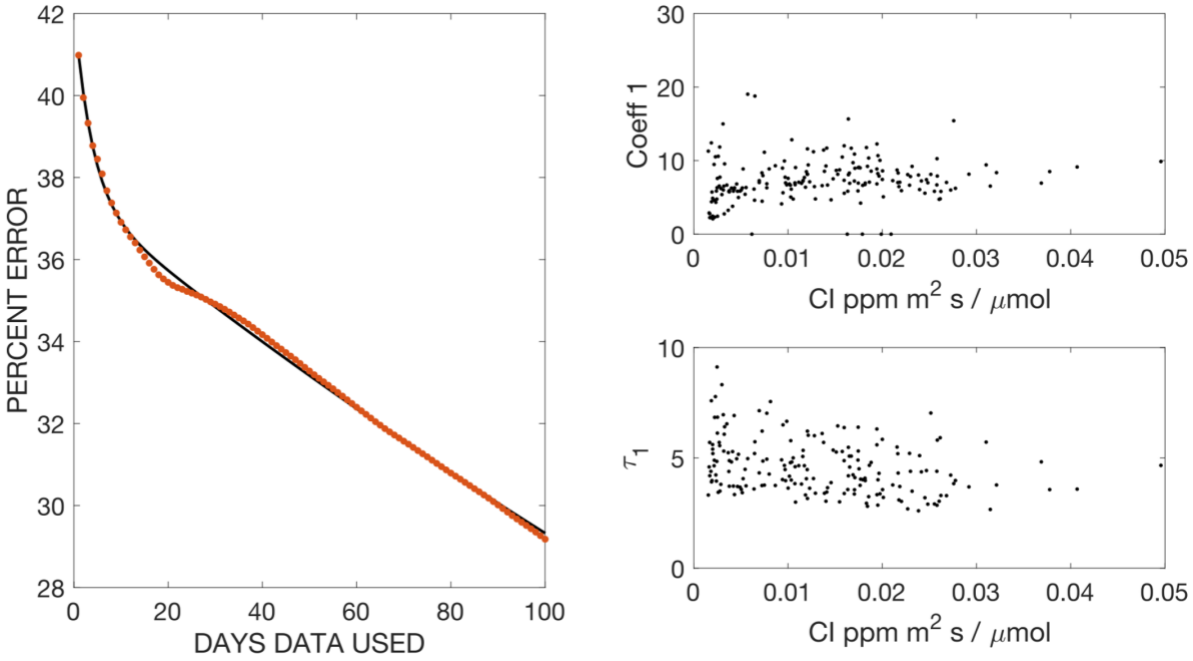

Figure 4.2. Left: Percent error from mean of highway traffic emissions as a function of number of days used. **Right:** Coefficients to fit to double exponential for traffic emissions from all highway pixels analyzed. CI on x axis is the average CI for a given pixel over the whole time period examined.

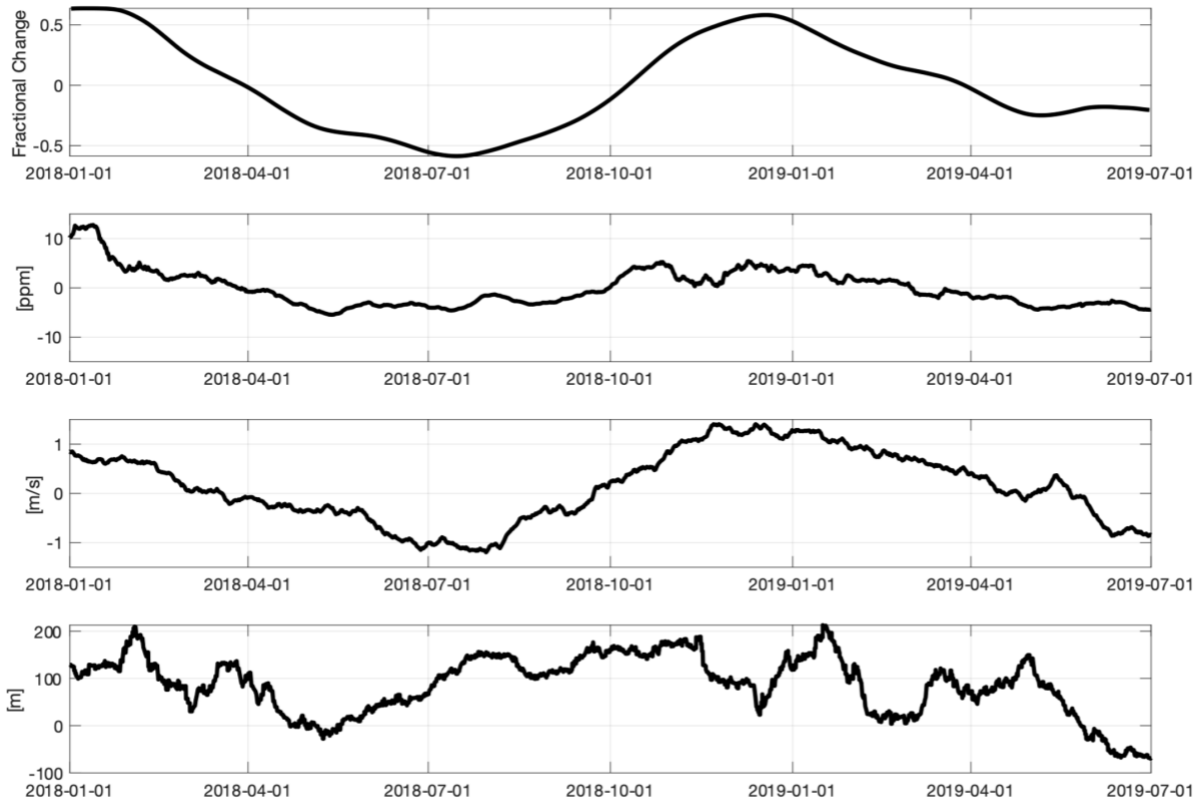

Figure 4.3. 30 day rolling averages of (1st) fractional change from mean highway traffic emissions (2nd) CO_2 enhancement error (3rd) windspeed error and (4th) boundary layer height error.

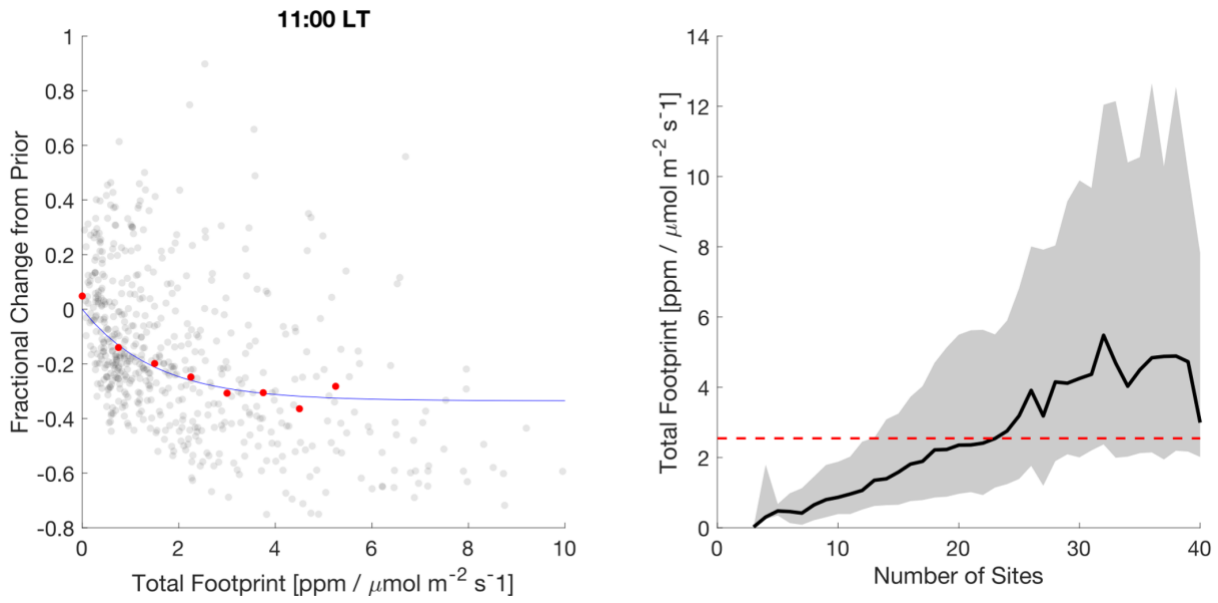

Figure 4.4. Left: Example percent change of posterior from prior for highway traffic emissions within the BEACO2N footprint area as a function of summed footprint (CI) over all highway pixels. Red dots represent binned median values of percent change. Blue line indicates fit to Eq. 4.6. **Right:** We show summed footprint over highway pixels as a function of number of BEACO$_2$N sites reporting CO_2 values for a given hour. Black line indicates median value and grey shaded area indicates one-sigma variance. Red dashed line represents the mean total footprint value across all hours with $R^2 > .5$ required for convergence.

Chapter 5 Conclusions

5.1. Summary

Because vehicle emissions represent the largest sectoral contribution of CO_2 emissions in US cities and contribute substantially to health inequities caused by exposure to co-emitted pollutants (Tessum, 2020), city and regional governments are increasingly developing and implementing measures to decrease emissions of CO_2 and $PM_{2.5}$ in an equitable way. To plan emission reduction strategies, governments need information regarding the sector and subsector breakdown, spatial origin, and temporal variability in emissions, as well as strategies for tracking emissions changes over the policy-relevant time scales of 1-3yrs.

In this dissertation, we outlined and evaluated methodology for using surface networks and real-time activity data to infer $PM_{2.5}$ and CO_2 emissions from vehicles in urban areas at the neighborhood scale. The work described in the previous chapters demonstrates that both regulatory monitoring sites and low-cost sensor networks can be used to quantify long-term trends and spatial heterogeneity sector and sub-sector specific emissions of CO_2 and $PM_{2.5}$. Applying these methods in combination with real-time, high-resolution traffic data, we can quantify not just emissions, but also emissions factors (g pollutant / unit activity).

W first develop a method for using HDV percentage and stationary, near-road regulatory sensors to derive Heavy Duty Vehicle emission factors – mass pollutant per unit activity (Fitzmaurice, *Chapter 2)*. In applying this method to the San Francisco Bay Area, we find that EFs decline by a factor of ~7 in the 2009-2020 period and are comparable to those derived in similar places with higher-cost measures. Additionally, we observe spatial heterogeneity in EFs across the Bay Area, possibly due to inconsistencies in compliance to HDV emissions regulations.

Second, we demonstrate that a high-density network of low-cost sensors, such as $BEACO_2N$ can resolve speed-dependent fuel efficiency at the scale of ~5km highway segments (Fitzmaurice, *2022a*), and that with exception of emissions during the morning rush hour, that $BEACO_2N$ observations are in line with fuel efficiencies generated using EMFAC2017 data.

Finally, we explore the dependence of the accuracy and precision of the $BEACO_2N$ network on background concentration estimate error, modeled meteorological error, and site density. We find that with the exception of stagnation events not reflected in modeled meteorology, that $BEACO_2N$-STILT emissions inferences are not biased by meteorological error. We present a method for exploring convergence of emissions estimates as a function of $BEACO_2N$ footprint density. We find that using the current inversion framework, the conditions for convergence of highway emissions are almost never met when less than 10 $BEACO_2N$ nodes are operational and almost always met when more than 30 $BEACO_2N$ nodes report data.

5.2. Future Directions

5.2.1. Observing long-term trends and spatially heterogeneity of HDV emissions across the United States

As shown in Tbl 2.1, most studies in the past decade documenting HDV EF have been conducted in the state of California. This is problematic for understanding the current and long-term impact of HDV on air quality across the United States, because HDV emissions control regulations (and likely the use of emissions control technology such as diesel particulate filters and selective catalytic reduction) differ from state to state.

A cross-country campaign to understand HDV EF from single plume analysis would be costly and time and labor intensive. However, because of the Clean Air Act, the United States has a long record of hourly, co-located $PM_{2.5}$ and CO measurements. More than 100 of these co-located sites across the country are located within 500 m of a major highway and many have been in operation for a decade or more. All US states track truck percentage and vehicle flow via dense, in-road magnetic sensor networks. Because of the accessibility of this data, the method described in Chapter 2 could be applied to datasets across the United States and over the past decade to uncover long-term trends and spatial variations in HDV EF. Furthermore, researchers interested in observing spatial heterogeneity in HDV EF across a specific city could apply this method in combination with a network of near-highway, low-cost sensors.

5.2.2. Additional learning about traffic emissions from the BEACO$_2$N-STILT system

In Chapter 3, we demonstrated that the BEACO$_2$N-STILT system can observe shifts in vehicle fuel efficiency associated with speed and vehicle type, by focusing on a short (~5 km) stretch of highway. This means that BEACO$_2$N-STILT can be used as a tool to evaluate and improve upon parameterizations used to generate activity-based emissions inventories. While we demonstrated that for my segment of interest, BEACO$_2$N-STILT-derived fuel efficiency generally matches fuel efficiency expected by using speed and vehicle-type as inputs to the EMFAC2017 model, several avenues of exploration remain.

One avenue is using BEACO$_2$N-STILT to identify and understand situations in which EMFAC2017 does not predict emissions accurately. For example, in Chapter 3, we describe a mismatch between EMFAC2017 model and the BEACO$_2$N-STILT observation system during the morning rush hour. Because we do not expect seasonal bias to have an hour-of-day specific impact on median emissions estimates over the time period examined, we expect this morning rush hour mismatch to persist after seasonal biases in the BEACO$_2$N-STILT are corrected. In the supplement to Chapter 3, we hypothesize the inability of hourly speed data to represent the complexity of acceleration and speeds traveled as a function of congestion, but that hypothesis remains to be verified. Beyond highway emissions, the BEACO$_2$N-STILT system has the potential to help us understand mobile emissions from surface streets. Most activity-based inventories estimate that surface streets account for ~25-30% of total on-road CO_2 emissions (McDonald et al., 2014), but those estimates have not been verified via atmospheric measurements, and the spatial distribution of these emissions is not well understood, especially because of the variability of traffic speeds on surface streets is not typically represented in activity-based inventories. Pairing BEACO$_2$N measurements with inventories created by urban science researchers leveraging cell-phone and UBER speed data to create high-resolution emissions estimates on surface streets (Ozturk, *in prep*) has the potential to refine our understanding of surface-street vehicle emissions. Finally, because each BEACO$_2$N sensor is equipped with $PM_{2.5}$, CO, NO, and NO_2 sensors, the BEACO$_2$N-STILT system has the potential

to evaluate long-term trends and spatial and temporal distribution of emissions and emission factors of these co-emitted species from vehicles. For example, preliminary BEACO$_2$N-STILT estimates of CO emissions (Asimow, *in prep*) show that while evening rush hour CO emissions are concentrated in highway pixels, morning rush hour emissions are distributed more evenly across pixels associated with surface streets, implying the importance of cold-start emissions of CO.

5.5.3. Refining the BEACO$_2$N-STILT Inversion Process

As discussed in Chapter 3, under the current inversion framework, BEACO$_2$N-STILT emissions output suffers from seasonal biases, likely caused by errors in background concentrations. Future work should explore methods for reducing such seasonal bias, either by employing different strategies for determining background concentrations as discussed in Karion et al. (2021) or by solving directly for background concentration values as in Henne et al. (2016) or Nickless et al. (2018). Future work should also explore methods for minimizing the seasonal impacts of wind and boundary layer height biases.

5.5.4. Expanding BEACO$_2$N-STILT analysis to additional sectors and locations

The BEACO$_2$N-STILT system has the potential to evaluate emissions from other sectors such as home heating, industrial sources, and the biosphere. Furthermore, BEACO$_2$N expansions to other locations (Los Angeles, Glasgow, Leicester, Providence) will allow for inter-city and inter-country comparisons of emission rates.

References:

A.B. 617, 2017 Biennium, 2017 Reg. Sess. (Cal. 2017). https://leginfo.legislature.ca.gov/faces/billTextClient.xhtml?bill_id=201720180AB617

Apte, J. S., Messier, K. P., Gani, S., Brauer, M., Kirchstetter, T. W., Lunden, M. M., Marshall, J.D., Portier, C.J., Vermeulen, R.C.H., Hamburg, S. P. High-Resolution Air Pollution Mapping with Google Street View Cars: Exploiting Big Data. Environmental Science and Technology, 51(12), 6999–7008. https://doi.org/10.1021/acs.est.7b00891 , 2017

Bay Area Air Quality Management District, West Oakland Environmental Indicators Project. 2019. Owning Our Air: the West Oakland Community Action Plan—Volume 1: the Plan. https://www.baaqmd.gov/~/media/files/ab617-community-health/west-oakland/100219-files/final-plan-vol-1-100219-pdf.pdf?la=en Retrieved December 13, 2021.

Balashov, N.V., Davis, K.J., Miles, N.L., Lauvaux, T., Richardson, S.J., Barkley, Z.R. and Bonin, T.A., 2020. Background heterogeneity and other uncertainties in estimating urban methane flux: Results from the Indianapolis Flux Experiment (INFLUX). *Atmospheric Chemistry and Physics*, *20*(7), pp.4545-4559. https://doi.org/10.5194/acp-20-4545-2020

Ban-Weiss, G.A., McLaughlin, J.P., Harley, R.A., Lunden, M.M., Kirchstetter, T.W., Kean, A.J., Strawa, A.W., Stevenson, E.D. and Kendall, G.R., 2008. Long-term changes in emissions of nitrogen oxides and particulate matter from on-road gasoline and diesel vehicles. *Atmospheric Environment*, *42*(2), pp.220-232., https://doi.org/10.1016/j.atmosenv.2007.09.049

Ban-Weiss, G.A., Lunden, M.M., Kirchstetter, T.W. and Harley, R.A., 2010. Size-resolved particle number and volume emission factors for on-road gasoline and diesel motor vehicles. *Journal of Aerosol Science*, *41*(1), pp.5-12., https://doi.org/10.1016/j.jaerosci.2009.08.001

Bishop, G.A., Hottor-Raguindin, R., Stedman, D.H., McClintock, P., Theobald, E., Johnson, J.D., Lee, D.W., Zietsman, J. and Misra, C., 2015. On-road heavy-duty vehicle emissions monitoring system. *Environmental science & technology*, *49*(3), pp.1639-1645., https://doi.org/10.1021/es505534e

Bishop, G.A., 2019. Three decades of on-road mobile source emissions reductions in South Los Angeles. *Journal of the Air & Waste Management Association*, *69*(8), pp.967-976., https://doi.org/10.1080/10962247.2019.1611677

Bishop, G. A. Does California's EMFAC2017 vehicle emissions model underpredict California light-duty gasoline vehicle NOx emissions? Journal of the Air and Waste Management Association, 71(5), 597–606. https://doi.org/10.1080/10962247.2020.1869121 , 2021.

Boswell, M. R., & Madilyn Jacobson, A. R. 2019 Report on the State of Climate Action Plans in California. https://ww2.arb.ca.gov/sites/default/files/2020-03/17RD033.pdf, last accessed: January 12, 2022, 2019.

Bréon, F.M., Broquet, G., Puygrenier, V., Chevallier, F., Xueref-Remy, I., Ramonet, M., Dieudonné, E., Lopez, M., Schmidt, M., Perrussel, O. and Ciais, P., 2015. An attempt at estimating Paris area CO 2 emissions from atmospheric concentration measurements. *Atmospheric Chemistry and Physics*, *15*(4), pp.1707-1724. https://doi.org/10.5194/acp-15-1707-2015

California Air Resources Board. (2018) Truck and Bus Regulation – Low Mileage Construction Truck Phase-in Option. Retrieved from: https://ww3.arb.ca.gov/msprog/onrdiesel/documents/faqconstructiontrucks.pdf

California Air Resources Board. 2018 PROGRESS REPORT: California's Sustainable Communities and Climate Protection Act, (November), 96. https://ww2.arb.ca.gov/sites/default/files/2018-11/Final2018Report_SB150_112618_02_Report.pdf, last accessed: January 12, 2022

Caubel, J. J., Cados, T. E., Preble, C. V., & Kirchstetter, T. W. A Distributed Network of 100 Black Carbon Sensors for 100 Days of Air Quality Monitoring in West Oakland, California. Environmental Science and Technology, 53(13), 7564–7573. https://doi.org/10.1021/acs.est.9b00282, 2019.

Choi, W., Winer, A.M. and Paulson, S.E., 2014. Factors controlling pollutant plume length downwind of major roadways in nocturnal surface inversions. *Atmospheric Chemistry and Physics*, *14*(13), pp.6925-6940., https://doi.org/10.5194/acp-14-6925-2014

City of Oakland: Oakland Equitable Climate Action Plan. https://cao-94612.s3.amazonaws.com/documents/Oakland-ECAP-07-24.pdf, last accessed January 12, 2022.

Dallmann, T.R., Harley, R.A. and Kirchstetter, T.W., 2011. Effects of diesel particle filter retrofits and accelerated fleet turnover on drayage truck emissions at the Port of Oakland. *Environmental science & technology*, *45*(24), pp.10773-10779., https://doi.org/10.1021/es202609q

Dallmann, T.R., Kirchstetter, T.W., DeMartini, S.J. and Harley, R.A., 2013. Quantifying on-road emissions from gasoline-powered motor vehicles: Accounting for the presence of medium-and heavy-duty diesel trucks. *Environmental science & technology*, *47*(23), pp.13873-13881., https://doi.org/10.1021/es402875u

Dallmann, T.R., DeMartini, S.J., Kirchstetter, T.W., Herndon, S.C., Onasch, T.B., Wood, E.C. and Harley, R.A., 2012. On-road measurement of gas and particle phase pollutant emission factors for individual heavy-duty diesel trucks. *Environmental science & technology*, *46*(15), pp.8511-8518., https://doi.org/10.1021/es301936c

Dallmann, T.R., Onasch, T.B., Kirchstetter, T.W., Worton, D.R., Fortner, E.C., Herndon, S.C., Wood, E.C., Franklin, J.P., Worsnop, D.R., Goldstein, A.H. and Harley, R.A., 2014. Characterization of particulate matter emissions from on-road gasoline and diesel vehicles using

a soot particle aerosol mass spectrometer. *Atmospheric Chemistry and Physics*, *14*(14), pp.7585-7599., https://doi.org/10.5194/acp-14-7585-2014

Davis, S. C., Diegel, S. W., & Boundy, R. G. Transportation Energy Data Book, Edition 29. Energy. https://tedb.ornl.gov/wp-content/uploads/2021/02/TEDB_Ed_39.pdf, last accessed January 12, 2022

Delaria, E.R., Kim, J., Fitzmaurice, H.L., Newman, C., Wooldridge, P.J., Worthington, K. and Cohen, R.C., 2021. The Berkeley Environmental Air-quality and CO 2 Network: field calibrations of sensor temperature dependence and assessment of network scale CO 2 accuracy. *Atmospheric Measurement Techniques*, *14*(8), pp.5487-5500. https://doi.org/10.5194/amt-14-5487-2021

Deng, A., Lauvaux, T., Davis, K.J., Gaudet, B.J., Miles, N., Richardson, S.J., Wu, K., Sarmiento, D.P., Hardesty, R.M., Bonin, T.A. and Brewer, W.A., 2017. Toward reduced transport errors in a high resolution urban CO2 inversion system. Elementa: Science of the Anthropocene, 5. https://doi.org/10.1525/elementa.133

Di, Q., Wang, Y., Zanobetti, A., Wang, Y., Koutrakis, P., Choirat, C., Dominici, F. and Schwartz, J.D., 2017. Air pollution and mortality in the Medicare population. *New England Journal of Medicine*, *376*(26), pp.2513-2522., https://doi:10.1056/NEJMoa1702747

Fanai, A.K, Claire, S.J., Dinh, T.M., Nguyen, Scultz, S.A. Bay Area Emissions Inventory Report: Criteria Air Pollutants: Base Year 2011, Bay Area Air Quality Management District. 2014

Fitzmaurice, H.L., Turner, A.J., Kim, J., Chan, K., Delaria, E.R., Newman, C., Wooldridge, P. and Cohen, R.C., 2022a. Assessing vehicle fuel efficiency using a dense network of CO 2 observations. *Atmospheric Chemistry and Physics*, *22*(6), pp.3891-3900.

Fitzmaurice, H.L. and Cohen, R.C., 2022b. A method for using stationary networks to observe long term trends of on-road emissions factors of primary aerosol from heavy duty vehicles. *Atmospheric Chemistry and Physics Discussions*, pp.1-13.

Gately, C. K., Hutyra, L. R., & Wing, I. S. Cities, traffic, and CO2: A multidecadal assessment of trends, drivers, and scaling relationships. Proceedings of the National Academy of Sciences of the United States of America, 112(16), 4999–5004. https://doi.org/10.1073/pnas.1421723112, 2015.

Gately, C.K. and Hutyra, L.R., 2017. Large uncertainties in urban-scale carbon emissions. *Journal of Geophysical Research: Atmospheres*, *122*(20), pp.11-242. https://doi.org/10.1002/2017JD027359

Gately, C.K., Hutyra, L.R., Peterson, S. and Wing, I.S., 2017. Urban emissions hotspots: Quantifying vehicle congestion and air pollution using mobile phone GPS data. *Environmental pollution*, *229*, pp.496-504. https://doi.org/10.1016/j.envpol.2017.05.091

Geller, M.D., Sardar, S.B., Phuleria, H., Fine, P.M. and Sioutas, C., 2005. Measurements of particle number and mass concentrations and size distributions in a tunnel environment. *Environmental Science & Technology*, *39*(22), pp.8653-8663., https://doi.org/10.1021/es050360s

Gurney, K.R., Razlivanov, I., Song, Y., Zhou, Y., Benes, B. and Abdul-Massih, M., 2012. Quantification of fossil fuel CO2 emissions on the building/street scale for a large US city. *Environmental science & technology*, *46*(21), pp.12194-12202. https://doi.org/10.1021/es3011282

Gurney, K.R., Liang, J., Roest, G., Song, Y., Mueller, K. and Lauvaux, T., 2021. Under-reporting of greenhouse gas emissions in US cities. *Nature communications*, *12*(1), pp.1-7. https://doi.org/10.1038/s41467-020-20871-0

Hamilton, S.D. and Harley, R.A., 2021. High-Resolution Modeling and Apportionment of Diesel-Related Contributions to Black Carbon Concentrations. *Environmental Science & Technology*, *55*(18), pp.12250-12260.

Haugen, M.J. and Bishop, G.A., 2017. Repeat fuel specific emission measurements on two California heavy-duty truck fleets. *Environmental science & technology*, *51*(7), pp.4100-4107., https://doi.org/10.1021/acs.est.6b06172

Hallegatte, Stephane, Mook Bangalore, Laura Bonzanigo, Marianne Fay, Tamaro Kane, Ulf Narloch, Julie Rozenberg, David Treguer, and Adrien Vogt-Schilb. 2016. Shock Waves: Managing the Impacts of Climate Change on Poverty. Climate Change and Development Series. Washington, DC: World Bank. doi:10.1596/978-1-4648-0673-5. License: Creative Commons Attribution CC BY 3.0 IGO, retrieved from: https://documents1.worldbank.org/curated/en/260011486755946625/pdf/ShockWaves-FullReport.pdf on April 1 2022

Haugen, M.J. and Bishop, G.A., 2018. Long-Term Fuel-Specific NO x and Particle Emission Trends for In-Use Heavy-Duty Vehicles in California. *Environmental science & technology*, *52*(10), pp.6070-6076., https://doi.org/10.1021/acs.est.8b00621

Hedelius, J.K., Liu, J., Oda, T., Maksyutov, S., Roehl, C.M., Iraci, L.T., Podolske, J.R., Hillyard, P.W., Liang, J., Gurney, K.R. and Wunch, D., 2018. Southern California megacity CO 2, CH 4, and CO flux estimates using ground-and space-based remote sensing and a Lagrangian model. *Atmospheric Chemistry and Physics*, *18*(22), pp.16271-16291. https://doi.org/10.5194/acp-18-16271-2018

Henne, S., Brunner, D., Oney, B., Leuenberger, M., Eugster, W., Bamberger, I., Meinhardt, F., Steinbacher, M. and Emmenegger, L., 2016. Validation of the Swiss methane emission inventory by atmospheric observations and inverse modelling. *Atmospheric Chemistry and Physics*, *16*(6), pp.3683-3710. https://doi.org/10.5194/acp-16-3683-2016

Hoegh-Guldberg, O., D. Jacob, M. Taylor, M. Bindi, S. Brown, I. Camilloni, A. Diedhiou, R. Djalante, K.L. Ebi, F. Engelbrecht, J. Guiot, Y. Hijioka, S. Mehrotra, A. Payne, S.I. Seneviratne,

A. Thomas, R. Warren, and G. Zhou, 2018: Impacts of 1.5ºC Global Warming on Natural and Human Systems. In: Global Warming of 1.5°C. An IPCC Special Report on the impacts of global warming of 1.5°C above pre-industrial levels and related global greenhouse gas emission pathways, in the context of strengthening the global response to the threat of climate change, sustainable development, and efforts to eradicate poverty [Masson-Delmotte,V., P. Zhai, H.-O. Pörtner, D. Roberts, J. Skea, P.R. Shukla,A. Pirani,W. Moufouma-Okia, C. Péan, R. Pidcock,S. Connors, J.B.R. Matthews,Y. Chen, X. Zhou, M.I. Gomis, E. Lonnoy,T. Maycock, M.Tignor, and T.Waterfield (eds.)]. In Press.

IPCC. (2014). Climate Change 2014 Part A: Global and Sectoral Aspects. Climate Change 2014: Impacts, Adaptation, and Vulnerability. Part A: Global and Sectoral Aspects. Contribution of Working Group II to the Fifth Assessment Report of the Intergovernmental Panel on Climate Change.

Karion, A., Lopez-Coto, I., Gourdji, S.M., Mueller, K., Ghosh, S., Callahan, W., Stock, M., DiGangi, E., Prinzivalli, S. and Whetstone, J., 2021. Background conditions for an urban greenhouse gas network in the Washington, DC, and Baltimore metropolitan region. *Atmospheric Chemistry and Physics*, *21*(8), pp.6257-6273. https://doi.org/10.5194/acp-21-6257-2021

Kirchstetter, T.W., Harley, R.A., Kreisberg, N.M., Stolzenburg, M.R. and Hering, S.V., 1999. On-road measurement of fine particle and nitrogen oxide emissions from light-and heavy-duty motor vehicles. *Atmospheric Environment*, *33*(18), pp.2955-2968., https://doi.org/10.1016/S1352-2310(99)00089-8

Kim, J., Shusterman, A. A., Lieschke, K. J., Newman, C., & Cohen, R. C. The Berkeley Atmospheric CO2 Observation Network: Field calibration and evaluation of low-cost air quality sensors. Atmospheric Measurement Techniques, 11(4), 1937–1946. https://doi.org/10.5194/amt 11-1937-2018, 2018.

Kim, J., Turner, A.J., Fitzmaurice, H.L., Delaria, E.R., Newman, C., Wooldridge, P.J. and Cohen, R.C., 2022. Observing Annual Trends in Vehicular CO2 Emissions. *Environmental Science & Technology*. https://doi.org/10.1021/acs.est.1c06828

Kim, J., Turner, A. J., Fitzmaurice, H. L, Cohen, R. C., and Berelson, W.M., A simple near-field model for inferring CO_2 emissions from continuous in-situ observations. (*in prep)*

Kort, E.A., Frankenberg, C., Miller, C.E. and Oda, T., 2012. Space-based observations of megacity carbon dioxide. *Geophysical Research Letters*, *39*(17). https://doi.org/10.1029/2012GL052738

Kwon, J., Varaiya, P., & Skabardonis, A. Estimation of Truck Traffic Volume from Single Loop Detectors with Lane-to-Lane Speed Correlation. Transportation Research Record, 684(1856), 106–117. https://doi.org/10.3141/1856-11 2003.

Lauvaux, T., Miles, N.L., Richardson, S.J., Deng, A., Stauffer, D.R., Davis, K.J., Jacobson, G., Rella, C., Calonder, G.P. and DeCola, P.L., 2013. Urban emissions of CO 2 from Davos, Switzerland: The first real-time monitoring system using an atmospheric inversion technique. *Journal of Applied Meteorology and Climatology*, *52*(12), pp.2654-2668. https://doi.org/10.1175/JAMC-D-13-038.1

Lauvaux, T., Miles, N. L., Deng, A., Richardson, S. J., Cambaliza, M. O., Davis, K. J., Gaudet, B. Gurney, K. R., Huang, J. O'Keefe, D., Song, Y., Karion, A., Oda, T., Patarsuk, R., Razlivanov, I., Sarmiento, D., Shepson, P, Sweeney, C. Turnbull, J. Wu, K. High-resolution atmospheric inversion of urban CO2 emissions during the dormant season of the Indianapolis flux experiment (INFLUX). Journal of Geophysical Research, 121(10), 5213–5236. https://doi.org/10.1002/2015JD024473, 2016.

Lauvaux, T., Gurney, K. R., Miles, N. L., Davis, K. J., Richardson, S. J., Deng, A., Nathan, B. J., Oda, T. Wang, J. A., Hutyra, L., Turnbull, J. Policy-relevant assessment of urban CO2emissions. Environmental Science and Technology, 54(16), 10237–10245. https://doi.org/10.1021/acs.est.0c00343, 2020.

Li, X., Dallmann, T.R., May, A.A., Stanier, C.O., Grieshop, A.P., Lipsky, E.M., Robinson, A.L. and Presto, A.A., 2018. Size distribution of vehicle emitted primary particles measured in a traffic tunnel. *Atmospheric Environment*, *191*, pp.9-18., https://doi.org/10.1016/j.atmosenv.2018.07.052

Lian, J., Bréon, F.M., Broquet, G., Lauvaux, T., Zheng, B., Ramonet, M., Xueref-Remy, I., Kotthaus, S., Haeffelin, M. and Ciais, P., 2021. Sensitivity to the sources of uncertainties in the modeling of atmospheric CO 2 concentration within and in the vicinity of Paris. *Atmospheric Chemistry and Physics*, *21*(13), pp.10707-10726. https://doi.org/10.5194/acp-21-10707-2021

Lian, J., Lauvaux, T., Utard, H., Bréon, F.M., Broquet, G., Ramonet, M., Laurent, O., Albarus, I., Cucchi, K. and Ciais, P., 2022. Assessing the Effectiveness of an Urban CO2 Monitoring Network over the Paris Region through the COVID-19 Lockdown Natural Experiment. *Environmental Science & Technology*. https://doi.org/10.1021/acs.est.1c04973

Liu, T., Meng, H., Yu, M., Xiao, Y., Huang, B., Lin, L., Zhang, H., Hu, R., Hou, Z., Xu, Y. and Yuan, L., 2021. Urban-rural disparity of the short-term association of PM2. 5 with mortality and its attributable burden. *The Innovation*, *2*(4), p.100171. https://doi.org/10.1016/j.xinn.2021.100171

Ma, L., Graham, D.J. and Stettler, M.E., 2021. Has the ultra low emission zone in London improved air quality?. *Environmental Research Letters*, *16*(12), p.124001. https://doi.org/10.1088/1748-9326/ac30c1

Martien, P., Fanai, A.K, Claire, S.J., Dinh, T.M., Nguyen, Scultz, S.A. Base Year 2011 Emission Inventory: Source Category Methodologies. Bay Area Air Quality Management District. 2014

California Air Resources Board. Community Air Protection Blueprint. 2018. Retrieved from: https://ww2.arb.ca.gov/sites/default/files/2020-03/final_community_air_protection_blueprint_october_2018_acc.pdf

Martin, C.R., Zeng, N., Karion, A., Mueller, K., Ghosh, S., Lopez-Coto, I., Gurney, K.R., Oda, T., Prasad, K., Liu, Y. and Dickerson, R.R., 2019. Investigating sources of variability and error in simulations of carbon dioxide in an urban region. *Atmospheric environment*, *199*, pp.55-69. https://doi.org/10.1016/j.atmosenv.2018.11.013

McDonald, B.C., McBride, Z.C., Martin, E.W. and Harley, R.A., High-resolution mapping of motor vehicle carbon dioxide emissions. Journal of Geophysical Research: Atmospheres, 119(9), pp.5283-5298. https://doi.org/10.1002/2013JD021219, 2014.

Moua, F., 2018 California Annual Fuel Outlet Report Results (CEC-A15), Energy Assessments Division, California Energy Comission, 2020. retrieved from: https://ww2.energy.ca.gov/almanac/transportation_data/gasoline/piira_retail_survey.html

Moua, F. (2020). California Annual Fuel Outlet Report Results (CEC-A15), Energy Assessments Division, California Energy Comission., https://www.energy.ca.gov/media/3874, last accessed January 13, 2022

Mueller, K., Yadav, V., Lopez-Coto, I., Karion, A., Gourdji, S., Martin, C., and Whetstone, J.: Siting Background Towers to Characterize Incoming Air for Urban Greenhouse Gas Estimation: A Case Study in the Washington, DC/Baltimore Area, J. Geophys. Res.-Atmos., 123, 2910–2926, https://doi.org/10.1002/2017JD027364, 2018.

Nathan, B.J., Lauvaux, T., Turnbull, J.C., Richardson, S.J., Miles, N.L. and Gurney, K.R., 2018. Source sector attribution of CO2 emissions using an urban CO/CO2 Bayesian inversion system. *Journal of Geophysical Research: Atmospheres*, *123*(23), pp.13-611. https://doi.org/10.1029/2018JD029231

Nathan, B., Kremser, S., Mikaloff-Fletcher, S., Bodeker, G., Bird, L., Dale, E., Lin, D., Olivares, G. and Somervell, E., 2021. The MAPM (Mapping Air Pollution eMissions) method for inferring particulate matter emissions maps at city scale from in situ concentration measurements: description and demonstration of capability. *Atmospheric Chemistry and Physics*, *21*(18), pp.14089-14108. https://doi.org/10.5194/acp-21-14089-2021

Newman, S., Xu, X., Gurney, K.R., Hsu, Y.K., Li, K.F., Jiang, X., Keeling, R., Feng, S., O'Keefe, D., Patarasuk, R. and Wong, K.W., Toward consistency between trends in bottom-up CO 2 emissions and top-down atmospheric measurements in the Los Angeles megacity. *Atmospheric Chemistry and Physics*, *16*(6), pp.3843-3863. https://doi.org/10.5194/acp-16-3843-2016, 2016.

Nickless, A., Rayner, P. J., Engelbrecht, F., Brunke, E.-G., Erni, B., and Scholes, R. J.: Estimates of CO_2 fluxes over the city of Cape Town, South Africa, through Bayesian inverse modelling,

Atmospheric Chemistry and Physics, 18, 4765–4801, https://doi.org/10.5194/acp-18-4765-2018, 2018.

Oda, T. and Maksyutov, S., 2011. A very high-resolution (1 km× 1 km) global fossil fuel CO 2 emission inventory derived using a point source database and satellite observations of nighttime lights. *Atmospheric Chemistry and Physics*, *11*(2), pp.543-556. https://doi.org/10.5194/acp-11-543-2011

Park, S.S., Vijayan, A., Mara, S.L. and Herner, J.D., 2016. Investigating the real-world emission characteristics of light-duty gasoline vehicles and their relationship to local socioeconomic conditions in three communities in Los Angeles, California. *Journal of the Air & Waste Management Association*, *66*(10), pp.1031-1044., https://doi.org/10.1080/10962247.2016.1197166

Park, S.S., Kozawa, K., Fruin, S., Mara, S., Hsu, Y.K., Jakober, C., Winer, A. and Herner, J., 2011. Emission factors for high-emitting vehicles based on on-road measurements of individual vehicle exhaust with a mobile measurement platform. *Journal of the Air & Waste Management Association*, *61*(10), pp.1046-1056., https://doi.org/10.1080/10473289.2011.595981

Preble, C.V., Cados, T.E., Harley, R.A. and Kirchstetter, T.W., 2018. In-use performance and durability of particle filters on heavy-duty diesel trucks. Environmental science & technology, 52(20), pp.11913-11921., https://doi.org/10.1021/acs.est.8b02977

Rajagopalan, S. and Landrigan, P.J., 2021. Pollution and the Heart. *New England Journal of Medicine*, *385*(20), pp.1881-1892. https://doi.org/10.1056/NEJMra2030281

Robinson, A.L., Grieshop, A.P., Donahue, N.M. and Hunt, S.W., 2010. Updating the conceptual model for fine particle mass emissions from combustion systems Allen L. Robinson. *Journal of the Air & Waste Management Association*, *60*(10), pp.1204-1222., https://doi.org/10.3155/1047-3289.60.10.1204

Rogelj, J., D. Shindell, K. Jiang, S. Fifita, P. Forster, V. Ginzburg, C. Handa, H. Kheshgi, S. Kobayashi, E. Kriegler, L. Mundaca, R. Séférian, and M.V. Vilariño, 2018: Mitigation Pathways Compatible with 1.5°C in the Context of Sustainable Development. In: Global Warming of 1.5°C. An IPCC Special Report on the impacts of global warming of 1.5°C above pre-industrial levels and related global greenhouse gas emission pathways, in the context of strengthening the global response to the threat of climate change, sustainable development, and efforts to eradicate poverty [Masson-Delmotte, V., P. Zhai, H.-O. Pörtner, D. Roberts, J. Skea, P.R. Shukla, A. Pirani, W. Moufouma-Okia, C. Péan, R. Pidcock, S. Connors, J.B.R. Matthews, Y. Chen, X. Zhou, M.I. Gomis, E. Lonnoy, T. Maycock, M. Tignor, and T. Waterfield (eds.)]. In Press.

Sargent, M., Barrera, Y., Nehrkorn, T., Hutyra, L.R., Gately, C.K., Jones, T., McKain, K., Sweeney, C., Hegarty, J., Hardiman, B. and Wang, J.A., 2018. Anthropogenic and biogenic CO2 fluxes in the Boston urban region. *Proceedings of the National Academy of Sciences*, *115*(29), pp.7491-7496. https://doi.org/10.1073/pnas.1803715115

Shah, R.U., Robinson, E.S., Gu, P., Robinson, A.L., Apte, J.S. and Presto, A.A., 2018. High-spatial-resolution mapping and source apportionment of aerosol composition in Oakland, California, using mobile aerosol mass spectrometry. *Atmospheric Chemistry and Physics*, *18*(22), pp.16325-16344., https://doi.org/10.5194/acp-18-16325-2018

Shusterman, A. A., Teige, V. E., Turner, A. J., Newman, C., Kim, J., & Cohen, R. C., The Berkeley Atmospheric CO2 Observation Network: Initial evaluation. Atmospheric Chemistry and Physics, 16(21), 13449–13463. https://doi.org/10.5194/acp-16-13449-2016, 2016.

Shusterman, A. A., Kim, J., Lieschke, K. J., Newman, C., Wooldridge, P. J., & Cohen, R. C. (2018). Observing local CO2 sources using low-cost, near-surface urban monitors. *Atmos. Chem. Phys*, *18*, 13773-13785.

Solomon, S., Plattner, G. K., Knutti, R., & Friedlingstein, P. (2009). Irreversible climate change due to carbon dioxide emissions. *Proceedings of the national academy of sciences*, *106*(6), 1704-1709.

Staufer, J., Broquet, G., Bréon, F.M., Puygrenier, V., Chevallier, F., Xueref-Rémy, I., Dieudonné, E., Lopez, M., Schmidt, M., Ramonet, M. and Perrussel, O., 2016. The first 1-year-long estimate of the Paris region fossil fuel CO 2 emissions based on atmospheric inversion. *Atmospheric Chemistry and Physics*, *16*(22), pp.14703-14726. https://doi.org/10.5194/acp-16-14703-2016

Tessum, C.W., Apte, J.S., Goodkind, A.L., Muller, N.Z., Mullins, K.A., Paolella, D.A., Polasky, S., Springer, N.P., Thakrar, S.K., Marshall, J.D. and Hill, J.D., 2019. Inequity in consumption of goods and services adds to racial–ethnic disparities in air pollution exposure. *Proceedings of the National Academy of Sciences*, *116*(13), pp.6001-6006., https://doi.org/10.1073/pnas.1818859116

Tessum, C. W., Paolella, D. A., Chambliss, S. E., Apte, J. S., Hill, J. D., & Marshall, J. D., PM2.5 polluters disproportionately and systemically affect people of color in the United States. Science Advances, 7(18), 1–7. https://doi.org/10.1126/sciadv.abf4491, 2021.

Texas A&M Transportation Institute. (2019). Urban Mobility Report 2019, 182. https://static.tti.tamu.edu/tti.tamu.edu/documents/umr/archive/mobility-report-2019.pdf, last accessed January 13, 2022.

Sumil K. Thakrar, Srinidhi Balasubramanian, Peter J. Adams, Inês M. L. Azevedo, Nicholas Z. Muller, Spyros N. Pandis, Stephen Polasky, C. Arden Pope, Allen L. Robinson, Joshua S. Apte, Christopher W. Tessum, Julian D. Marshall, and Jason D. Hill
Environmental Science & Technology Letters **2020** *7* (9), 639-645
DOI:10.1021/acs.estlett.0c00424

Title 13, Section 2025, California Code of Regulations Regulation to Reduce Emissions of Diesel Particulate Matter, Oxides of Nitrogen and Other Criteria Pollutants from In-Use Heavy-Duty Diesel-Fueled Vehicles.

Turner, A.J., Kim, J., Fitzmaurice, H., Newman, C., Worthington, K., Chan, K., Wooldridge, P.J., Köehler, P., Frankenberg, C. and Cohen, R.C., 2020. Observed impacts of COVID-19 on urban CO 2 Emissions. Geophysical Research Letters, 47(22), p.e2020GL090037.Geophysical Research Letters, 47(22), 1–6. https://doi.org/10.1029/2020GL090037, 2020a.

Turner, A. J., Köhler, P., Magney, T. S., Frankenberg, C., Fung, I., & Cohen, R. C., A double peak in the seasonality of California's photosynthesis as observed from space. Biogeosciences, 17(2), 405–422. https://doi.org/10.5194/bg 17-405-2020, 2020b.

Turner, A. J., Shusterman, A. A., McDonald, B. C., Teige, V., Harley, R. A., & Cohen, R. C., Network design for quantifying urban CO2 emissions: Assessing trade-offs between precision and network density. Atmospheric Chemistry and Physics, 16(21), 13465–13475. https://doi.org/10.5194/acp-16-13465-2016, 2016.

United Nations, Human Rights Council. (2019) Climate Change and Poverty

Wu, L., Broquet, G., Ciais, P., Bellassen, V., Vogel, F., Chevallier, F., Xueref-Remy, I. and Wang, Y., 2016. What would dense atmospheric observation networks bring to the quantification of city CO 2 emissions?. *Atmospheric Chemistry and Physics*, *16*(12), pp.7743-7771. https://doi.org/10.5194/acp-16-7743-2016

Zhang, Y., Gao, Z., Li, D., Li, Y., Zhang, N., Zhao, X. and Chen, J., 2014. On the computation of planetary boundary-layer height using the bulk Richardson number method. *Geoscientific Model Development*, *7*(6), pp.2599-2611. https://doi.org/10.5194/gmd-7-2599-2014

Zimmerman, N., Presto, A.A., Kumar, S.P., Gu, J., Hauryliuk, A., Robinson, E.S., Robinson, A.L. and Subramanian, R., 2018. A machine learning calibration model using random forests to improve sensor performance for lower-cost air quality monitoring. *Atmospheric Measurement Techniques*, *11*(1), pp.291-313., https://doi.org/10.5194/amt-11-291-2018.